



**Politecnico
di Torino**

Politecnico di Torino

Master of Science in Environmental & Land Engineering

A.Y. 2021/2022

Graduation Session July 2022

**Data Extraction from River Area using Very
High-Resolution Multispectral UAS Imagery
and Artificial Intelligence**

Supervisor:

Andrea Maria Lingua

Candidate:

Masoume Mahboubi

Co-Supervisor:

Elena Belcore

Francesca Matrone

Acknowledgment

I would like to show my deep appreciation to my partner whose presence in my life is something I will always cherish. He helped me in all challenges throughout my life and during the sleepless nights of doing this thesis. I would also like to thank my friends and family who supported me even from thousand miles away.

I wish to acknowledge that the data are provided by the Geomatics Lab of Politecnico di Torino, and they are acquired by the data acquisition team led by Paolo Felice Maschio. Also, I would like to express my gratitude to my colleague Emanuele Pontoglio whose valuable presence and assistance allowed my studies to go the extra mile.

Last but not least, I want to thank myself for believing in me, for doing all this hard work, for having no days off, for never quitting, and even for taking the extra step of publishing and presenting a paper from this valuable work in the AGILE (Association of geographic information laboratories in Europe) conference.

Abstract

Unmanned Aerial System (UAS) imagery has enabled very high-resolution multispectral image acquisition. In this study images acquired by UAS or generally known as drones are our main data, which have been used to perform the Structure from Motion (SfM) Approach and produce the Digital Elevation Model (DEM) and orthophotos (orthomosaics) of five spectral bands of Red, Green, Blue, Red-Edge and Near-Infrared.

Detection of wet areas and classification of land cover based on these images using the Machine Learning (ML) algorithm named Random Forest (RF) is our main purpose in this project. Orthophotos of the SfM process have been used as inputs for a machine learner in different scenarios. Starting from Random Forest Classifier, 3 different datasets consisting of RGB only, Multispectral only consisting of Red-Edge and Near-Infrared, RGB plus Multispectral for classification of the area have been used in three different test areas in two time epochs.

Therefore, another objective of this study is to investigate the performance of spectral bands (number of included bands and related wavelength) in the classification and wet area detection, to probe whether RGB (visible) light provides better results for our goal or multispectral data (Red-Edge and NIR) outperform in this analysis, or whether combining visible and Multispectral data is a superior alternative or not.

In our case study for the sake of simplicity of comparison between implemented methods of classification and strength of datasets and to probe the most effective features in all seasonal conditions, only three classes have been analyzed including Vegetation, Water, and Ground.

Furthermore, in another time epoch in the summertime, in addition to spectral features used in the previous epoch, the capability of vegetation indices, elevation, and texture features in the classification of land cover and detection of the wet riparian area in the case study are assessed. There are many existing methods for the classification of land cover based on UAS images, but very high-resolution centimetre-level data are of main importance in this analysis. Outstanding results have been produced in both epochs considering three extremely accurate performance

analyzers of precision, recall, and F-core which are originally based on True Positive, True Negative, False Positive, False Negative concepts.

Additionally, in this research, the most decisive and effective features based on a selection tool in python programming language have been discovered to compromise the accuracy of the classification and the number of effectual features and save processing time and power in future similar studies.

Keywords: Machine learning, classification, UAS, spectral features, land cover.

Table of Contents

1- Introduction	1
2- State of the Art.....	9
3- Methodology.....	17
3-1- Theoretical Background	17
3-1-1- Structure from Motion	17
3-1-2- Machine Learning Classification	18
3-1-3- Performance Assessment.....	20
3-2- Data Acquisition and study areas	22
.....	22
3-3- Processing Steps.....	23
3-3-1-Structure from Motion (SfM)	23
3-3-1-1- Adding photos:	23
3-3-1-2- Quality control of photos	23
3-3-1-3- Interior orientation of the camera	24
3-3-1-4- Settings.....	25
3-3-1-5- Align photos.....	25
3-3-1-6- Georeferencing.....	27
3-3-1-7- Optimal Alignment	30
3-3-1-8- Building Dense Point Cloud	30
3-3-1-9- Build Mesh.....	31
3-3-1-10- Build Texture	32
3-3-1-11- Building Digital Elevation Model.....	33
3-3-1-12- Building Orthomosaic	34
3-3-2- Machine Learning- Random Forest- April Epoch.....	40
3-3-2-1- First Test Area.....	41
3-3-2-1-1- RGB+ Red-Edge+ Near Infrared dataset	41
3-3-3- Machine Learning- RF- July Epoch.....	55

3-3-3-1- Feature Selection.....	55
4-1- Random Forest - April Epoch - First test area.....	56
4-1-1- RGB + Red-Edge + NIR	56
4-1-2- RGB dataset.....	59
4-1-3- Red-Edge + NIR dataset.....	61
4-2- Random Forest- April Epoch- Second Test Area.....	65
4-2-1- RGB dataset.....	65
4-2-2- Red-Edge + NIR dataset.....	68
4-2-3- RGB+ Red-Edge+ NIR dataset	70
4-3- Random Forest- April Epoch- Third Test Area	73
4-3-1- RGB dataset.....	73
4-3-2- Red-Edge + NIR dataset.....	76
4-3-3- RGB+ Red-Edge+ NIR dataset	78
4-4- Random Forest- July epoch	83
5- Conclusions and Suggestions	86
References.....	89

List of Figures

Figure 1. Up left: DJI phantom4 camera, up right: 6 spectral bands of phantom4 drone, bottom: Thermal camera XT2 16

Figure 2. Structure from Motion procedure..... 18

Figure 3. Study area, Salbertrand town, Salbertrand river 22

Figure 4. Quality Control for images- Red band..... 24

Figure 5. Camera interior calibration..... 24

Figure 6. Tie points of blue band and technical characteristics 26

Figure 7. Tie points of green band and technical characteristics..... 26

Figure 8. Tie points of red band and technical characteristics..... 26

Figure 9. Tie points of Red-Edge band and technical characteristics..... 27

Figure 10. Tie points of NIR band and technical characteristics 27

Figure 11. Camera Positions on RGB Tie Points 27

Figure 12. GCPs on the Tie points- RGB..... 29

Figure 13. . right: F6 marker on the RGB image, left: two markers on the NIR image..... 29

Figure 14. Dense Cloud of RGB bands..... 31

Figure 15. Solid Model of RGB bands..... 32

Figure 16. Textured Model of RGB bands 32

Figure 17. Different views of the 3D model 33

Figure 18. Different views of the 3D model 33

Figure 19. DEM- RGB band 38

Figure 20. Orthophoto-left: Blue Band, right: green band..... 39

Figure 21. Orthophoto-left: red Band, right: Red-Edge band..... 39

Figure 22. Orthomosaic- left: NIR Band, right: RGB band..... 39

Figure 23. Composite raster of RGB, Red-Edge & NIR bands..... 42

Figure 24. identify value in 16 bit for one pixel..... 43

Figure 25. identify value after converting the format to 8 bit 43

Figure 26. Training raster 44

Figure 27. training polygons for 3 classes: Green (Vegetation), Yellow (Ground), Blue (Water) ... 45

Figure 28. Water training raster..... 46

Figure 29. Assigning label '11' for water class..... 46

Figure 30. Reading training data into the python script..... 47

Figure 31. packages and libraries used in the training phase..... 47

Figure 32. Splitting training dataset for cross-validation purpose..... 48

Figure 33. Script of cross-validation step for best parameters determination for 4 folds 49

Figure 34. possible values for each parameter 49

Figure 35. Test raster, 1st test area..... 51

Figure 36. packages and libraries necessary for the prediction and evaluation phase..... 52

Figure 37. Head function for bringing balance to the unbalanced training dataset.....	52
Figure 38. Reading training dataset into the script	52
Figure 39. setting hyper-parameters for RF classifier, fitting a model on the training data, and predicting accuracy on training data.....	53
Figure 40. Reading unseen testing dataset into the script, prediction of labels for each point, exporting it to the determined directory	53
Figure 41. Validation polygons for 3 classes: Green (Vegetation), Yellow (Ground), Blue (Water)	54
Figure 42. Prediction (Segmented) map of testing based on RGB + Red-Edge + NIR dataset.....	56
Figure 43. The precision-Recall curve for 3 classes- for 1st test area- RGB+RE+NIR dataset.....	58
Figure 44. Predicted (Segmented) image of the 1st Test area based on RGB dataset.....	59
Figure 45. Precision-Recall curve of 1st test area- RGB dataset	61
Figure 46. Predicted (classified) map of 1st test area- based on Red-Edge + NIR dataset	62
Figure 47. Precision-Recall curve of 1st test area based on Red-Edge + NIR dataset	64
Figure 48. Results of 1st test area using 3 different datasets.....	64
Figure 49. Left: 2nd test area. Right: classified map of 2nd test area	65
Figure 50. Validation polygons on the 2nd test area, Green (Vegetation), Blue (Water), Yellow (Ground)	66
Figure 51. Precision-recall curves for 3 classes.....	67
Figure 52. Left: 2nd Testing area- RE + NIR dataset. Right: segmented map of 2nd testing area based on RE + NIR dataset.....	68
Figure 53. Precision-recall curves for 3 classes	69
Figure 54. Left. 2nd testing area, RGB+ RE+ NIR dataset. Right: Segmented map of the 2nd testing area	70
Figure 55. Precision- Recall curves.....	71
Figure 56. Results of 2nd test area using 3 different datasets	72
Figure 57. Left: 3rd testing area-RGB dataset. Right: segmented map of the 3rd testing area based on RGB dataset	73
Figure 58. Validation Polygons on the 3rd testing area. Green (Vegetation), blue (Water), Yellow (Ground)	74
Figure 59. Precision-Recall curves.....	75
Figure 60. Left: 3rd testing area- Red-Edge + NIR dataset. Right: classified map of the 3rd testing area based on Red-Edge + NIR dataset	76
Figure 61. Precision-recall curve.....	77
Figure 62. Left: 3rd testing area- RGB+ RE+ NIR dataset. Right: Segmented map of 3rd testing area based on RGB+ RE+ NIR dataset.....	78
Figure 63. Precision-Recall curves.....	80
Figure 64. Results of 3rd test area using 3 different datasets	81
Figure 65. Importance of all features in percentage	84

List of Tables

<i>Table 1. Vegetation indexes and corresponding references</i>	5
<i>Table 2. Technical characteristics of the sensor</i>	16
<i>Table 3. Number of Check and control points in all bands</i>	30
<i>Table 4. Cross Validation result for RGB + Red-Edge + NIR dataset</i>	50
<i>Table 5. Accuracy on training dataset for 4 folds and optimum parameters</i>	50
<i>Table 6. Accuracy errors of Red Band for control and check points</i>	34
<i>Table 7. Accuracy errors of green Band for control and check points</i>	35
<i>Table 8. Accuracy errors of blue band for control and check points</i>	35
<i>Table 9. Accuracy errors of Red-Edge band for control and check points</i>	36
<i>Table 10. Accuracy errors of NIR band for control and check points</i>	36
<i>Table 11. Accuracy errors of RGB for control and check points</i>	37
<i>Table 12. Check points Errors of all bands</i>	38
<i>Table 13. Confusion Matrix for 1st test area- RGB+RE+NIR dataset</i>	57
<i>Table 14. Accuracy parameters for 1st test area- RGB+RE+NIR dataset</i>	57
<i>Table 15. Cross-Validation result for RGB dataset</i>	59
<i>Table 16. . Confusion matrix of 1st test area- RGB dataset</i>	60
<i>Table 17. Accuracy parameters of 1st test area- RGB dataset</i>	60
<i>Table 18. Cross Validation Result for Red-Edge + NIR dataset</i>	62
<i>Table 19. Confusion Matrix of 1st test area based on Red-Edge + NIR dataset</i>	63
<i>Table 20. Accuracy parameters of 1st test area based on Red-Edge + NIR dataset</i>	63
<i>Table 21. Confusion matrix of 2nd test area- RGB dataset</i>	66
<i>Table 22. Accuracy parameters of 2nd test area- RGB dataset</i>	67
<i>Table 23. Confusion matrix of 2nd Testing area- RE + NIR dataset</i>	68
<i>Table 24. Accuracy parameters of 2nd Testing area- RE + NIR dataset</i>	70
<i>Table 25. Confusion Matrix of 2nd testing area, RGB+ RE+ NIR dataset</i>	71
<i>Table 26. Accuracy Parameters of 2nd testing area, RGB+ RE+ NIR dataset</i>	71
<i>Table 27. Confusion Matrix of the 3rd testing area- based on RGB dataset</i>	74
<i>Table 28. Accuracy parameters of the 3rd testing area- based on RGB dataset</i>	75
<i>Table 29. Confusion Matrix of 3rd testing area- Red-Edge + NIR dataset</i>	77
<i>Table 30. Accuracy Parameters of the 3rd testing area based on Red-Edge + NIR dataset</i>	77
<i>Table 31. Confusion Matrix of the 3rd testing area- RGB+ RE+ NIR dataset</i>	79
<i>Table 32. Accuracy Parameters of the 3rd testing area based on RGB+ RE+ NIR dataset</i>	80
<i>Table 33. Results of all test areas for all available dataset</i>	82
<i>Table 34. Results of performance analysis with all features vs only selected features.</i>	85

List of Abbreviations and Symbols

<i>Symbol</i>	<i>Quantity</i>
UAV	Unmanned Aerial Vehicle
UAS	Unmanned Aerial System
SfM	Structure from Motion
R	Red
G	Green
B	Blue
RE	Red-Edge
NIR	Near-Infrared
NDVI	Normalized Difference Vegetation Index
NDWI	Normalized Difference Water Index
NDRE	Normalized Difference Red-Edge
ARI	Anthocyanin Reflectance Index
EVI2	Enhanced Vegetation Index2
SAVI	Soil Adjusted Vegetation Index
SIPI	Structure Insensitive Pigment Index
GNSS	Global Navigation Satellite System
DTM	Digital Terrain Model
nDSM	Normalized Digital Surface Model
ML	Machine Learning
AI	Artificial Intelligence
RF	Random Forest
GCP	Ground Control Points
CP	Check points

Chapter 1

1- Introduction

According to several reports, consequences of global warming and climate change including severe droughts, saltwater intrusion into groundwater, shrinkage of glaciers, in addition to the increased water demand due to economic developments, fast urbanization, and population increase, have combined to result in an estimated 40% global water shortage by the year 2030. Hence, in addition to improvements in the conservation, distribution, and management of water resources, ensuring that new sources of fresh water can be readily available is essential in order to meet the increasing demand (Clara Skuse, 2021).

Classification of land cover to detect wet and moist areas is highly important for urban and environmental planning (Chaturvedi and de Vries, 2021). Furthermore, one of the crucial pillars of climate change is connected to water in different media, from lakes and rivers to soil water (Mahboubi, et al., 2022). Hence, detecting water in various environmental media is one of the essential steps in facing climate change (Lidberg et al., 2020). Since as climate changes and the earth warms up, the drier areas of earth become drier and lose all their wet resources from the lake, rivers, and even soil moisture. Since there is no direct and straightforward way to measure rainfall and evaporation from the surface, automatic artificial intelligence tools for the detection of wet areas enables researchers to detect dried areas, especially in the riparian river area, which

is expected to be the moistest areas and assess the effect of climate change (Schneider, et al., 2010).

Today, the widespread use of UAS imagery has provided a variety of very high-resolution image data sources for machine learning classifiers. There are several reasons that UAS or drones are a pleasant choice for scientists nowadays. To name a few, we can mention drones' appropriateness for hazardous and hard-to-reach areas, where it contains risks for human/operator health, and they can easily fly over the hazardous area with the drone. The second enormous advantage of drones would be their cost-efficiency. Considering that in a short period, there is the possibility of several flights and the acquisition of thousands of images, they are an extremely economic choice. Furthermore, the possibility of reacquisition of data helps to have high-quality data at the end of the acquisition phase. Last but not least, very high-resolution data acquired by drones, which is a result of GPS systems enabled on drones, enables researchers to have very accurate results for different purposes such as identification of weeds, monitoring crop health, crop damage, crop assessment, field soil analysis, Irrigation Monitoring, classification, etc. (Singh, et al., 2022).

The efficiency and potential of machine learning classifiers have made the classification purpose more precise and efficient (Jiang et al., 2021). UAS outperforms traditional approaches for data acquisition thanks to their high temporal and spatial resolution (Merlino et al., 2020; Banerjee et al., 2020). Considering their low cost, it is possible to have several flights in different epochs (Jiménez-Jiménez et al., 2021).

After data acquisition, to have a 3D map of the area, the Structure from Motion (SfM) approach was implemented. SfM lies in the simplified concept of production of a 3-D model or a digital twin from a bunch of 2-D images, and in order to produce this model, it looks up for similar features in the images and finds the corresponding points in each couple of images. Hence, to have a successful 3-D model, there should be overlap in the images in the acquisition phase, the amount of overlap can be controlled by the operator in the acquisition phase (Francisco Agüera-Vega, 2018).

Classification of the study area is based on a Machine Learning algorithm in this project. Machine learning is a sub-category of Artificial Intelligence and it can be referred s predictive modeling. Machine learning involves the use of algorithms that receive and analyze some input data/features and predict output values based on these algorithms. These algorithms learn from new data and

optimize their operations in order to improve performance and accuracy, hence they gradually become intelligent.

The four types of machine learning algorithms are supervised, semi-supervised, unsupervised, and reinforcement learning. Our focus will be on the Supervised algorithms, since we are able to provide training data for our algorithms, in other words, can teach the machine by some examples. Based on some known inputs and outputs for the machine by users, its responsibility is to figure out how to reach those outputs based on the given inputs, hence, it intelligently tries to figure out the methodology. Operators know the right answers to problems, but algorithms identify patterns in data, learn from observations, and predict. Level of accuracy and performance attained by the algorithm by making predictions will be checked by the operator until it reaches a high degree of performance.

There are Three kinds of supervised learning:

- a) **Classification:** Machine learning programs are used for classification tasks, where they draw conclusions from observed values and determine which values are relevant to which class.
- b) **Regression:** In regression, machine learning programs are required to estimate - and understand - how variables are related and what is the pattern in the data (Mahboubi, et al., 2022).
- c) **Forecasting:** Based on past and present data, forecasting makes predictions about the future and is often used to analyze trends (F.Y., et al., 2017).

In Unsupervised algorithms, clustering is based on similarities and differences between data themselves, so there is no information about classes and their characteristics in the first place. In a semi-supervised, there is some information available about labels, and the relationship between data and input data, in this method portion of labeled data is a few in respect to unlabeled data. In reinforcement learning, there are methods for each step of the model.

Our focus will be on the classification task of machine learning considering three available classes in the riparian river area. There are several methods for the classification of multispectral UAS data (Iglhaut et al., 2019).

Random Forest (RF) Classifier is based on the decision of several trees, meaning that it uses several trees (so a forest) and the concept of sub-sampling to make the prediction more precise and more accurate (Rodriguez-Galiano et al., 2012; Lowe and Kulkarni, 2015). Random forest algorithms are

built on decision trees. Decision trees are tree-like structures that provide decision support. There are three components to a decision tree: decision nodes, leaf nodes, and the root node. Training datasets are divided into branches that are further divided into sub-branches by a decision tree algorithm. A leaf node is reached at the end of this sequence, which cannot be divided anymore. In a decision tree, nodes show the attributes that can be used to predict outputs, and decision nodes provide the linkage with leaves.

The following steps represent the steps of the Random Forest classifier:

- a) Random forest takes n random records from a data set with k records
- b) A decision tree is constructed for each sample
- c) Decision trees produce output
- d) The final output is decided based on the majority number of votes based on several decision trees.

Random Forest is used for our classification purpose, Figure i shows a schematic diagram of the RF structure for a classification purpose for a given dataset (Random Forest Models, 2022).

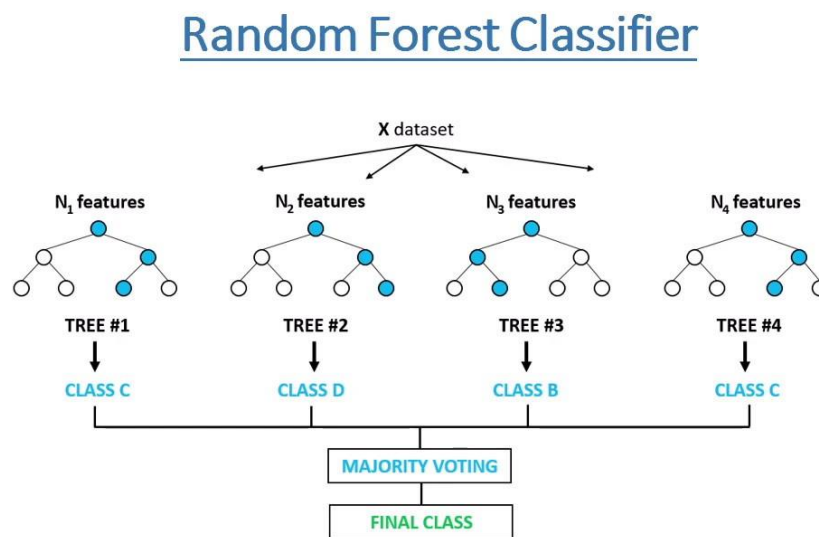


Figure i. Random Forest Structure

In the following chapters, after the introduction of sensor characteristics, acquired data, and study area, the first Structure from Motion procedure will be illustrated considering all steps and results of Orthophotos of different spectral bands, and Digital Elevation Model (DEM) will be presented.

Then in the next part, the Machine Learning classifier, RF will be used in different scenarios in two different time epochs for three different test areas to detect the wet areas in the Riparian region of a river and perform the classification. Hence, in this study, the performance of the RF classifier in classification and wet area detection, based on three different combinations of spectral bands will be assessed, and then, the classifier's improvement after adding some extra features including spectral indices, elevation, and texture features for the second time epoch will be analyzed, and the most effectual features for classification of land cover and detection of wet soil and waterbed will be discovered.

Table 1 shows different spectral indexes. The most useful features are selected using the "Select from Model" function in the scikit-learn package.

Table 1. Vegetation indexes and corresponding references

Index	Abbreviation	Formula	Author and Year
Normalized Difference Vegetation Index	NDVI	$\frac{NIR - RED}{NIR + RED}$	(Abderrazak et al., 1996)
Normalized Difference Water Index	NDWI	$\frac{Green - NIR}{Green + NIR}$	(Ceccato et al., 2002)
Normalized Difference Red-Edge	NDRE	$\frac{NIR - RE}{NIR + RE}$	(Clarke et al., 2001)
Anthocyanin Reflectance Index	ARI	$\frac{1}{Green} - \frac{1}{RE}$	(Miura et al., 2008)
Enhanced Vegetation Index 2	EVI2	$2.4 * \frac{NIR - RED}{NIR + RED + 1}$	(Miura et al., 2008)
Soil Adjusted Vegetation Index	SAVI	$\frac{NIR - RED}{(NIR + RED + L)} * (1 + L)$	(Ahamed et al., 2011)
Structure Insensitive Pigment Index	SIPI	$SIPI = \frac{NIR - Blue}{NIR - Red}$	(Xue & Su, 2017)

NDVI: the most basic way to assess if vegetation is healthy or not. Negative values of NDVI show there is probably water instead of vegetation. Low values of NDVI show the presence of less or no vegetation, a high value shows the presence of dense vegetation.

NDWI: the most basic index to evaluate the water/moisture content of vegetation.

NDRE: another index for measuring the health of vegetation based on multispectral data, in other words, it measures the amount of chlorophyll in the plants.

ARI: Weakening vegetation contains higher concentrations of anthocyanins, so this index is one measure of stressed vegetation. Increases in ARI1 indicate canopy changes in foliage via new growth or death. It uses reflectance measurements in the visible spectrum to take advantage of the absorption signatures of stress-related pigments.

EVI2: it has improved sensitivity in high biomass regions and a reduction in atmosphere influences.

SAVI: it attempts to minimize soil brightness influences using a soil-brightness correction factor.

SIPI: it maximizes sensitivity to the bulk carotenoids to chlorophyll ratio while minimizing the impact of the variable canopy structure. Larger SIPI values represent more stress.

Most of the processings in this project are performed by two tools:

- a) **QGIS software:** QGIS stands for Quantum Geographic Information Systems. This publicly available and free software is mainly used for mapping and related geospatial tasks. As a license is not needed, any type of user can make use of QGIS. There is no limitation on the tools that can be utilized, and numerous plug-ins can be easily installed to execute different complex processes. This geospatial software has very good data processing times compared to other technologies of the same kind such as some of the ESRI Desktop tools. QGIS was mainly used for vector data preprocessing steps such as digitization and for raster visualization of RF predictions (QGIS, 2022).
- b) **Python Programming language:** a very popular computer programming language that is being used in different disciplines. It has an object-oriented approach that facilitates coding in a logical and clear way. It can be applied in a wide range of small- and large-scale projects,

allowing to conduct data analysis, software development, and complex data visualization. Python is an open-source and freely available service that supports a wide variety of modules and libraries that assist users in different fields. Libraries and geopackages are user-friendly and easy to import and execute. The machine learning model and random forest classifier that was used for class prediction were based on python language (Python Programming Language, 2022).

As for limitations of this project is consideration of only three classes of water, vegetation, and ground, but since our purpose is focused on the methodology development itself and best features detection, we have continued with these three classes, and then, in future work, the selected features can be used to perform the classification for a larger number of classes, for example, different types of vegetation, grass, large trees, bushes, etc.

Another limitation of this study is focusing on only five multispectral bands. In a more developed work, hyperspectral data with more spectral features can be considered (Maimaitijiang, et al., 2020).

Therefore, what is examined in this thesis is to answer the following questions:

- ✓ Whether UAV data can perform the classification of the riparian area and detect wet areas?
- ✓ Whether visible bands of the UAV data are able to perform classification of the riparian area and detect wet areas?
- ✓ Whether adding other multispectral bands to visible bands improves the classification?
- ✓ Whether adding other features of elevation/ vegetation indices/ texture improves the classification?
- ✓ Which features play the most decisive role in the classification?

The overall overview of investigations carried out in this thesis is presented in Figure j:

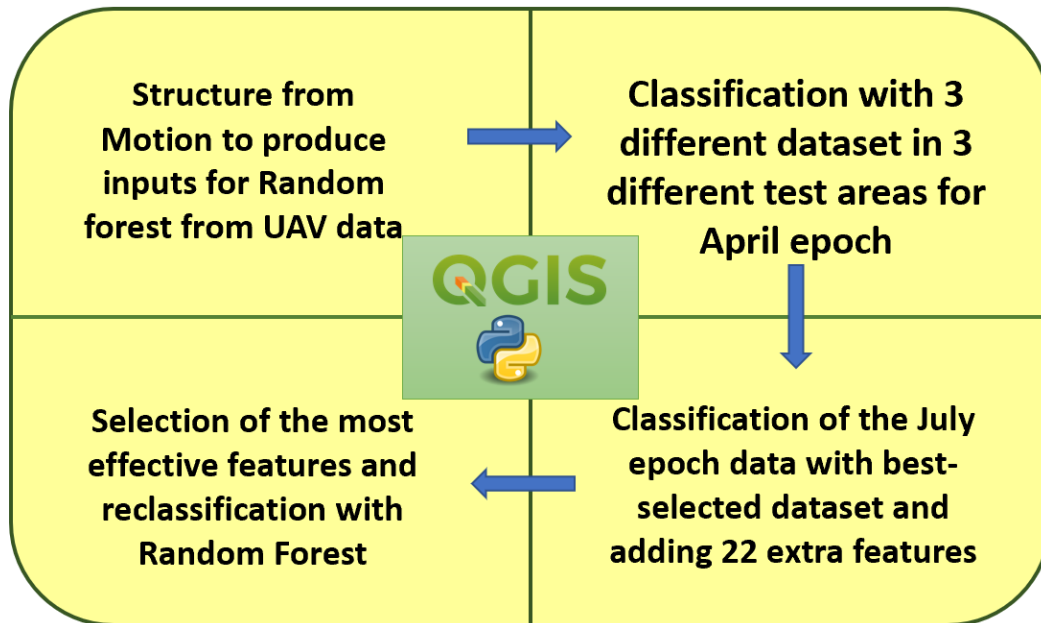


Figure j. General procedure and steps

Chapter 2

2- State of the Art

For data acquisition, UAVs outperform traditional approaches. The high temporal and spatial resolution of the UAV systems is impressive (Merlino et al., 2020; Banerjee et al., 2020). Considering their low cost, it is possible to have several flights in different epochs (Jiménez-Jiménez et al., 2021) and investigate the area for different purposes for example their evolution. After data acquisition to have a 3D map of the area, the Structure from Motion (SfM) approach will be implemented, which can be considered as a combination of computer vision and image analysis (Iglhaut, et al., 2019). In traditional softcopy photogrammetric methods, the 3-D location and pose of the camera (s), or the 3-D location of ground control points, must be known in order to facilitate the triangulation and reconstruction of a scene, on the other hand, a highly redundant bundle adjustment based on matching features in multiple overlapping, offset images is used by the SfM method to solve camera pose and scene geometry simultaneously and automatically (Westoby, et al., 2012).

Classification of a riparian area of the river has high importance for decision-makers. Land-use planning for water-quality security can benefit from an understanding of the connections between land use, landscape patterns, and riverine water quality (Zhang, et al., 2022). In (Zhang, et al., 2022) 67 water samples were collected and analyzed in northwest China's Jing River Watershed (JRW) from 2016-2017. The Canadian Water Quality Index (CWQI) was calculated using remote

sensing images from Sentinel-2. In a riparian buffer zone, Random Forest classification was used to describe current LULC patterns and compute landscape metrics. By collecting geospatial data continuously over large areas, remote sensing technology makes it possible to understand riparian shape, function, and change over time (Rusnák, et al., 2022). A review of studies published from 1991 to 2021 that used remote sensing techniques to map and understand riparian habitats and their ecological functions is provided in (Rusnák, et al., 2022). The 257 articles reviewed fell into six major categories (physical channel properties; morphology and vegetation or field surveys; canopy detection; use of vegetation and water indices; riparian vegetation; and fauna habitat assessment). In most studies, aerial RGB imagery was used for river reaches up to 100 km in length, and Landsat satellite imagery for river reaches of 100 to 1000 km in length. Based on (Rusnák, et al., 2022), over the past decade, unmanned aerial vehicles (UAVs) have been widely used for low-cost monitoring and mapping of riverine and riparian environments. A major challenge remains the transfer of RS data to managers and stakeholders for systematic monitoring in order to ensure the successful management of riparian zones.

As a result of climate change, flash floods are expected to intensify and become more frequent in the Mediterranean region. This will also have an impact on the adjacent riparian vegetation (Koutalakis, et al., 2020). In this study, UAV images were used to capture and record flood debris events and fluvial-geomorphological changes along the Kallifytos torrent in northern Greece. By using UAV images validated using field data and a visual protocol, a novel approach was developed for detecting changes in riparian vegetation and assessing conditions. Following major floods, the orthomosaics clearly showed changes in the torrent bed and debris flow events. UAV images are highly useful for capturing, recording, and monitoring fluvio-geomorphological events and riparian vegetation (Koutalakis, et al., 2020).

There are several methods for the classification of multispectral UAV data such as support vector machine (SVM), neural networks, maximum likelihood, and Random Forest (RF). Random Forest Classifier is based on several decision trees, in which for classification purposes, each tree decides a class, and at the end, the class with a maximum number of votes is selected as a class for the input (Maimaitijiang, et al., 2020), hence the analysis is based on the decision of several trees, and it results in a highly accurate and precise classification (Rodriguez-Galiano et al., 2012). Neural

networks on the other hand produce more accurate and satisfying results in the presence of a large number of images for their training purpose (Lowe & Kulkarni, 2015; Osco, et al., 2021)

Classification based on the UAV data can be performed for different contexts. For instance, Using UAV imagery, (Gevaert, et al., 2017) gets high classification accuracy in challenging classification problems for the analysis of informal settlements based on integrating 2D radiometric and textural features, 2.5D topographic features, and 3D geometric features. The aim is to identify salient features for specific objects in heterogeneous urban environments by comparing UAV datasets from informal settlements in two different countries.

Classification based on machine learning algorithms can be either feature-based or object-based. An example of an object-based approach is presented in (Franklin & Ahmed, 2018), As a result of segmenting images, the resulting objects were visually confirmed to correspond to the sampled tree crowns. An independent validation sample of 23 tree crowns produced results of approximately 78% accuracy based on machine-learning classification using the Random Forest algorithm and finally, the most distinct species were birch and aspen; maples were confused with each other and with immature trees and shrubs under the understory.

Scientific studies also utilize RF for a variety of topics, for instance, (Zhang, et al., 2022) uses two machine learning methods of Multilayer Perceptron (MLP) and Random Forest (RF) for the prediction of coal self-ignition tendency (Zhang, et al., 2022), and (Nasir, et al., 2022) uses Machine learning algorithm for Water quality classification (Nasir, et al., 2022). (Al-Awar, et al, 2022) utilizes four machine learning algorithms of support vector machine (SVM), random forest (RF), regression tree (CART), and backpropagation network (BPN) to select the most robust one for classification of the crop maps (Al-Awar, et al, 2022).

Focusing on agricultural purposes, in (Shen, et al., 2022) study, UAV multispectral and UAV data are used to perform a crop yield prediction estimation based on a long short-term memory neural network and random forest (LSTM-RF) tool, and finally LSTM-RF model obtained better prediction results compared to the LSTM.

With the same token, (Alabi, et al., 2022) did soybean yield estimation. Based on the multispectral images of UAV from five variety trials during the 2020 growing season in Nigeria. UAV-based spectral bands, canopy height, vegetation indices, and texture features have been utilized to estimate crop grain yield using five machine learning (ML) regression models, including Cubist, Extreme Gradient Boosting (XGBoost), Stochastic Gradient Boosting (GBM), Support vector machine (SVM), and Random Forest (RF).

In a similar study, (Impollonia, et al., 2022) considers multispectral images of UAV in Italy and the UK in 2021 and 2022 to analyze the possibility of high-throughput phenotyping (HTP) of novel *Miscanthus* hybrids to estimate the yield prediction, to do this, they use Random Forest using VIs time series and predicted yield using peak descriptor derived from VIs time series.

In order to perform change detection on macro landforms, (Tavakol, et al., 2022) performs a classification. The methodology performed is based on two approaches, first, a supervised classification based on Random Forest, the three major classes of soil microforms, vegetation, and galls were identified and classified into five classes, then a deep learning neural network is used to classify area into 5 classes (Tavakol, et al., 2022).

(Nikolakopoulos, et al., 2022) propose a method to acquire UAV data over landslide areas with various characteristics. In this study, ortophotos and digital surface model is produced based on the SfM method, as is ours in this research.

An analysis of multispectral UAV images to classify burn severity is presented in (Shin, et al., 2019) study. In the analysis of burn area severity, determining the burned surface area is challenging since it appears unburned in aircraft or satellite images. They processed a mosaic reflectance image from a RedEdge multispectral UAV image after a forest fire. As training and validation samples, hundreds of samples were collected for each burn severity class. In order to classify the data, maximum likelihood methodology (MLH), spectral angle mapper (SAM), and thresholding of the normalized difference vegetation index (NDVI) were employed. Even though unburned pine and unburned deciduous trees exhibited some confusion, the classifiers also showed high accuracy for identifying burned surfaces.

The study performed by (Feng, Liu, & Gong, 2015) includes analyzing how classification accuracy changes with texture window size in urban vegetated areas using a hybrid method using Random Forest and texture analysis. To add ancillary data to RGB images, six less-correlated second-order texture measures were calculated at nine different window sizes. The spectral-textural feature space was classified using a Random Forest classifier consisting of 200 decision trees. According to the results, Random Forest outperformed traditional Maximum Likelihood classifiers and matched object-based image analysis in urban vegetation classification, and incorporating texture features improved classification accuracy significantly (Feng, Liu, & Gong, 2015).

A ranking-based approach is proposed by (Ramos, et al., 2020) to further potentialize the RF method for predicting maize yields. In this approach, the correlation coefficient between individual vegetation indices (VIs) is used as a method of estimation. VIs were ranked using RF against a baseline method to measure the improvement in Pearson's correlation coefficient. As a result, the RF model only included the most relevant VIs. Using multispectral imagery from UAVs (unmanned aerial vehicles), 33 VIs were extracted. The ranking-based analysis found that NDVI, NDRE, and GNDVI combined were the top three factors in predicting maize yields. Moreover, their approach outperformed previous machine learning methods, such as support vector machines and artificial neural networks (Ramos, et al., 2020).

(Zeybek, 2021) talks about the importance of classification in a general context. A two-dimensional cadastral map or a topographic map can be produced using three-dimensional (3D) point clouds in the form of UAV-based images. It is necessary to classify point clouds since they are subjected to various analyses for the purpose of extracting further information from direct point clouds. The high density of point clouds makes it challenging and time-consuming to process data and gather information. As a result, the classification process enables the acquisition of valuable information in an optimal manner. Random forest machine learning algorithms are applied to radiometric features (Red band, Green band, Blue band) as well as geometric features (curvature, omnivariance, flatness, linearity, surface variance, anisotropy, normalized terrain surface). Additionally, the proposed methodology is tested against UAV-based point clouds to obtain accuracy and performance using the random forest method (Zeybek, 2021).

In (Zan, et al., 2020), a method for automatic detection of maize tassels by random forest (RF) and VGG16 was developed based on time series RGB images from unmanned aerial vehicles (UAVs) with maize at the flowering stage. To determine potential tassel regions, the RF first segmented UAV images into tassel and non-tassel regions; then, morphological methods were employed and they randomly selected 50 plots from UAV images to demonstrate the performance of the proposed method (Zan, et al., 2020).

Some studies perform a similar methodology with a different kind of input dataset. In (Ayala-Izurieta, et al., 2017), a spectral vegetation index (SVI) and ancillary geographic data were used to map vegetation based on random forest and to analyze variables that help differentiate vegetation cover, and (3) to evaluate the reliability of the vegetation cover classification in hard-to-reach Ecuadorian mountain regions. Satellite images from Landsat 7 ETM+, a Random Field Coefficient algorithm, and stratified sampling were used. As with the traditional and often used normalized difference vegetation index (NDVI) in other settings, the altitude, and the two-band enhanced vegetation index (EVI2) give more information on vegetation cover than the traditional and usually used two-band enhanced vegetation index (EVI2) (Ayala-Izurieta, et al., 2017).

With the help of UAV imagery, (Marin, et al., 2021) propose a method of detecting Coffee leaf rust (CLR) severity. Farmers can improve disease management procedures and reduce losses associated with CLR by identifying the symptoms, severity, and spatial distributions of the disease. So for this purpose vegetation indices alongside machine learning algorithms have been used (Marin, et al., 2021).

The most essential objective of my study is to investigate the performance of datasets (number of considered features) in the classification and if adding other features, including elevation (Normalized Digital Surface Model (nDSM)), spectral (thermal data and vegetation indexes), and texture features can be of benefits for classification. There are several studies to investigate the classification capability based on an RF classifier (Jiang, et al., 2021; Rodriguez-Galiano, et al., 2012), but focusing on the goal of wet area detection considering different combinations of very high-resolution multispectral bands (centimeter-level data) and adding other features, including

elevation, spectral (thermal data and vegetation indexes), and texture in two different epochs highlights the innovation of this research.

Data were acquired using a commercial solution drone DJI Phantom 4. The drone contains an RGB sensor and separate blue, green, red, RE, and NIR sensors. During the data collection, some GCPs have been surveyed to assess the accuracy of the georeferencing of the embedded GNSS dual-frequency sensor.

The study area was mapped using the DJI Phantom 4 drone. Besides the RGB camera, the sensor contains blue, green, red, red-edge, and near-infrared multispectral cameras. Among the sensor's unique features are its integrated sunlight sensor. Positioned on the body's upper part, the sensor detects the sun's irradiation, optimizing the quality of the collected data. In addition, RTK positioning accuracy without internet connection is enhanced by connecting P4 Multispectral to D-RTK 2 high precision GNSS mobile station, or NTRIP protocol (for RTCM data transfer over the internet) via a 4G dongle or WiFi hotspot. By using DJI's TimeSync system, it is possible to capture accurate, real-time positioning data by capturing images from six cameras.

The TimeSync system continuously updates the attitude of the flight controller, the RGB and NB cameras, and the RTK module, keeping the positioning data accurate at the center of the CMOS sensor and providing accurate metadata for each image. Calibration of all cameras includes measuring radial and tangential lens distortions.

To adapt the post-production software to the needs of each user, distortion parameters are acquired and saved in the metadata. According to DJI, this new platform comes with the same powerful features as its Phantom 4 series drones, such as a flight time of 27 minutes and a transmission distance of seven kilometers. Figure 1 shows the sensors and multispectral bands utilized for data acquisition including the DJI phantom4 drone for multispectral data acquisition in both April and July epochs and Thermal XT2 camera in the July epoch. Table 2 shows the technical characteristics of phantom4 drone.



Figure 1. Up left: DJI phantom4 camera, up right: 6 spectral bands of phantom4 drone, bottom: Thermal camera XT2

Table 2. Technical characteristics of the DJI phantom4 sensor

Sensors	Six 1 / 2.9 ° CMOS sensors, including an RGB sensor for visible light images and five monochrome sensors for multispectral image acquisition. Each Sensor: 2.08MP Effective Pixels (2.12MP Total)
Filters:	Blue (B): 450nm ± 16nm, Green (G): 560nm ± 16nm, Red (R): 650nm ± 16nm, Red-Edge (RE): 730nm ± 16nm, near infrared (NIR): 840 nm ± 26 nm
Aims	FOV (field of view): 62.7 ° Focal length: 5.74mm (35mm equivalent format: 40mm), ∞ autofocus Aperture: f / 2.2
RGB sensor ISO range	200 - 800
Gain of the monochrome sensor	1 - 8x
Global electronic shutter	1/100 - 1/20000 s (visible light); 1/100 - 1/10000 s (multispectral)
Maximum image size	1600 × 1300 (4: 3.25)
Photo format	JPEG (visible light images) + TIFF (multispectral images)
Supported file systems	FAT32 (≤ 32GB); exFAT (> 32 GB)
Supported SD cards	microSD with a minimum write speed of 15 MB / s. Capacity: 128GB. Class 10 or UHS-1 standard
Operating temperature	0 - 40 ° C

Chapter 3

3- Methodology

3-1- Theoretical Background

3-1-1- Structure from Motion

The two most important methodologies used in this study are Structure from Motion (SfM) and Classification based on the Random Forest classifier. SfM technique works on the fact that several images are acquired from different angles from the object or in our case the area and overlapped photogrammetry produces 3D structures (Iglhaut, et al., 2019). After data acquisition in order to have a 3D mapping of the area besides producing a Digital Elevation model and orthomosaic of the area, an approach is implemented in the Metashape software, which can be considered as a combination of computer vision and image analysis. SfM technique works on the fact that several images are acquired from different angles (both nadiral and oblique) from the object or in our case the area and overlapped photogrammetry produce 3D structures. The concept behind this technique is called SIFT or Scale-Invariant Feature Transform (Francisco Agüera-Vega, 2018). Data acquired by high-resolution UAV systems follow a chaotic behavior meaning that there is high rotational and angular variation during acquisition time and high distortions. So, the post-processing technique for producing 3D models and DEM should be strong for this purpose. that is

the reason for using the introduced SIFT method for UAV imagery data processing since it has a steady behavior in presence of translation and rotation of the UAV images. On-board GNSS receivers of the UAVs allow for location data acquisition in the collection phase and in order to increase the positioning accuracy Ground Control Points can be manually collected during the campaign, in this way the result is a high accuracy DEM and Orthomosaic (Darren Turner *, 2012). The flowchart in Figure 2 represents the main steps included in the SfM (Iglhaut et al., 2019).

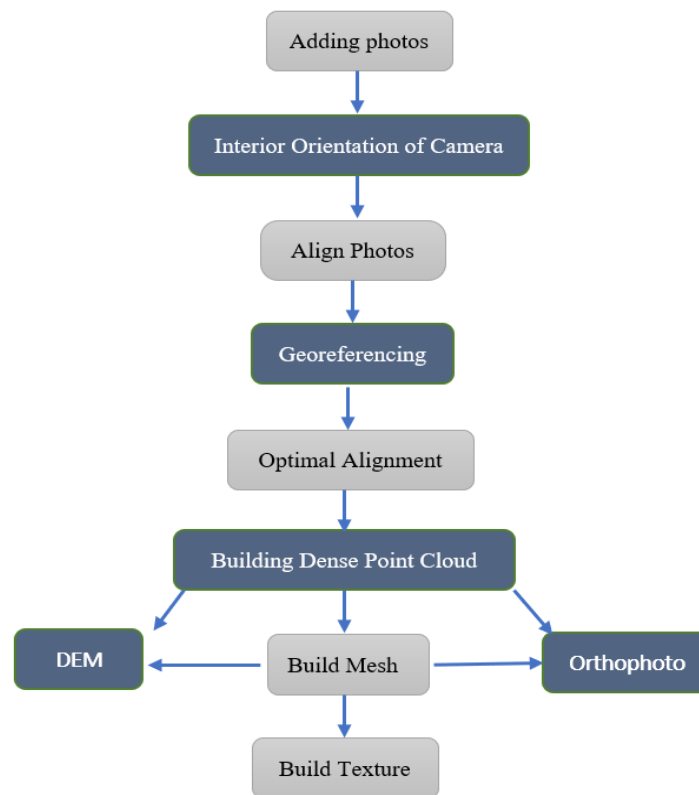


Figure 2. Structure from Motion procedure

3-1-2- Machine Learning Classification

So-called Intelligent Systems are frequently employed for the task of supervised classification. Artificial Intelligence has been used to develop a large number of techniques (Logic-based techniques, Perceptron-based techniques) as well as Statistics (Bayesian Networks, Instance-based techniques). Using predictor features, supervised learning builds a concise model of the distribution of class labels. As a result of the classifier, class labels are assigned to instances that

have known predictor features but unknown class labels (Kotsiantis, Zaharakis, & Pintelas, 2006). Remotely sensed imagery can be effectively and efficiently classified using machine learning. Handling data with high dimensionality and complex characteristics are two of the strengths of machine learning (Maxwell, Warner, & Fang, 2018).

Random Forest Classifier as can be understood from its name is based on several decision trees in which for classification purposes, each tree decides a class and at the end, the class with the maximum number of votes is selected as a class for the input, hence the analysis is based on the decision of several trees, and it results in a highly accurate and precise classification (Barrett Lowe, 2015). Each tree in the random forest spits out a class prediction and the class with the most votes becomes our model's prediction. The fundamental concept behind random forest is a simple but powerful one, the wisdom of crowds: A large number of relatively uncorrelated models (trees) operating as a committee will outperform any of the individual constituent models. In other words, A random forest is a meta estimator that fits a number of decision tree classifiers on various sub-samples of the dataset and uses averaging to improve the predictive accuracy and control overfitting in this project (Ronald Kemker C. S., 2018).

In the April epoch, orthophotos of 5 multispectral bands have been used as input features for the RF classifier. Furthermore in the summer epoch, besides 5 considered spectral channels, Elevation data of Normalized Digital Surface Model, Spectral data including Thermal data and Vegetation Indexes including NDVI, NDWI, NDRE, ARI, EVI2, SAVI, SIPI, and Texture features including Angular Second Moment, Contrast, Correlation, Variance, Inverse Difference Moment, Sum Average, Sum Variance, Sum Entropy, Entropy, Difference Variance, Difference Entropy, Information Measures of Correlation, Maximal Correlation Coefficient as described in (ROBERT M. HARALICK, 1973) have been added with the purpose of improving the classification result. Considering all features and bands into account generally 27 attributes for each pixel are available in the dataset.

In the summer epoch, the best-selected dataset from the previous epoch beside extra features including nDSM, thermal and vegetation indexes, and texture features, are added to improve the classification (Haralick et al., 1973) and to find out about the most effective features in the

classification of the area using RF. Considering all features and bands, 27 attributes for each pixel are available in this dataset.

3-1-3- Performance Assessment

Validation- Evaluation of classification goodness- Python: in this level, the prepared validation data will be as input for the python program and classification goodness will be examined through evaluation tools. For this purpose, first, some concepts for accuracy assessment should be explained.

Performance Assessment: Before introducing performance analyzers, four basic concepts of machine learning techniques for classification should be established. True Positive, True Negative, False Positive, False Negative.

True Positive (TP): positive outcomes that the model predicted correctly.

True Negative (TN): negative outcomes that the model predicted correctly.

False Positive (FP): positive outcomes that the model predicted incorrectly. This is also known as Type I error.

False Negative (FN): negative outcomes that the model predicted incorrectly. This is also known as Type II error.

Classification Accuracy: Classification accuracy or simply accuracy is the ratio of the number of correct predictions to the total number of input samples and it usually works well when the number of samples in classes is mostly symmetrical, otherwise when the dataset includes misbalanced classes accuracy may give us the false sense of achieving high accuracy.

$$Accuracy = \frac{TP + TN}{TP + FP + TN + FN}$$

Precision: The number of correct positive results divided by the number of positive results predicted by the classifier.

$$Precision = \frac{TP}{TP + FP}$$

Recall: It is the number of correct positive results divided by the number of all actual samples.

$$Recall = \frac{TP}{TP + FN}$$

F1 Score: The F1 Score is the weighted average or Harmonic Mean between precision and recall. The range for F1 Score is [0, 1] and it represents how precise the classifier is (how many instances it classifies correctly), as well as how robust it is (it does not miss a significant number of instances).

$$F1\ score = 2 * \frac{Precision * Recall}{Precision + Recall} = \frac{2 * TP}{2 * TP + FP + FN}$$

Confusion Matrix: A Confusion matrix is an N x N matrix used for evaluating the performance of a classification model, where N is the number of target classes. The matrix compares the actual target values with those predicted by the machine learning model. This gives us a holistic view of how well our classification model is performing and what kinds of errors it is making. Classification accuracy can hide the detail needed to diagnose the performance of the model. But details can be detected by using a confusion matrix and generally the confusion matrix shows the ways in which the classification model is confused when it makes predictions.

Validation in python: The input file in this stage is the prepared validation data and the idea is that based on the Random Forest Classifier, the predicted label of points will be compared to the known label of the point, and this procedure will get repeated for all points in the validation data and finally an accuracy score based on the probability of correct predictions will be computed. Crucial libraries from Scikitlearn package for this stage includes 'confusion_matrix', 'plot_confusion_matrix', 'precision_recall_fscore_support' and 'precision_recall_curve'.

Nine different scenarios considering three datasets for three test areas in the winter epoch have been analyzed. In the following, the best-selected dataset from the winter epoch with the addition of some other features consisting of Elevation (Normalized Digital Surface Model), Spectral (Thermal data and Vegetation Indexes of Normalized Difference Vegetation Index, Normalized difference water index, Normalized Difference Red-Edge, Anthocyanin Reflectance Index, Enhanced vegetation index, Soil-adjusted vegetation index, Structure Insensitive Pigment Index) and Texture (Angular Second Moment, Contrast, Correlation, Variance, Inverse Difference

Moment, Sum, Average, Sum Variance, Sum Entropy, Entropy, Difference Variance, Difference Entropy, Information Measures of Correlation, Maximal Correlation Coefficient) have been taken into account to analyze the performance of the classifier on the summer epoch of the acquired area.

3-2- Data Acquisition and study areas

UAV Data acquired in this area are provided in two epochs: one during April in winter and the other one during July in summer. For this study, data has been acquired in the Salbertrand town in northwest Italy in two different epochs of April and July. Salbertrand, as is shown in **Error! Reference source not found.** is a municipality in the province of Torino with an elevation of 1039 meters and studied riparian area located in the Salbertrand. Since the data is acquired on the river and the surrounding area, the focus of this study will be on the riparian area and wet area detection in the riverbed and riparian areas.

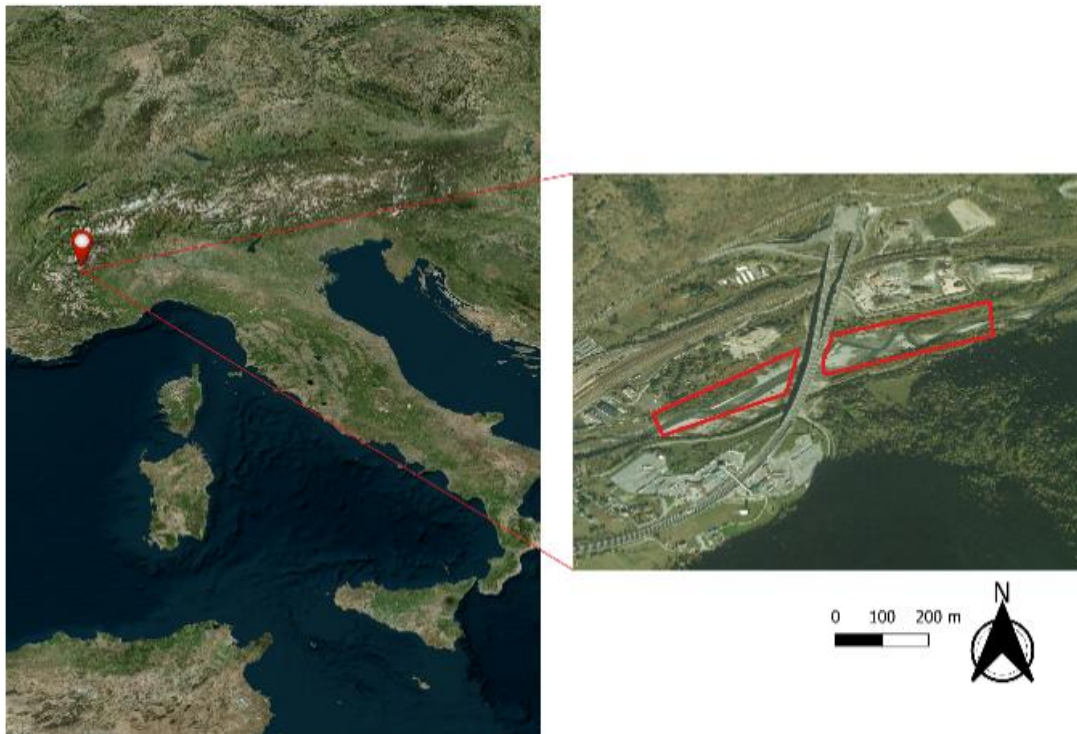


Figure 3. Study area, Salbertrand town, Salbertrand river

3-3- Processing Steps

The main idea of the present study contains the following steps:

- a) produce orthophotos and DEM based on the Structure from Motion approach from raw UAV multispectral data which has been acquired in the Salbertrand area in Piedmont, Italy in two different epochs of April and July.
- b) The concentration of this study is on the riparian area of the river; hence the final goal is to assess the strength of Artificial Intelligence methods in the identification of wet areas besides detection of all other classes and to analyze the performance of Artificial intelligence techniques, specifically talking Machine Learning technique named Random Forest (RF) for classification purpose.
- c) Then a feature selection method will be used in the second method to discover the most effective and decisive features for the classification.

3-3-1-Structure from Motion (SfM)

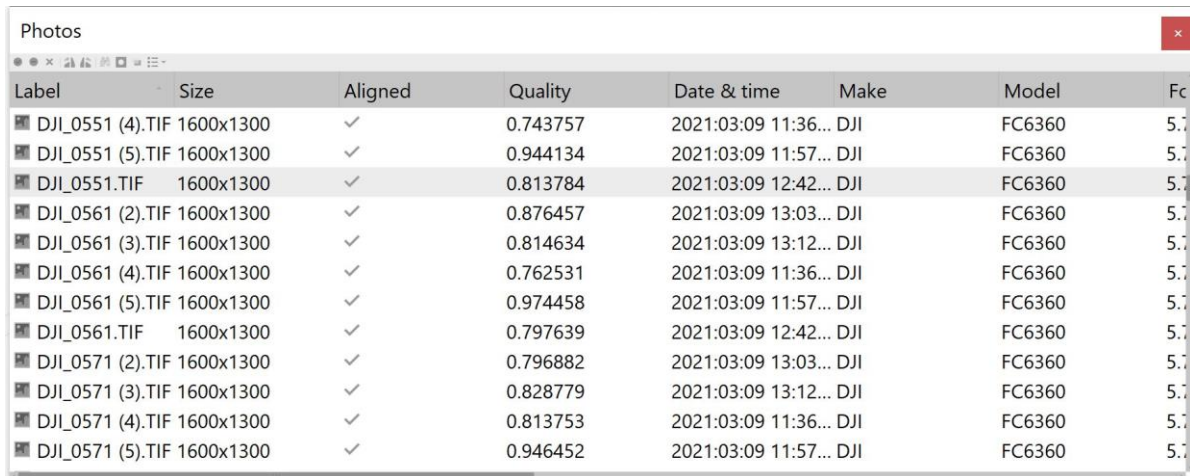
3-3-1-1- Adding photos:

In this step, there are two options to import photos into software. Either by adding a folder in which all photos are included or by selecting all photos and adding them. If the selected folder only includes needed photos, adding a folder is a better option. It is worth mentioning that photos will be imported to the already selected chunk in the project. In the project for the sake of simplicity, each band of the multispectral camera including Red, Green, Blue, Red-Edge, Near Infrared, and RGB are imported in separate chunks. Once the photos have been added to the project, the software will call them camera which implies camera location or camera position.

3-3-1-2- Quality control of photos

In order to be sure that there are not any blurry or defective photos in our dataset quality control of photographs is necessary. For this purpose, the “Estimate Image Quality” option has been performed on photographs. Quality values range between 0 to 1. And on average values below 0.5 should be considered blurry and unqualified to be used in the 3D modeling process. As an

example, image quality values related to the Red band are presented in Figure 4. Quality values of all other bands similar to the red band were quite high.



Label	Size	Aligned	Quality	Date & time	Make	Model	Fc
DJI_0551 (4).TIF	1600x1300	✓	0.743757	2021:03:09 11:36...	DJI	FC6360	5.7
DJI_0551 (5).TIF	1600x1300	✓	0.944134	2021:03:09 11:57...	DJI	FC6360	5.7
DJI_0551.TIF	1600x1300	✓	0.813784	2021:03:09 12:42...	DJI	FC6360	5.7
DJI_0561 (2).TIF	1600x1300	✓	0.876457	2021:03:09 13:03...	DJI	FC6360	5.7
DJI_0561 (3).TIF	1600x1300	✓	0.814634	2021:03:09 13:12...	DJI	FC6360	5.7
DJI_0561 (4).TIF	1600x1300	✓	0.762531	2021:03:09 11:36...	DJI	FC6360	5.7
DJI_0561 (5).TIF	1600x1300	✓	0.974458	2021:03:09 11:57...	DJI	FC6360	5.7
DJI_0561.TIF	1600x1300	✓	0.797639	2021:03:09 12:42...	DJI	FC6360	5.7
DJI_0571 (2).TIF	1600x1300	✓	0.796882	2021:03:09 13:03...	DJI	FC6360	5.7
DJI_0571 (3).TIF	1600x1300	✓	0.828779	2021:03:09 13:12...	DJI	FC6360	5.7
DJI_0571 (4).TIF	1600x1300	✓	0.813753	2021:03:09 11:36...	DJI	FC6360	5.7
DJI_0571 (5).TIF	1600x1300	✓	0.946452	2021:03:09 11:57...	DJI	FC6360	5.7

Figure 4. Quality Control for images- Red band

3-3-1-3- Interior orientation of the camera

In this step, camera calibration parameters should be adjusted internal parameters such as focal length, camera type, and pixel size will be set using imported photos in the software based on the bundle block adjustment method (Figure 5).

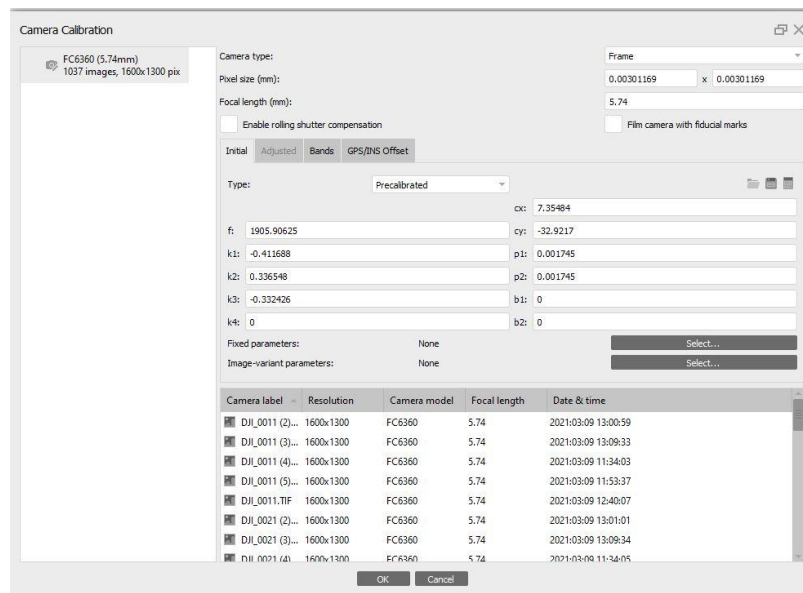


Figure 5. Camera interior calibration

3-3-1-4- Settings

Some settings should be checked in the software before starting the modeling process. For instance, in the “Metashape Preferences tool” two options of “load camera location accuracy from XMP metadata” and “Load GPS/INS offset from XMP metadata” should be activated, in this way, all data recorded in the metadata during acquisition will be added to the project to increase initial accuracy of the project.

3-3-1-5- Align photos

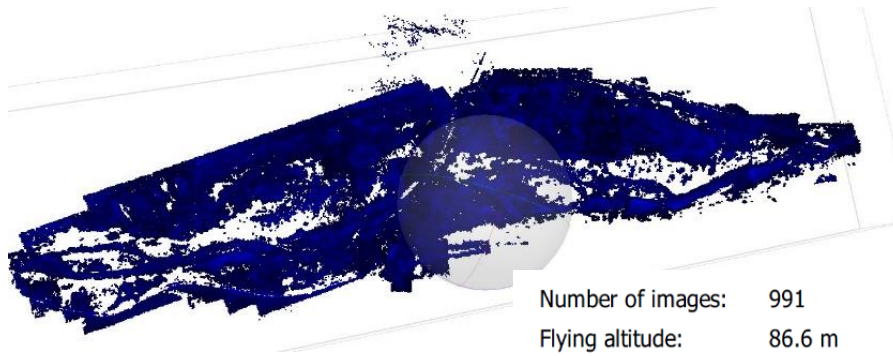
The next step in the workflow is aligning photos. The result of this step is initial camera locations and sparse point cloud or named tie points. Alignment in the Metashape is based on Scale Invariant Feature Transform (SIFT) algorithm. Scale Invariant Feature Transform (SIFT) is an image descriptor for image-based matching developed by (Lowe D. G., 2004). As a descriptor, this can be used for a variety of tasks in computer vision, including point matching between different views of a 3-D scene and view-based object recognition. The SIFT descriptor is invariant to translations, rotations, and scaling transformations in the image domain as well as moderate perspective transformations and illumination variations. Under real-world conditions, the SIFT has proven to be very useful for robust image matching (Darren Turner *, 2012).

It is worth mentioning that the initial alignment of the photos was based on the GNSS positioning of the cameras. Accuracy has been set to the “high” in this step meaning that photos are used in their original size. By decreasing the accuracy level photos will be downscaled by a factor.

Results of this step are provided in the following table for each band separately and they represent tie points of each band and initial camera positions by blue rectangles on them. There is the possibility that not all of the photos of each chunk get aligned successfully because of the low resolution of some photos or low overlap between some images.

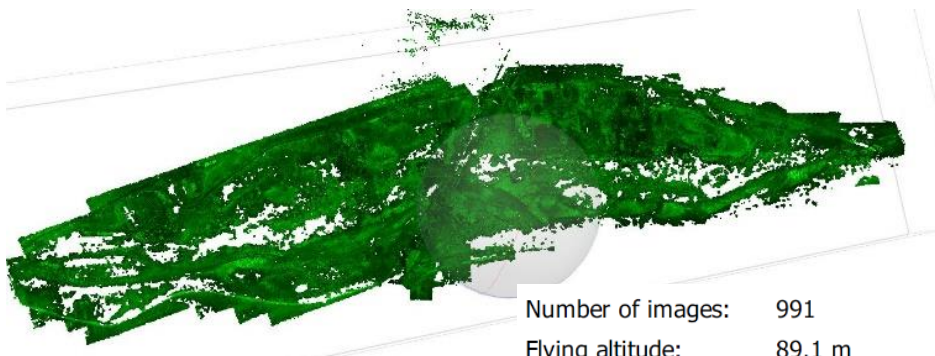
Tie points resulting from aligning process for all chunks (bands) are presented in **Error! Reference source not found., Error! Reference source not found.**

Figure 11 shows the hypothetical position of the cameras during the acquisition phase on the tie points.



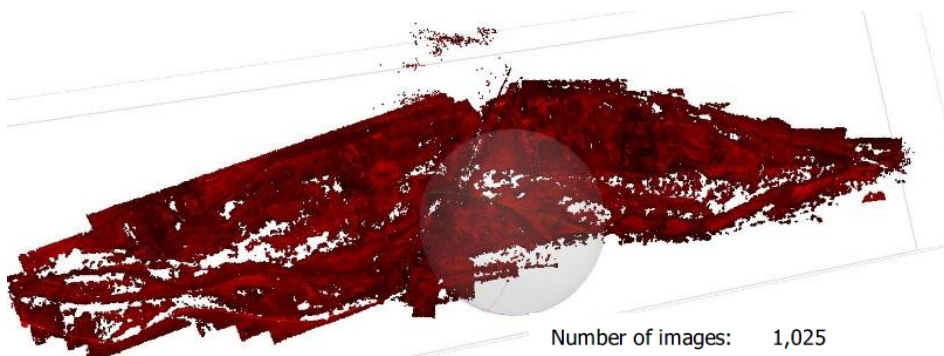
Number of images:	991	Camera stations:	991
Flying altitude:	86.6 m	Tie points:	1,009,952
Ground resolution:	4.1 cm/pix	Projections:	3,546,213
Coverage area:	0.407 km ²	Reprojection error:	0.422 pix

Figure 6. Tie points of blue band and technical characteristics



Number of images:	991	Camera stations:	991
Flying altitude:	89.1 m	Tie points:	1,219,412
Ground resolution:	4.09 cm/pix	Projections:	4,259,433
Coverage area:	0.4 km ²	Reprojection error:	0.41 pix

Figure 7. Tie points of green band and technical characteristics



Number of images:	1,025	Camera stations:	1,025
Flying altitude:	78.2 m	Tie points:	1,372,144
Ground resolution:	4.12 cm/pix	Projections:	4,798,995
Coverage area:	0.411 km ²	Reprojection error:	0.391 pix

Figure 8. Tie points of red band and technical characteristics

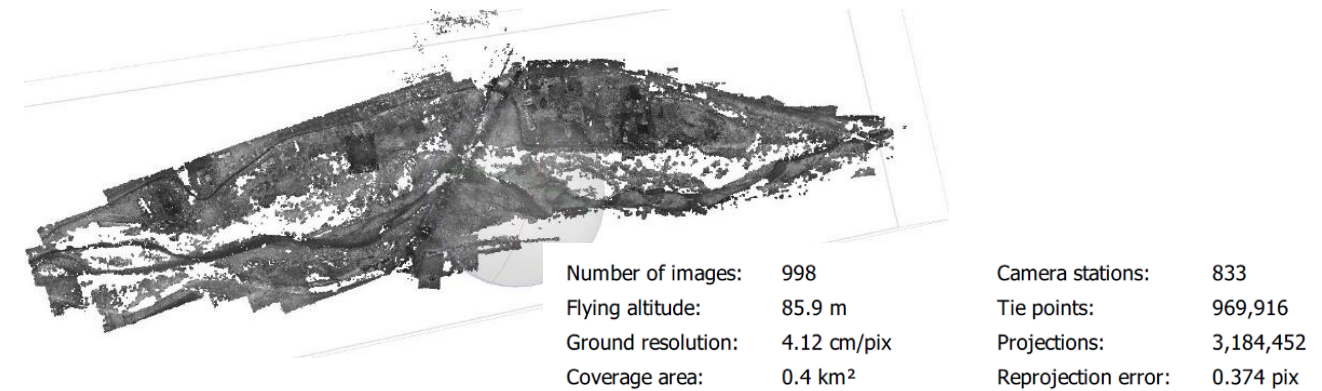


Figure 9. Tie points of Red-Edge band and technical characteristics

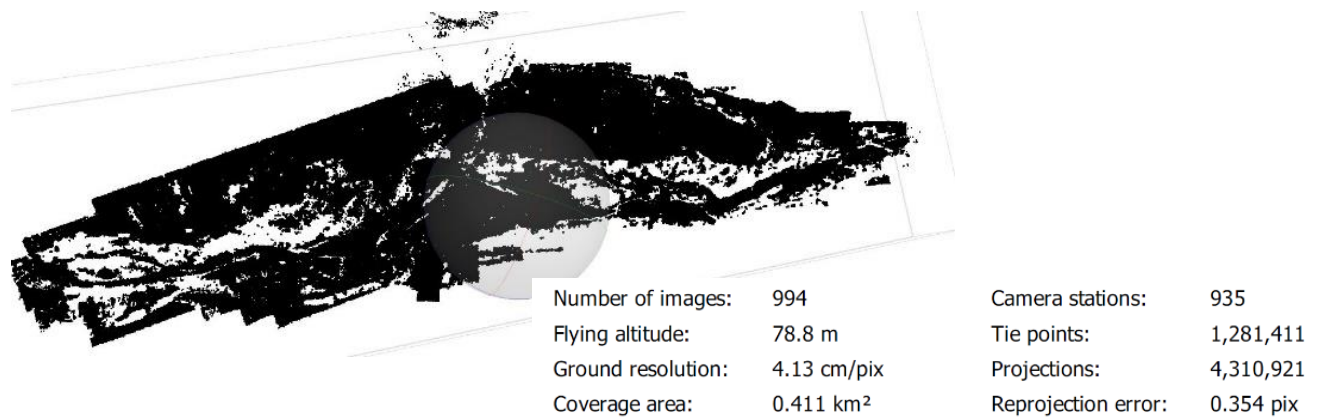


Figure 10. Tie points of NIR band and technical characteristics

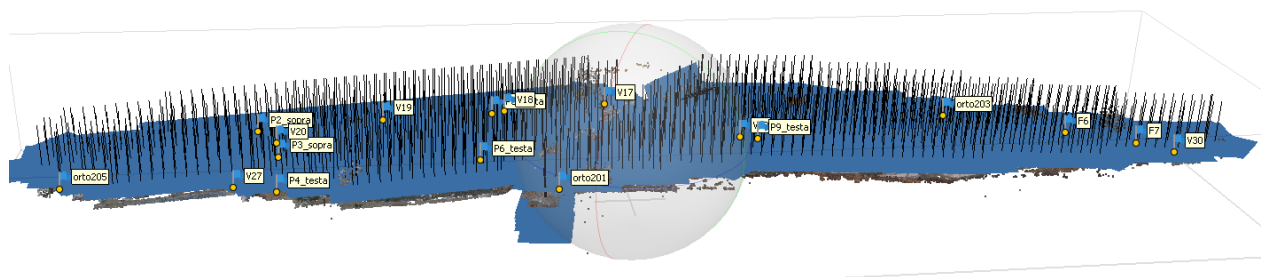


Figure 11. Camera Positions on RGB Tie Points

3-3-1-6- Georeferencing

On-board GNSS receiver of the UAVs allow for location data acquisition in the collection phase and in order to increase the positioning accuracy Ground Control Points can be manually collected

during the campaign, in this way the result is a high accuracy digital terrain model and orthomosaic of the study area based on the SfM procedure (Turner et al., 2012).

During the data collection phase, some Ground Control Points have been surveyed. Adding these points to the project and optimizing alignment based on these GCPs can result in increasing the accuracy of modeling. In order to integrate ground control points into a project, a text file of points including 'Name of the marker', 'Easting', 'Northing' and 'Altitude' of points should be imported into the project. Coordinate system related to points should be set correctly during import process which in our case is projected into Universal Transverse Mercator (UTM), Zone 32 North. The targets used in this project are photogrammetric, meaning that they are selected on the existing stable objects on the ground to provide multi-temporal analysis for the future. For points, only position data are acquired, and orientation data (Yaw, Pitch, Roll) are not provided.

Once the GCPs have been imported into the project, the setting related to the reference system in the project should be checked, at this moment there are three coordinate systems that should be set correctly:

- 1) coordinate system of the project and outputs: since objective is to acquire all results in the metric system so the coordinate system should be projected to UTM,32N.
- 2) Camera reference related to acquired images: which is the reference system during the acquisition time
- 3) Marker reference system related to surveyed Ground Points.

Since all cameras, markers, and also the project is georeferenced in the same reference system, markers will be detected on the tie points as soon as they are imported into the project, but to fix the exact location of markers and avoid some inaccuracies, markers should be placed on images again manually, for this purpose 'Filter photos by marker' is performed, which separates images related to each marker and allows user to place markers in each image in the exact location. After detection of the marker in 2 or 3 images and updating the project, the marker will be modified in the rest of the images and its location became even more accurate. Thus, the marker placing process will become easier and easier. Figure 12 shows the location of GCPs on the tie points of

the area. Generally, 27 markers were surveyed for this case study and as beforementioned ground control points in this case study are photogrammetric meaning they are signs on existing objects or detectable corners of objects. Hence, some markers in some images were not detectable with good accuracy, and in the end number of projected images for some markers was not enough, hence in order to make consistency this kind of marker has been removed from the project.



Figure 12. GCPs on the Tie points- RGB

To provide some examples some of the photogrammetric targets on the RGB, NIR, Red-Edge, and Blue cameras are presented in Figure 13.

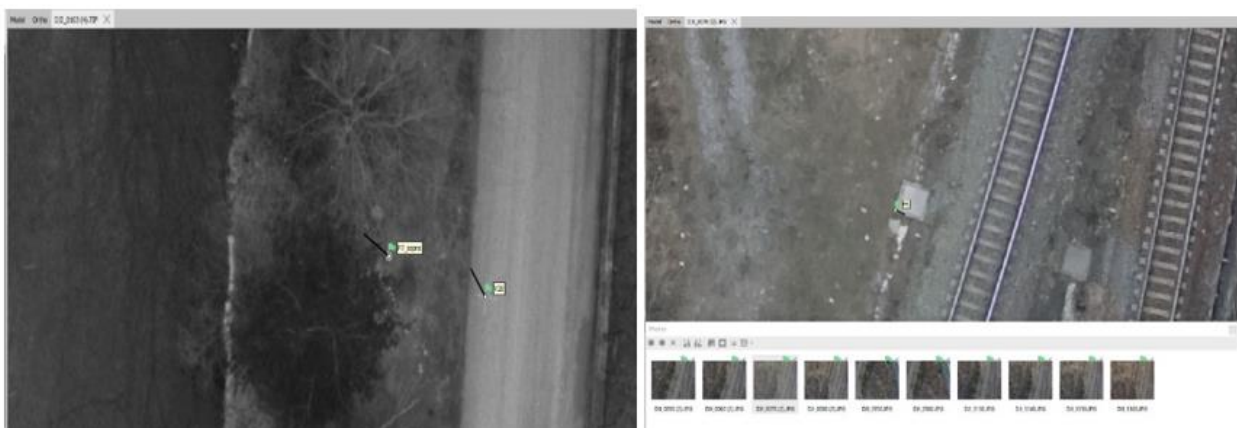


Figure 13. . right: F6 marker on the RGB image, left: two markers on the NIR image

3-3-1-7- Optimal Alignment

After detecting GCP on the images for all chunks the whole project should be updated and georeferenced based on very accurate Ground Control Points. Then optimal alignment function should be performed to improve initial alignment and generate a camera calibration based on GCP which takes GCP into account for the alignment process. Of all GCPs, some of them should be selected as checkpoints to check alignment accuracy. The number of checkpoints should be in a reasonable proportion with respect to the total number of ground control points, in a way that assessment of the accuracy of the model based on checkpoints gives us a reasonable overview. In the following table, the number of checkpoints and control points for each band is presented in Table 3.

Table 3. Number of Check and control points in all bands

Band	Num of Control points	Num of Checkpoints
Red	17	4
Green	17	4
Blue	17	4
Red-Edge	16	4
NIR	15	4
RGB	18	4

3-3-1-8- Building Dense Point Cloud

This step uses generated sparse cloud in the previous step and camera locations and produces a dense cloud in Figure 14. Quality setting in this step determines down sampling factor for photos, for instance, if 'High' quality gets selected down-sampling factor will be 4. This is also the case for our project. 'Depth Filtering' setting is related to the behavior of software with outliers and depth calculation. For our project, the default parameter has been kept.

The ability to produce dense clouds from lower density data (tie points) is one of the great advantages of the UAV drones in comparison to other acquisition platforms for instance LIDAR system. Since with a low price we can achieve high-density point cloud and high accuracy (Tao, Lei, & Mooney, 2011). The produced dense cloud in this step will be used to produce mesh for the area.



Figure 14. Dense Cloud of RGB bands

3-3-1-9- Build Mesh

This step generates a polygonal model based on a dense cloud. One of the important setting parameters required for this step is related to 'Surface Type'. Usually, surface type can be set in 2 ways. 'Arbitrary' type can be used for any kind of object such as oblique or complex. 'Height Field' type is appropriate to model a surface orthogonal to the reference system, hence when the main objective is to produce DEM, this type can be suitable. It is worth mentioning that this step is based on the interpolation of points to generate Mesh (Figure 15). Where a point cloud saves the location for millions of points, a mesh converts those points into triangles (Bassier, Vergauwen, & Poux, 2020).

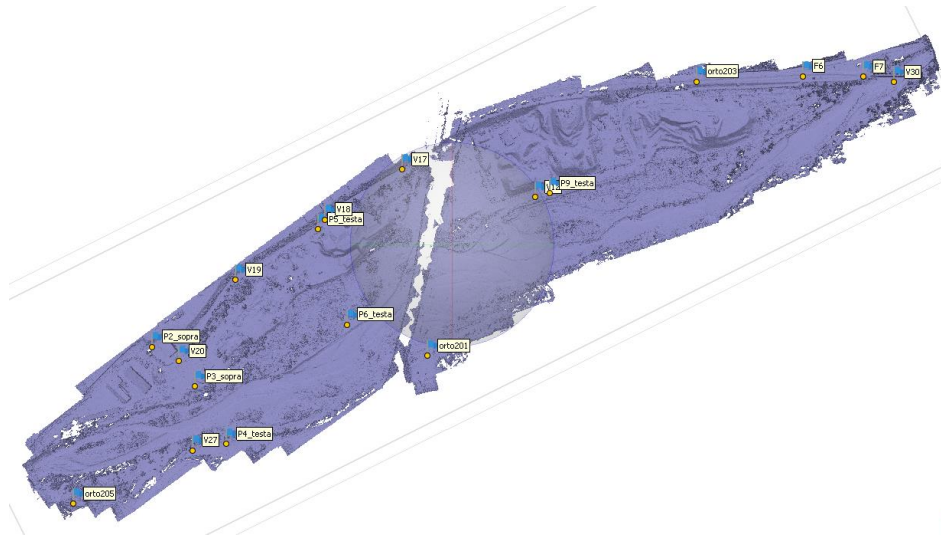


Figure 15. Solid Model of RGB bands

3-3-1-10- Build Texture

To have a representation of color and texture, a color overlay of the point cloud is needed. All parameters have been set to default values. Figure 16 and Figure 17 and Figure 18 show the 3-D model of the area, as it can be seen from different views of the 3-D model, the studied area consists of vegetation, road, ground, riverbed, and some rocks, stocks (very low buildings or storages) and some taller buildings at the very edge of the area. In the next stages, only some portions of the area will be clipped to be used in the Machine Learning processing.



Figure 16. Textured Model of RGB bands



Figure 17. Different views of the 3D model



Figure 18. Different views of the 3D model

3-3-1-11- Building Digital Elevation Model

Since Ground Control Points are provided for the project, generation of DEM product is possible, in this step coordinate system of DEM should be the same as the coordinate system of GCP. Although during the export process of DEM, the coordinate system can be modified. Both dense Cloud and Mesh can be used as source data in this step. Using Dense Cloud, provide more accurate results since it is actual data, while the mesh is based on interpolation. DEM is produced for the

RGB band and it will be used as a source for the next step which is orthomosaic production. The resolution of the DEM is 7.97 cm/pixel and the point density is 150 points/m².

3-3-1-12- Building Orthomosaic

Building orthomosaic was not possible if the texture had not been added to the project. Both DEM and Mesh can be a source for producing orthomosaic.

In our case, the Digital Elevation Model of RGB bands is the reference for producing orthomosaic of all other bands including Red filter, Green filter, Blue filter, Red-Edge, and NIR bands. The reason for doing this is to avoid any difference between bands from a spatial point of view and bring orthophotos of all bands perfectly to each other. In this step, pixel size should be set for orthomosaic. Recommended value based on ground sampling resolution is suitable although increasing this value may result in a lower file size. At the end of this process for each band in the reference pane, a list of Ground control points, checkpoints and their East Error, North Error, Altitude Error, and overall error in meter and pixel units are provided.

Table 5, Table 6, Table 7, Table 8, and Table 9, Table 9 represent accuracy errors for check and control points in three directions for red, green, blue, Red-Edge, and NIR respectively.

Table 4. Accuracy errors of Red Band for control and checkpoints

Markers	East err (m)	North err (m)	Alt. err (m)	Accuracy (m)	Error (m)	Projections	Error (pix)
✓ F6	0.002504	0.000375	-0.000187	0.005000	0.002539	11	0.604
✓ F7	-0.002829	0.000158	0.002953	0.005000	0.004093	9	0.905
✓ P2_sopra	0.000142	0.005503	0.000242	0.005000	0.005510	3	0.800
✓ P3_sopra	0.013748	0.004313	0.001634	0.005000	0.014501	8	0.952
✓ P4_testa	-0.003275	-0.004141	-0.000011	0.005000	0.005280	10	0.738
✓ P5_testa	0.013153	0.014344	0.004144	0.005000	0.019898	12	1.122
✓ P6_testa	-0.000364	-0.009278	0.001055	0.005000	0.009344	11	2.116
✓ P9_testa	0.000023	-0.000580	0.002309	0.005000	0.002381	13	0.635
✓ V12				0.005000		0	0.000
✓ V17	-0.001453	-0.001808	-0.000272	0.005000	0.002335	8	0.305
✓ V18	-0.014621	-0.005289	-0.002531	0.005000	0.015753	12	0.855
✓ V19	-0.005009	0.012841	-0.056592	0.005000	0.058247	8	0.237
✓ V20	-0.005886	0.000700	0.000088	0.005000	0.005928	8	0.487
✓ V30	0.004650	-0.001447	-0.069466	0.005000	0.069637	11	1.051
✓ orto201	-0.000370	-0.000498	0.000466	0.005000	0.000776	6	0.504
✓ orto203	-0.000126	-0.001121	0.020672	0.005000	0.020703	8	0.510
✓ orto205	-0.000541	-0.000733	0.009114	0.005000	0.009159	5	0.468
Total Error							
Control points	0.007291	0.005703	0.001867		0.009443		0.989
Check points	0.003428	0.006496	0.046202		0.046783		0.702

Table 5. Accuracy errors of green Band for control and checkpoints

Markers	East err (m)	North err (m)	Alt. err (m)	Accuracy (m)	Error (m)	Projections	Error (pix)
✓ F6	0.000959	0.000731	-0.000447	0.005000	0.001286	11	0.978
✓ F7	-0.002046	0.001703	0.002891	0.005000	0.003930	9	1.447
✓ P2_sopra	-0.000744	0.002201	-0.000043	0.005000	0.002324	5	0.834
✓ P3_sopra	0.013557	0.005645	0.003062	0.005000	0.015001	11	0.851
✓ P4_testa	-0.002755	-0.003024	-0.000185	0.005000	0.004095	10	0.705
✓ P5_testa	-0.001880	0.011623	0.003203	0.005000	0.012202	11	0.795
✓ P6_testa	-0.001868	-0.008978	0.001189	0.005000	0.009247	8	2.206
✓ P9_testa	-0.001027	-0.001924	0.002598	0.005000	0.003392	13	0.521
✓ V12				0.005000		0	0.000
✓ V17	-0.002947	0.000011	-0.000295	0.005000	0.002962	8	1.140
✓ V18	0.000367	-0.001916	-0.001729	0.005000	0.002607	13	0.358
✓ V19	0.002348	0.002818	-0.000358	0.005000	0.003685	9	0.251
✓ V20	-0.016806	-0.015828	-0.035874	0.005000	0.042660	8	0.164
✓ V30	0.002499	-0.011696	-0.099361	0.005000	0.100078	8	0.456
✓ orto201	0.000066	-0.005700	0.026184	0.005000	0.026797	6	0.256
✓ orto203	0.000791	0.000776	0.000773	0.005000	0.001351	9	0.462
✓ orto205	-0.002365	-0.002636	0.000709	0.005000	0.003612	5	0.065
Total Error							
Control points	0.004283	0.004838	0.001830		0.006716		0.969
Check points	0.008577	0.010329	0.054419		0.056051		0.291

Table 6. Accuracy errors of the blue band for control and checkpoints

Markers	East err (m)	North err (m)	Alt. err (m)	Accuracy (m)	Error (m)	Projections	Error (pix)
✓ F6	0.000904	-0.000202	0.000238	0.005000	0.000957	10	0.644
✓ F7	0.000237	0.005362	0.003139	0.005000	0.006218	8	1.183
✓ P2_sopra	-0.000251	-0.000388	-0.000966	0.005000	0.001071	7	1.285
✓ P3_sopra	0.013260	0.003976	0.001367	0.005000	0.013911	9	1.108
✓ P4_testa	-0.039900	-0.010752	0.071044	0.005000	0.082188	8	0.420
✓ P5_testa	0.021840	0.024766	0.006223	0.005000	0.033602	11	1.880
✓ P6_testa	-0.005639	-0.002481	0.000649	0.005000	0.006195	10	0.563
✓ P9_testa	-0.000814	-0.000088	0.003401	0.005000	0.003499	7	1.175
✓ V12				0.005000		0	0.000
✓ V17	-0.005347	-0.004923	-0.003523	0.005000	0.008077	8	0.426
✓ V18	-0.017868	-0.013304	-0.003514	0.005000	0.022552	13	1.026
✓ V19	0.000785	-0.001953	-0.000617	0.005000	0.002193	8	0.398
✓ V20	-0.001575	-0.000859	0.001421	0.005000	0.002289	8	0.934
✓ V30	-0.000878	-0.011089	-0.046083	0.005000	0.047406	12	1.320
✓ orto201	-0.000377	-0.001438	0.000945	0.005000	0.001761	5	0.639
✓ orto203	0.000754	-0.000548	0.000275	0.005000	0.000972	8	0.491
✓ orto205	-0.000420	-0.005115	-0.000558	0.005000	0.005163	5	1.658
Total Error							
Control points	0.009171	0.008407	0.002568		0.012704		1.054
Check points	0.020134	0.008500	0.042378		0.047682		1.066

Table 8 shows the accuracy errors of the control and checkpoints in three directions and the average value in both meter and pixel units for the blue band, the representation for each marker is available as well, which can show us which markers have better accuracy in comparison to others. Table 9 shows these results for the Red-Edge band. As it can be seen from the results of all bands, errors are in the order of mm or cm level, which shows a very high level of accuracy for remotely-sensed data.

Table 7. Accuracy errors of Red-Edge band for control and checkpoints

Markers	East err (m)	North err (m)	Alt. err (m)	Accuracy (m)	Error (m)	Projections	Error (pix)
<input checked="" type="checkbox"/> F6	-0.001667	0.003920	0.000563	0.005000	0.004297	9	0.958
<input checked="" type="checkbox"/> F7	0.001905	-0.000226	0.001070	0.005000	0.002196	6	1.482
<input checked="" type="checkbox"/> P2_sopra	-0.002921	-0.002919	0.000948	0.005000	0.004237	6	0.857
<input checked="" type="checkbox"/> P3_sopra	0.006148	0.002798	0.003568	0.005000	0.007639	9	0.798
<input checked="" type="checkbox"/> P4_testa	-0.006139	-0.001596	0.000174	0.005000	0.006346	10	0.486
<input checked="" type="checkbox"/> P6_testa	-0.011858	0.004027	0.000710	0.005000	0.012543	5	1.219
<input checked="" type="checkbox"/> P9_testa	-0.000882	-0.000703	0.001995	0.005000	0.002292	9	0.505
<input checked="" type="checkbox"/> V12				0.005000		0	0.000
<input checked="" type="checkbox"/> V17	-0.000634	0.001987	-0.000271	0.005000	0.002103	7	0.840
<input type="checkbox"/> V18	0.025068	0.001687	0.054161	0.005000	0.059705	10	0.602
<input checked="" type="checkbox"/> V19	0.006724	-0.002593	-0.000082	0.005000	0.007207	6	0.654
<input checked="" type="checkbox"/> V20	0.001934	-0.004012	-0.003092	0.005000	0.005422	8	0.860
<input type="checkbox"/> V30	-0.005161	-0.006629	-0.034194	0.005000	0.035211	9	0.806
<input type="checkbox"/> orto201	-0.003457	0.001261	0.041384	0.005000	0.041547	6	0.613
<input checked="" type="checkbox"/> orto203	0.002397	-0.001121	0.000285	0.005000	0.002662	9	0.918
<input type="checkbox"/> orto205	-0.004268	-0.005521	-0.014902	0.005000	0.016455	5	0.166
Total Error							
Control points	0.005107	0.002681	0.001633		0.005995		0.877
Check points	0.013088	0.004440	0.038850		0.041235		0.629

Table 10 represents the results of 3-D model accuracy for the Near-Infrared band.

Table 8. Accuracy errors of NIR band for control and checkpoints

Markers	East err (m)	North err (m)	Alt. err (m)	Accuracy (m)	Error (m)	Projections	Error (pix)
<input checked="" type="checkbox"/> F6	-0.006670	0.008922	0.000092	0.005000	0.011140	8	1.032
<input checked="" type="checkbox"/> F7	0.006329	-0.012209	-0.000499	0.005000	0.013761	9	1.102
<input checked="" type="checkbox"/> P3_sopra	0.011347	0.005672	-0.001271	0.005000	0.012749	10	0.745
<input checked="" type="checkbox"/> P4_testa	-0.005999	-0.001411	-0.000779	0.005000	0.006212	10	0.444
<input type="checkbox"/> P6_testa	-0.000022	-0.016641	0.051593	0.005000	0.054211	7	0.599
<input checked="" type="checkbox"/> P9_testa	-0.001212	-0.000608	0.000078	0.005000	0.001358	11	0.461
<input checked="" type="checkbox"/> V12				0.005000		0	0.000
<input checked="" type="checkbox"/> V17	-0.003138	0.001450	-0.001451	0.005000	0.003749	7	0.570
<input type="checkbox"/> V18	0.020179	-0.006639	0.079080	0.005000	0.081884	10	0.174
<input checked="" type="checkbox"/> V19	-0.005724	0.000019	-0.001338	0.005000	0.005878	8	0.555
<input checked="" type="checkbox"/> V20	-0.000061	-0.000866	0.001034	0.005000	0.001350	8	0.284
<input type="checkbox"/> V30	-0.006975	0.016947	0.003879	0.005000	0.018733	12	1.277
<input checked="" type="checkbox"/> orto201				0.005000		0	0.000
<input checked="" type="checkbox"/> orto203	0.004049	-0.002511	-0.000089	0.005000	0.004765	9	0.925
<input type="checkbox"/> orto205	-0.002835	-0.004681	0.006881	0.005000	0.008792	5	0.581
Total Error							
Control points	0.005866	0.005501	0.000910		0.008094		0.728
Check points	0.010769	0.012551	0.047376		0.050180		0.841

Table 9. Accuracy errors of RGB for control and checkpoints

Markers	East err (m)	North err (m)	Alt. err (m)	Accuracy (m)	Error (m)	Projections	Error (pix)
<input checked="" type="checkbox"/> F6	-0.001360	0.000783	0.000123	0.005000	0.001574	10	0.880
<input checked="" type="checkbox"/> F7	0.003963	-0.004418	0.000009	0.005000	0.005935	9	1.102
<input type="checkbox"/> P2_sopra	-0.008469	-0.014433	0.031060	0.005000	0.035280	8	0.573
<input checked="" type="checkbox"/> P3_sopra	0.006691	0.006009	-0.000349	0.005000	0.009000	12	0.803
<input checked="" type="checkbox"/> P4_testa	-0.006056	0.002773	-0.000212	0.005000	0.006665	9	0.669
<input checked="" type="checkbox"/> P5_testa	-0.004451	-0.004850	-0.000098	0.005000	0.006584	13	0.800
<input checked="" type="checkbox"/> P6_testa	-0.006147	0.001981	0.000464	0.005000	0.006475	13	0.527
<input checked="" type="checkbox"/> P9_testa	0.000223	0.000168	0.000058	0.005000	0.000285	13	0.507
<input checked="" type="checkbox"/> V12				0.005000		0	0.000
<input checked="" type="checkbox"/> V17	-0.000789	0.001214	-0.000117	0.005000	0.001452	7	0.185
<input type="checkbox"/> V18	0.021941	0.013246	0.005688	0.005000	0.026252	12	0.418
<input checked="" type="checkbox"/> V19	0.003570	-0.001459	-0.000155	0.005000	0.003860	8	0.289
<input checked="" type="checkbox"/> V20	0.003653	-0.002105	-0.001069	0.005000	0.004349	8	0.360
<input checked="" type="checkbox"/> V27	-0.000751	-0.005939	0.000489	0.005000	0.006006	5	0.520
<input type="checkbox"/> V30	-0.006068	0.009569	-0.001620	0.005000	0.011446	12	0.966
<input checked="" type="checkbox"/> orto201				0.005000		0	0.000
<input checked="" type="checkbox"/> orto203	-0.000578	0.000111	-0.000172	0.005000	0.000613	8	1.203
<input type="checkbox"/> orto205	-0.001521	-0.003416	-0.011308	0.005000	0.011910	4	0.449
Total Error							
Control points	0.003919	0.003351	0.000394		0.005171		0.726
Check points	0.012168	0.011034	0.016789		0.023488		0.682

In Table 10, results of georeferencing accuracy for checkpoints in all bands of R, G, B, RE, NIR, and RGB camera are presented for the April epoch, which is considered a measure of 3D model accuracy.

As it is evident from the table, all errors are in mm or cm level and represent a high level of accuracy, especially considering that data are remote sensing data and there is the possibility of having several flights in the area with this level of accuracy. Hence, such accurate data can be very interesting for the machine learning classifier, which will be explored in the next chapters.

The main outputs of Structure from Motion, besides the 3-D model, would be the orthomosaic of the area in five spectral channels and the Digital Elevation Model. Produced orthomosaics will be used in the next step to perform machine learning. Figure 19 shows the Digital Elevation Model of the Salbertrand area, and Figure 20, Figure 21, and Figure 22 are the produced orthomosaics of the Salbertrand area in each multispectral band.

Table 10. Check points Errors of all bands

Band	East Error (m)	North Error (m)	Alt. Error (m)	Total Error (m)
Red	0.003	0.006	0.046	0.047
Green	0.008	0.01	0.054	0.056
Blue	0.02	0.008	0.042	0.048
Red-Edge	0.01	0.004	0.039	0.041
NIR	0.01	0.012	0.047	0.05
RGB	0.012	0.011	0.017	0.023

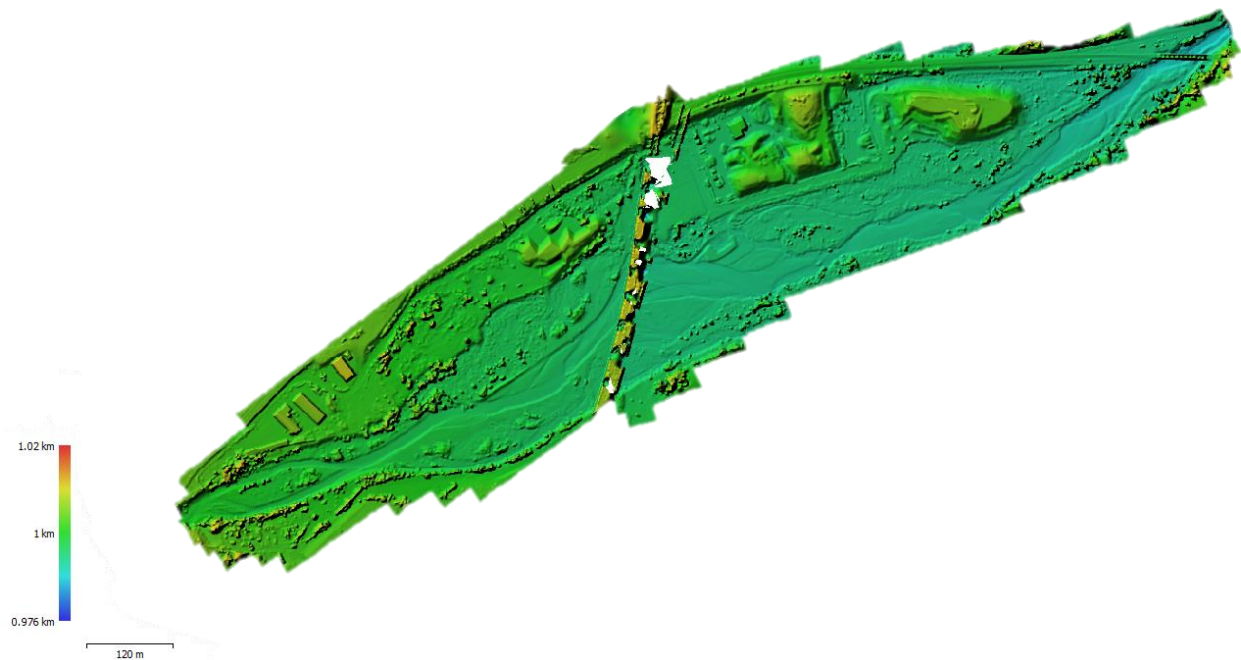


Figure 19. DEM- RGB band

In the following figures, orthophotos of all bands have been shown.

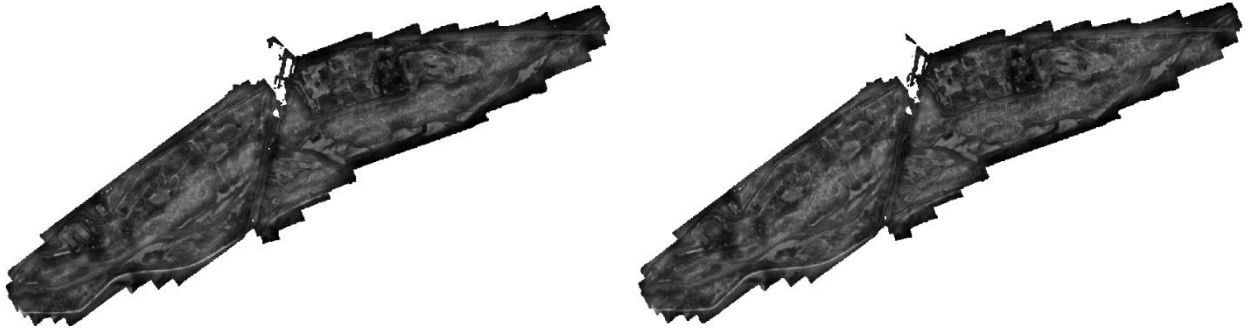


Figure 20. Orthophoto-left: Blue Band, right: green band



Figure 21. Orthophoto-left: red Band, right: Red-Edge band



Figure 22. Orthomosaic- left: NIR Band, right: RGB band

3-3-2- Machine Learning- Random Forest- April Epoch

UAV Data acquired in this area are provided in two epochs: one during April in winter and the other one during July in summer. The processing phase started with the Winter epoch. In order to choose the optimized dataset accuracy measures of precision, Recall and F-score value have been taken into account, and the optimized dataset for the classification purpose of the April epoch has been used to perform classification of the Summer epoch, although in the summer epoch also some Elevation (Normalized Digital Surface Model), Spectral (Thermal data and Vegetation Indexes) and Texture features (Angular Second Moment, Contrast, Correlation, Variance, Inverse Difference Moment, Sum Average, Sum Variance, Sum Entropy, Entropy, Difference Variance, Difference Entropy, Information Measures of Correlation, Maximal Correlation Coefficient as described in (ROBERT M. HARALICK, 1973)) have been added to discover the most effective features in the classification of the area using Random Forest Classifier and to explore whether the classification quality improves or not.

Classification of the Salbertrand area in April has been performed using three different datasets:

- a) combination of RGB and Multispectral datasets
- b) Only RGB datasets
- c) Only Multispectral Dataset including Red-Edge and Near-Infrared bands.

Nine different scenarios considering three datasets for three test areas in the winter epoch have been analyzed. In the following, the best-selected dataset from the winter epoch with the addition of some other features consisting of Elevation (Normalized Digital Surface Model), Spectral (Thermal data and Vegetation Indexes of Normalized Difference Vegetation Index, Normalized difference water index, Normalized Difference Red-Edge, Anthocyanin Reflectance Index, Enhanced vegetation index, Soil-adjusted vegetation index, Structure Insensitive Pigment Index) and Texture (Angular Second Moment, Contrast, Correlation, Variance, Inverse Difference Moment, Sum, Average, Sum Variance, Sum Entropy, Entropy, Difference Variance, Difference Entropy, Information Measures of Correlation, Maximal Correlation Coefficient) have been taken into account to analyze the performance of the classifier on the summer epoch of the acquired

area. Moreover, the feature selection approach has been utilized in python to detect the most important features and explore a compromise between accuracy and the number of utilized features. Our purpose is to see how datasets perform separately and how they perform when they are used together.

In order to perform an accurate classification 4 different portions of the study area have been clipped, one for training and three others for testing and validation. For different input datasets, these portions will remain constant spatially in order to perform an analytical comparison at the end, although for each dataset the radiometric values will be different. The following steps should be performed for all datasets to have a final classified map and an evaluation of the accuracy of the results and the same procedure will be repeated for two other test areas to produce a generalized result and conclusion for the performance of Random Forest classifier and machine learning technique.

- a) Data preparation for Training dataset- QGIS
- b) Cross validation- Python
- c) Data preparation for Testing dataset- QGIS
- d) Classification of Unseen testing dataset- Python
- e) Data preparation for Validation dataset- QGIS
- f) Validation- Evaluation of classification goodness- Python

3-3-2-1- First Test Area

3-3-2-1-1- RGB+ Red-Edge+ Near Infrared dataset

As previously mentioned, data acquired by phantom4 drone include 5 bands, of which three are associated with red, green, and blue filters and 2 of them are Red-Edge and Near-Infrared bands. Hence by combining orthophotos of these 5 bands together, an orthophoto consisting of 5 radiometric values for each pixel, will be obtained. It is worth mentioning that the final orthophoto resulting from the Structure from Motion approach had a pixel size of 4 cm, but for the sake of processing time, the combined orthophoto resampled with the pixel size of 6 cm.

Data preparation for Training dataset – QGIS: Mainly machine learning approach for our purpose has been performed in Python and based on Random Forest Classifier, so training, testing, and validation data should be prepared and exported in the appropriate format using QGIS, open-source software to be used later in python. The following steps should be performed to get training data ready.

1. Build Virtual Raster from Red, Green, Blue, Red-Edge, and NIR bands: as soon as the combined raster has been produced in the software, it should be exported in the Geotiff format, otherwise, since it is a virtual raster it will not be saved in the long-term memory and will be lost after closing software. Figure 23 shows a false-color representation of the area, with NIR in the Red channel, red in the blue channel, and green and green channel.

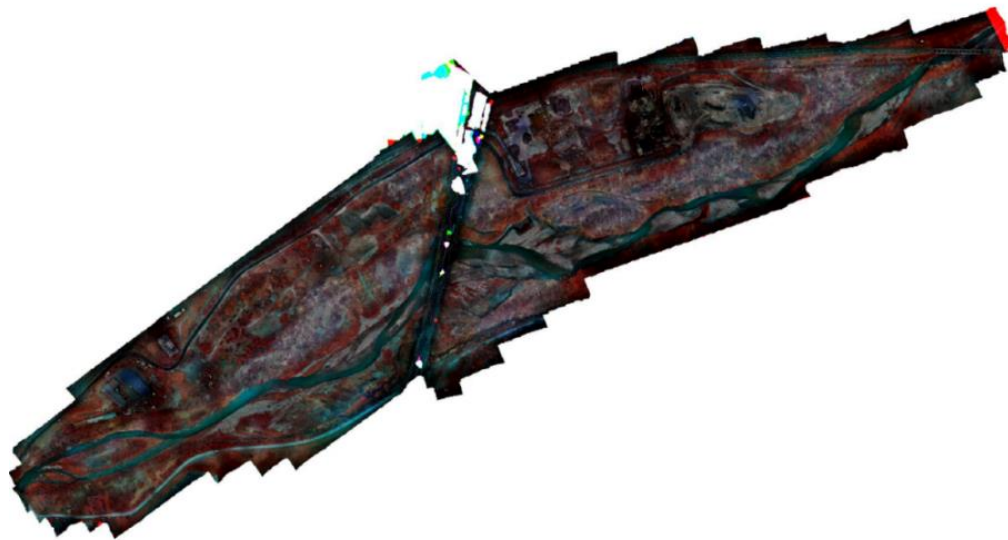


Figure 23. Composite raster of RGB, Red-Edge & NIR bands

2. Resample with 6 cm resolution: this step can be implemented by getting a 'save as' from the raster and the resolution value should have been changed during the save as process.
3. Translate (Convert Format) from 16 bit to 8 bit: using the "-scale 0 65535" command in the console, pixel values change from 16 bit to 8 bit (Figure 24 and Figure 25). Value of 65535 is the maximum value in the 16bit scale, so this value may be different for other data, and it should be checked in the 'properties' of the raster. As a result of this step, all pixel values should become a

value between 0 and 255. hence in order to check if the translation has been performed correctly “identify” tool can be used.

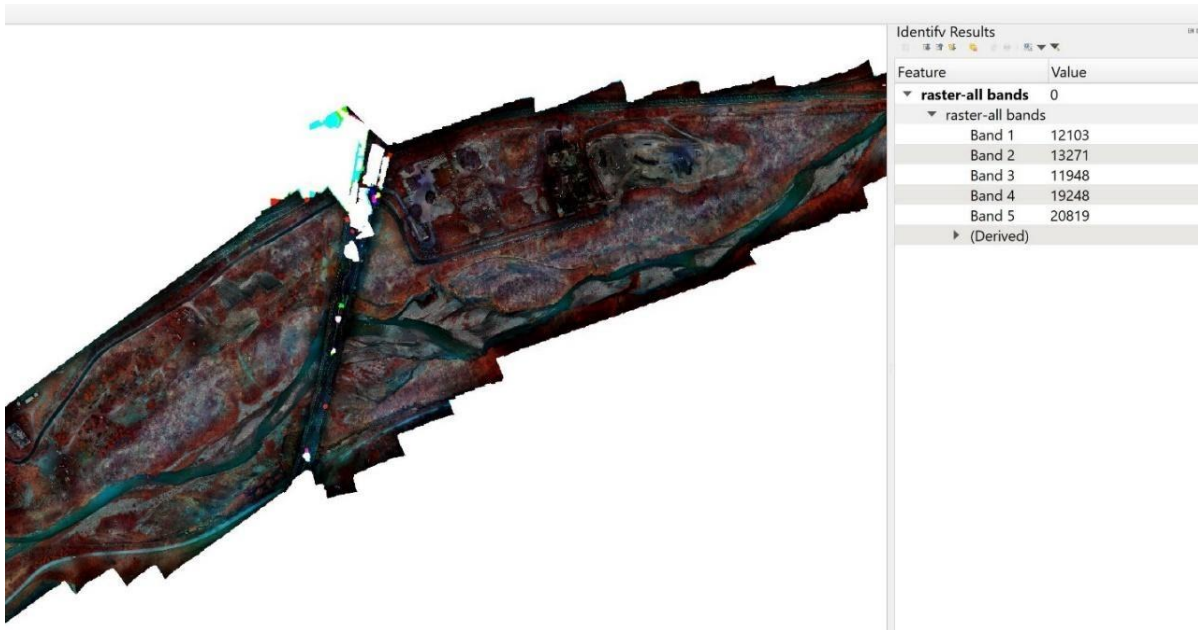


Figure 24. identify value in 16 bit for one pixel



Figure 25. identify value after converting the format to 8 bit

4. Clip raster by training mask and save as training raster: the objective of this step is to clip raster of the whole area with the training perimeter, the final raster will be called training raster (Figure 26) and will be used in the rest of the procedure. The coordinate system should be set here, and it is the same coordinate system of ground control points: WGS, UTM 32N.

5.



Figure 26. Training raster

5. Create polygons of 3 classes, each in an individual layer: for this purpose, three new layers should be created, one for each class, then each of the layers should be started for editing, and polygons will be drawn manually in each layer.

It is noteworthy that in drawing polygons only areas should be selected that we are confidently sure about their label since we are in the training stage and any wrong selection in the labels, will affect the final result of training and may end in inaccurate classification. It is also crucial to keep in mind that the number of points in 3 classes should be at least in the same order of magnitude

to have a balanced dataset, the more similar the number of points, the more accurate will be the results. Figure 27 shows the training polygons for the training area, in which yellow polygon represents the ground class, green ones are the vegetation areas and blue areas are the wet or water class. The more the number of polygons for each class, the more tried and accurate will be the classifier, but a very large and unreasonable number of training polygons may cause an overfitting problem.

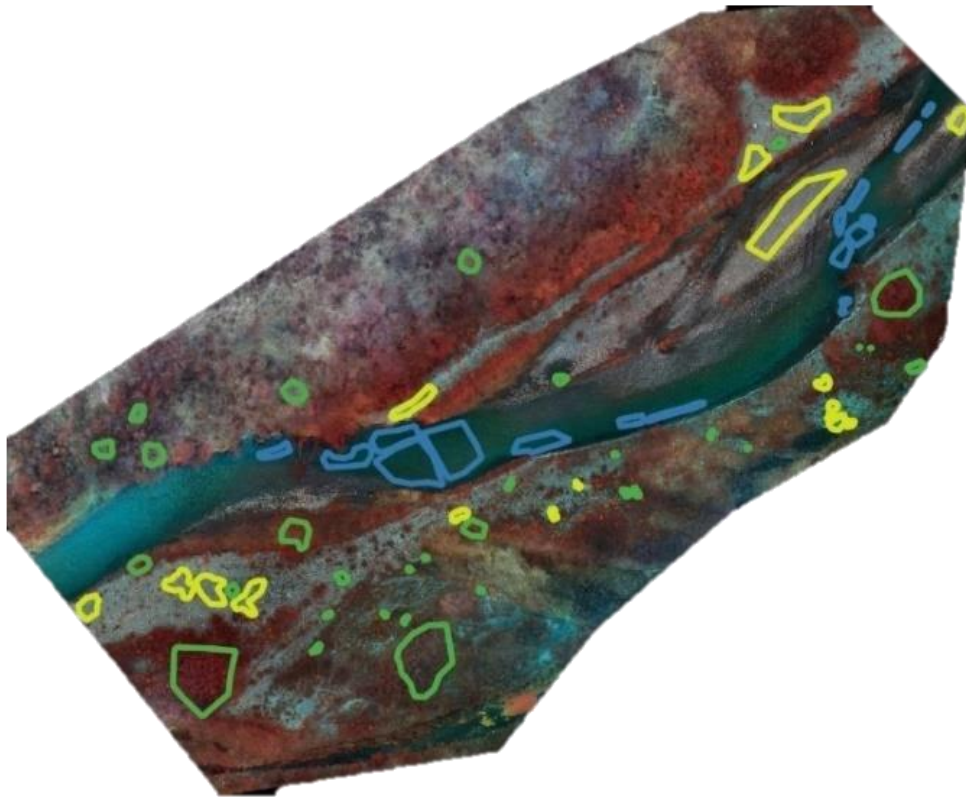


Figure 27. training polygons for 3 classes: Green (Vegetation), Yellow (Ground), Blue (Water)

6. Clip training raster with polygons and produce raster of each class: if the training raster gets clipped with 3 vector files (one for polygons of each class) the final result will be 3 new raster files: Vegetation raster, Water raster (Figure 28), Ground Raster.
7. Convert raster pixel2points: this step should be repeated for three rasters of Vegetation, Ground, and Water, the result of this step is the vector file of 3 layers.

11. Merge 3 vector layers of 3 classes: 3 vector files of ground, vegetation, and water should be selected as input data. Furthermore, the coordinate system should be set in the UTM, 32N as has been set in all other steps.

12. Export merged vector as comma-separated values (CSV) file: in this step, only the fields that we want to be present in the text file should be checked, which are as followings: R, G, B, RE, NIR, Class. Besides geometry type should be set to point, the coordinate system should be selected, and the final directory of exported file can be determined here. The result of this step is the final result of the preparation of training data, and it is a text file that will be imported for machine learning in python.

Cross-Validation- Python: Cross-validation has been performed in Python. Input data for cross-validation is the text file resulting from the previous step including points with R, G, B, RE, NIR, and Class (label) fields (Figure 30).

```
### TRAINING DATASET LOADING
df_train_data = pd.read_csv("D:\\Masoume\\Salbertrand\\DATASET\\RGB+RE+NIR-1st\\training\\training data-final.csv")
features = df_train_data.drop(columns=['Class'], axis='columns')
labels = df_train_data['Class']
```

Figure 30. Reading training data into the python script

predefined packages and libraries necessary for this step are as Figure 31:

```
import pandas as pd
import numpy as np
from scipy.sparse import coo_matrix
from sklearn.utils import shuffle
from sklearn import model_selection
from sklearn.preprocessing import StandardScaler
from sklearn.model_selection import train_test_split
from sklearn.model_selection import cross_val_score
from sklearn.model_selection import GridSearchCV
from sklearn.metrics import make_scorer
from sklearn.ensemble import RandomForestClassifier
import time
```

Figure 31. packages and libraries used in the training phase

- Numpy is for processing N-dimensional array objects, Linear Algebra, Fourier Transformation, etc.

- Scipy is for Mathematics and Engineering processing.
- Scikitlearn is for predictive data analysis including classification, Regression, Clustering, dimensionality reduction, and preprocessing of data.
- Coo-matrix can transform a sparse matrix into the coordinate format.
- Preprocessing is for transforming input data such as text files to be used in Machine Learning.
- StandardScaler standardizes features by removing mean and scaling to unit variance.
- Cross-val-score evaluates score by cross-validation.
- Model selection: for comparing, validating, choosing parameters and models or generally parameter tuning which specifically includes GridSearchCV, train_test_split, and cross_val_score.
- train_test_split is for splitting data into training and testing data with a specified percentage by the user which in our case is 20% for testing and 80% for training data (Figure 32).
- GridSearchCV is for searching over estimated parameters to find optimized and best cross-validation parameters. If cross-validation is based on the K-fold approach the observation set will be divided into K groups or folds of approximately the same size, first fold will be the validation set and the method will be fit on the remaining (K-1) folds. In our case number of folds is 4.

```
### DATASET SPLITTING FOR CROSS/VALIDATION --- StandardScaler() NORMALIZATION --- RANDOMIZING OF IT
X_train, X_test, y_train, y_test = train_test_split(features, labels, test_size=0.2, random_state=0)

features_scaler = StandardScaler()
X_train = features_scaler.fit_transform(X_train)
X_test = features_scaler.transform(X_test)

X_train, y_train = shuffle(X_train, y_train)
```

Figure 32. Splitting training dataset for cross-validation purpose

RandomForestClassifier is the used classifier for the Machine Learning approach here. The random forest has a large number of parameters that should be set for our purpose. For instance, 'number of estimators' or number of trees which has been set to values of 10-25 or 50. 'Criterion' can be 'Gini' or 'Entropy' and it represents the quality of split. 'Minimum samples split' is the minimum number of features required to split the internal node. 'Minimum

samples leaf' is the minimum number of samples required to be a leaf node. 'Maximum features' present the maximum number of features to consider when looking for the best split and it can be 'auto' or 'log2' for our purpose. It is the responsibility of the Cross-validation process to select the optimized values for these parameters among the possible values assigned by the user (Figure 33 and Figure 34).

```
### ALGORITHM CHOOSE (RF), CV CALCULATION (cross_val_score), RESULTS PRINTING
t1 = time.time()
classifier = RandomForestClassifier(n_estimators=10)
all_accuracies = cross_val_score(estimator=classifier, X=X_train, y=y_train, cv=4)
print("Accuracy on training dataset with different cv=4 folds:", all_accuracies)
print("Mean accuracy on training dataset through CV:", all_accuracies.mean())
print("Standard deviation reached in training dataset (if <1% is good -> very LOW variance):", all_accuracies.std())
precision = cross_val_score(classifier, X_train, y_train, cv=4, scoring='precision_macro')
recall = cross_val_score(classifier, X_train, y_train, cv=4, scoring='recall_macro')
f1 = cross_val_score(classifier, X_train, y_train, cv=4, scoring='f1_macro')
print("Precision train CV=4:", precision)
print("Recall train CV=4:", recall)
print("F1 train CV=4:", f1)
t2 = time.time()
print ('\n\n### %s ### \nCV and statistical parameters Time: %s s' % (RandomForestClassifier, round(t2-t1,5)))
```

Figure 33. Script of cross-validation step for best parameters determination for 4 folds

```
grid_param = {
    'n_estimators': [10, 25, 50],
    'criterion': ['gini', 'entropy'],
    'max_features': ['auto', 'log2'],
    'min_samples_split': [5, 7, 10],
    'min_samples_leaf': [4, 6, 10],
    'random_state': [None, 0, 42]
}
```

Figure 34. possible values for each parameter

The cross-validation result for this dataset is as in Table 11.

Data preparation for Testing dataset- QGIS, the steps are as follows:

- Importing orthophoto of the area (combined raster of all 5 bands) into QGIS
- Translating 16-bit raster into 8-bit raster
- Importing testing polygon perimeter
- Clip raster by testing mask layer to produce test raster (Figure 35).

Table 11. Cross-Validation result for RGB + Red-Edge + NIR dataset

N-Estimators	50
Criterion	Entropy
Max-features	Auto
Min-samples-leaf	4
Min-samples-split	5
Random state	None
Accuracy on training	98%

Table 12 shows the accuracy of the training dataset for 4 sets of cross-validation:

Table 12. Accuracy on training dataset for 4 folds and optimum parameters

Accuracy on training dataset with different CV = 4 folds	[0.984 0.984 0.983 0.984]
Mean accuracy of the training dataset	0.98
Standard deviation reached in the training dataset	0.0002
Precision in CV = 4 folds	[0.984 0.983 0.983 0.983]
Recall in CV = 4 folds	[0.984 0.983 0.983 0.984]
F1 Score in CV = 4 folds	[0.984 0.984 0.983 0.983]

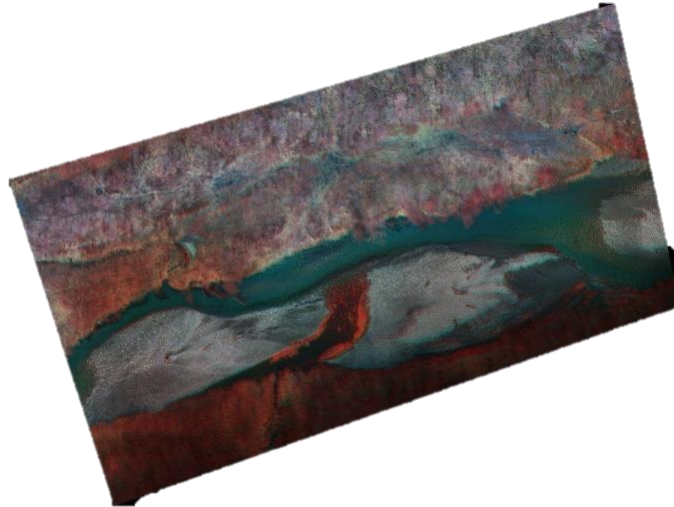


Figure 35. Test raster, 1st test area

- Raster pixel2points
- Clip vector by testing mask layer
- Point sampling tool
- Add X/Y fields to the layer.
- Export final vector into CSV file.

Most of the procedure of preparation of the testing dataset is similar to the training phase, except for the fact that labels or classes are not determined in the testing dataset, furthermore, coordinates should be added in this stage to the layer (step 8) because final classified orthophoto will be represented in the software visually, hence it should be spatially correct. The result of this step is a text file including R, G, B, RE, NIR, and X, Y values of all points of the testing area.

Classification of Unseen testing dataset- Python: Some packages and libraries are added in this step to perform the classification of the testing dataset (Figure 36). LabelEncoder is for encoding target labels with a value between 0 to (Number of classes-1). In this phase presence of some libraries is crucial in order to analyze the accuracy of testing data such as accuracy_score. Classification-report and libraries related to the confusion matrix will be used in the validation stage.

```

import pandas as pd
import numpy as np
from sklearn.preprocessing import LabelEncoder
from scipy.sparse import coo_matrix
from sklearn.utils import shuffle
from sklearn.ensemble import RandomForestClassifier
import time
from sklearn.metrics import accuracy_score
from sklearn.metrics import classification_report
from sklearn.metrics import confusion_matrix
from scikitplot.metrics import plot_confusion_matrix
import matplotlib.pyplot as plt

```

Figure 36. packages and libraries necessary for the prediction and evaluation phase

One crucial stage here that cannot be ignored is to use the ‘Head’ function which works based on the number of points in each class of training data (Figure 37). The purpose of this function is to make a balance among number of points of 3 land cover classes, so if there is the confidence that the classes are more or less balanced regarding number of points head function can be ignored, otherwise, the head function must be set based on a minimum number of points, in this way the program uses only ‘head’ number of points for all classes and automatically brings balance to the training phase.

```

### Portioning if you have unbalanced labels - otherwise don't use it
portion = df_train_data.groupby('Class', sort=False).head(145402)
features = portion[feature_columns]
labels = portion['Class']

```

Figure 37. Head function for bringing balance to the unbalanced training dataset

The procedure is to first train the classifier for 3 classes using the training dataset, and after setting the optimized hyperparameters for the random forest classifier resulting from the Cross-Validation stage, the prediction of class or label for testing data will be implemented (Figure 38).

```

### Upload dataset for training and validation through accuracy parameters
df_train_data = pd.read_csv("D:\Masoume\Salbertrand\DATASET\RGB+RE+NIR-1st\training\training data-final.csv",
df_train_data = df_train_data.dropna()
feature_columns = ['R', 'G', 'B', 'RE', 'NIR']
features = df_train_data[feature_columns]
labels = df_train_data['Class']
print(labels.value_counts())

```

Figure 38. Reading training dataset into the script

Figure 39 shows the steps of hyper parameters setting for RF classifier, then fits a model on the training data and predicts accuracy on training data.

```
### Model training and accuracy on the training dataset (generalization ability) -> insert CV and GridSearchCV for optimization of RF hyperparameters
model = RandomForestClassifier(criterion='gini', n_estimators=25,max_features='auto', min_samples_leaf=10, min_samples_split=5, random_state= 42)
t1 = time.time()
model.fit(features, labels)
t2 = time.time()
print ('\n\n### %s ### \nTraining Time: %s s' % (RandomForestClassifier, round(t2-t1,5)))
y_pred_train = model.predict(features)
accuracy = round(accuracy_score(labels, y_pred_train) * 100,2)
print ("\tAccuracy on Train: %s" % (accuracy))
```

Figure 39. setting hyper-parameters for RF classifier, fitting a model on the training data, and predicting accuracy on training data

Figure 40 reads an unseen dataset and performs the classification on it for each point, and exports it to the set directory.

```
### Classification and exportation of the 2nd unseen dataset
df_testing = pd.read_csv("D:\Masoume\Salbertrand\DATASET\SECOND TEST AREA\NIR+RE\testing points-final.csv")
df_testing_clean = df_testing.dropna().drop(columns=['x', 'y'])
feature_columns_test = ['R','G','B','RE','NIR']
features_test = df_testing[feature_columns_test]
CLASSIFIED_DATASET = model.predict(df_testing_clean)

tot_df = pd.concat([df_testing,df_testing_clean],axis=1).dropna()
my_data_1 = np.vstack((tot_df.T.drop(['R','G','B','RE','NIR']),CLASSIFIED_DATASET))
my_data_1 = my_data_1.T

np.savetxt('D:\Masoume\Salbertrand\DATASET\SECOND TEST AREA\NIR+RE\results\Classification_Testdata2.txt',
```

Figure 40. Reading unseen testing dataset into the script, prediction of labels for each point, exporting it to the determined directory

The output of this step is a text file consisting of coordinates and a class of points, accordingly, in order to have a visualization of the predicted map, the text file should be presented in the QGIS. The steps for preparing results and representing them in software are as follows:

1. Import CSV file into the software.
2. Export text file as point shapefile
3. Rasterize point shapefile based on a class field.
4. change the visualization to pseudo color.
5. assign appropriate colors for 3 classes of ground, water, and vegetation.

Data preparation for Validation dataset- QGIS: The validation step is decisive to see whether the results of classification are acceptable for us or not. In this stage, preparation should be implemented on the testing raster considering that classes of some points or areas are well-known to us and the goal is to see if these areas are classified correctly during the classification of unseen datasets or not. The steps of data preparation here are similar to training data preparation, the

only difference is the input data, which is testing raster here. Figure 41 shows the validation polygons. Thus, the steps are in such a way:

1. Importing testing raster into software
2. Drawing polygons for each class in 3 different layers

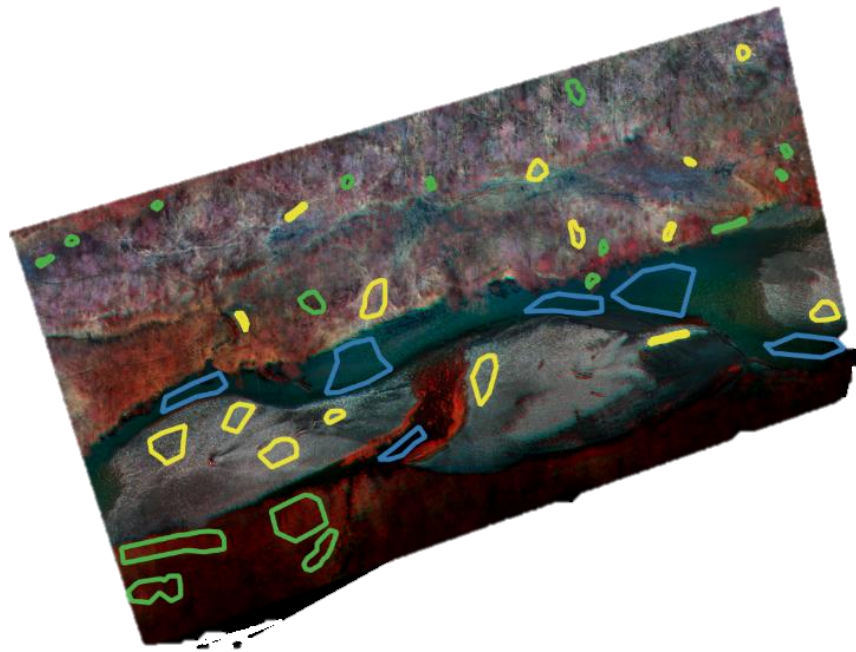


Figure 41. Validation polygons for 3 classes: Green (Vegetation), Yellow (Ground), Blue (Water)

3. Clip test raster by polygons: The result will be three rasters for each class.
4. Converting raster pixel2 points: the result will be 3 vector layers.
5. Removing zero values from attribute table of 3 layers
6. Point sampling tool: to add radiometric R, G, B, RE, and NIR values into layers.
7. Adding Coordinates of X/Y features into layers
8. Adding class or label field in the attribute table of each layer
9. Merging 3 vector layers
10. Extracting merged file into CSV format file: final output to be used in the next validation step in python.

3-3-3- Machine Learning- RF- July Epoch

In order to have an analysis regarding the performance of the Random Forest classifier in the summertime epoch in the same study area, orthomosaics of the area in the July season have been taken into account. Based on the results from previously analyzed scenarios in the winter epoch, all of the channels together had a better performance, hence in the summer data analysis, only this dataset in only one test area has been considered. Furthermore in the summer epoch, besides 5 considered spectral channels, Elevation data of Normalized Digital Surface Model, Spectral data including Thermal data and Vegetation Indexes including NDVI, NDWI, NDRE, ARI, EVI2, SAVI, SIPI, and Texture features including Angular Second Moment, Contrast, Correlation, Variance, Inverse Difference Moment, Sum Average, Sum Variance, Sum Entropy, Entropy, Difference Variance, Difference Entropy, Information Measures of Correlation, Maximal Correlation Coefficient as described in (ROBERT M. HARALICK, 1973) have been added with the purpose of improving the classification result. Considering all features and bands into account generally 27 attributes for each pixel are available in the dataset.

In the summer epoch, the best-selected dataset from the previous epoch beside extra features including nDSM, thermal and vegetation indexes, and texture features, are added to improve the classification (Haralick et al., 1973) and to find out about the most effective features in the classification of the area using RF. Considering all features and bands, 27 attributes for each pixel are available in this dataset.

3-3-3-1- Feature Selection

Using the “Select from Model” function in the scikit-learn package of python the most useful features have been selected considering the highest accuracy.

The used 27 features in this epoch are:

- a) Spectral features: Red, Green, Blue, RE, NIR, and thermal.
- b) Vegetation Indexes: NDVI, NDWI, NDRE, ARI, EVI2, SAVI, SIPI
- c) Texture features: Angular Second Moment, Contrast, Correlation, Variance, Inverse Difference Moment, Sum Average, Sum Variance, Sum Entropy, Entropy, Difference Variance, Difference Entropy, Information Measures of Correlation, Maximal Correlation Coefficient.

Chapter 4

4- Results and Discussion

4-1- Random Forest - April Epoch - First test area

4-1-1- RGB + Red-Edge + NIR

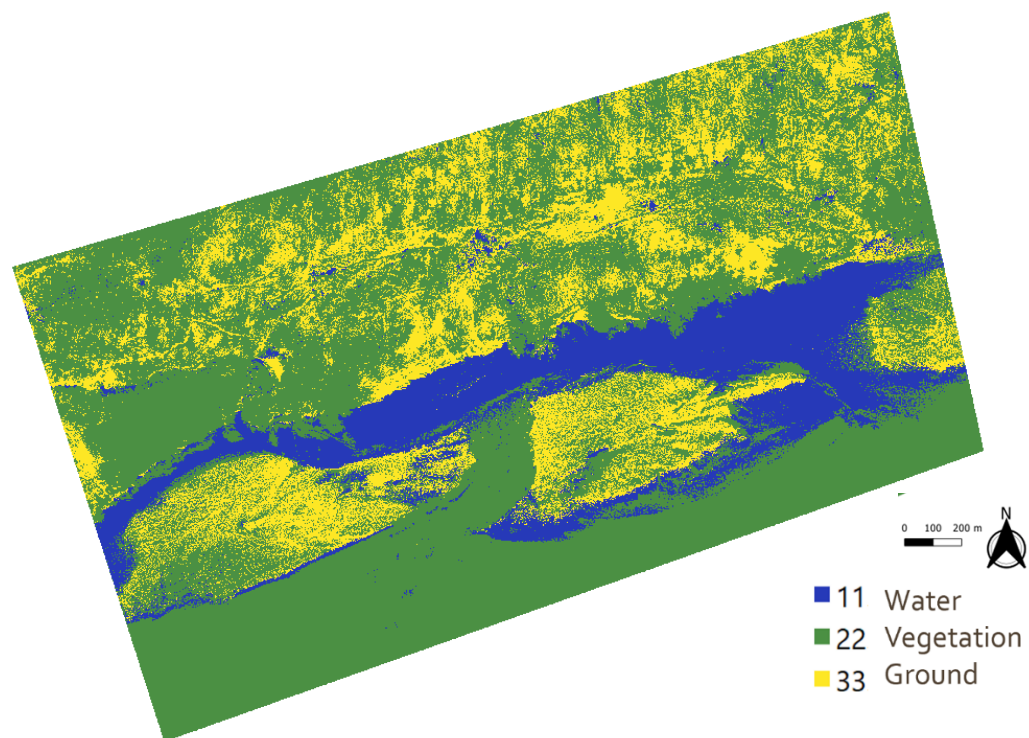


Figure 42. Prediction (Segmented) map of testing based on RGB + Red-Edge + NIR dataset

Figure 42 shows the classified map of the Salbertrand testing area based on all spectral bands of Red, Green, Blue, Red-Edge, and NIR, based on the Random Forest classifier. In the classified map, the water area is presented in blue, the vegetation in green, and the ground in yellow colors. As it is evident riverbed is detected almost accurately, as is the vegetated area, but to have an accurate measure of classification goodness, Table 13 represents the confusion matrix of the classified map. In the confusion matrix, diagonal numbers represent the correct classified pixels, which dedicates to the majority number of pixels in a good classification. Non-diagonal values represent misclassification between three classes, As it is obvious from the table, most of the misclassification is between vegetation and water class. Also, there are high values of misclassification between vegetation and ground. It is worth mentioning that values are not pixels, for the sake of simplicity they are presented in square meter units.

Table 13. Confusion Matrix for 1st test area- RGB+RE+NIR dataset

Unit:m ²	Water	Vegetation	Ground
Water	822.6	176	0.05
Vegetation	0.8	727	5.3
Ground	1.2	136	437.5

Table 14. Accuracy parameters for 1st test area- RGB+RE+NIR dataset

Table 14 presents other accuracy measures of precision, recall, and F-score. Precision shows how many of the classified pixels are correct. And recall shows how many correct pixels are classified correctly, and F-score is the weighted average of these two values. Similar to the results of the confusion matrix, lower values of precision, recall and f-score is between water and vegetation couple, as well as vegetation and ground couple. But, taking all misclassifications into account, results still are promising and present an f-score of an average of 86%.

	Precision	Recall	F-score	AUC
Water	0.99	0.82	0.90	0.99
Vegetation	0.69	0.99	0.82	0.99
Ground	0.98	0.76	0.86	0.98
Average	0.87	0.86	0.86	0.99

The precision-recall curve is another measure of model performance and represents the classifier's ability to distinguish between classes. Based on Table 14, high values of precision have been acquired, so in this case, the class has a high ability to distinguish between classes for a random dataset. Figure 43 shows the curve for three classes and almost all the classes, it tends to be close to 1 for both precision and recall measures. In other words, this curve is an easier and faster visual way of analyzing the results in comparison to numerical results presented in the precision, recall, and f-score table.

recision-Recall curve for Water (11), Vegetation (22), Ground/Gravel bars classe

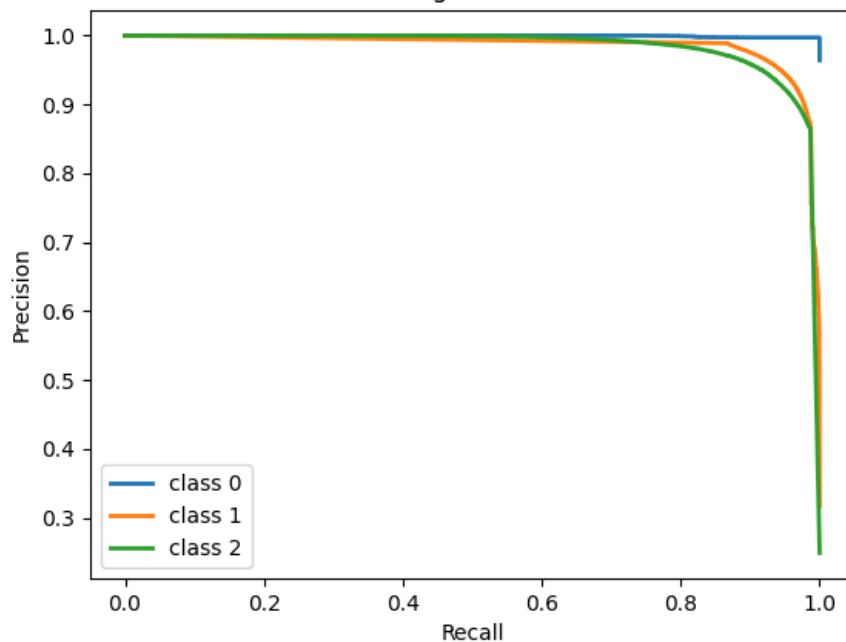


Figure 43. The precision-Recall curve for 3 classes- for 1st test area- RGB+RE+NIR dataset

4-1-2- RGB dataset

The cross-validation result for this dataset are as follows in Table 15, this result is based on the cross-validation library in the scikit-learn package in python, and shows the optimized values of random forest parameters. Optimization is based on the accuracy of training data.

Table 15. Cross-Validation result for RGB dataset

N-Estimators	50
Criterion	Gini
Max-features	Auto
Min-samples-leaf	10
Min-samples-split	10
Random state	None
Accuracy on training	90 %

Classification of Unseen testing dataset- Python is in Figure 44 . As it is obvious, the river bed is partly detected in the classified map, and there seem to be lots of misclassification between vegetation and ground.

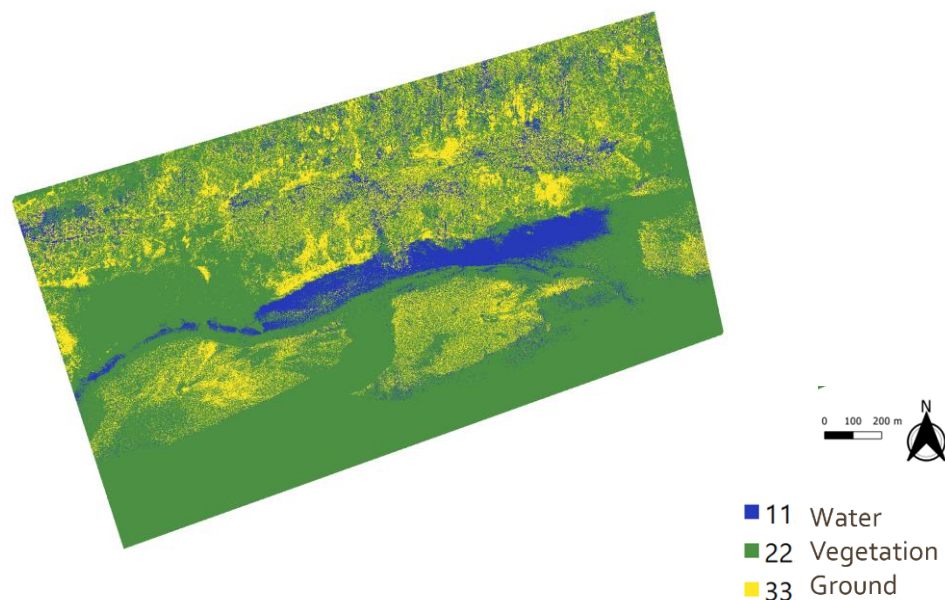


Figure 44. Predicted (Segmented) image of the 1st Test area based on RGB dataset

Evaluation of classification goodness based on the confusion matrix for this dataset is presented in Table 16. High values are related to the diagonal ones, as expected, but there are also very high values in misclassification between water and vegetation, and also between vegetation and ground, very low values of recall for water and ground, and low precision of vegetation is proof for this misclassification in Table 17. All three classes have low values of f-score and the average f-score value for all classes is 72%, which represents high problems in classification for this dataset.

Table 16. Confusion matrix of 1st test area- RGB dataset

Unit:m²	Water	Vegetation	Ground
Water	576.2	422	0.63
Vegetation	41.6	678.5	13
Ground	34.9	135.7	404.2

Table 17. Accuracy parameters of 1st test area- RGB dataset

	Precision	Recall	F-score	AUC
Water	0.88	0.58	0.70	0.85
Vegetation	0.55	0.92	0.69	0.88
Ground	0.96	0.70	0.81	0.98
Average	0.80	0.72	0.72	0.85

Figure 45 shows the precision-recall curve for the results of this dataset, and as it is evident, curves tend to decrease immediately from 1, especially for water and vegetation. Ground class decreases a bit slower with respect to two other classes and it has better results of F-score based on Table 17. The easiest way to interpret this curve is to analyze its curviness, the more it is tending to run away from 1 value on both axes, the less the precision, recall values, and the less accurate is the classification.

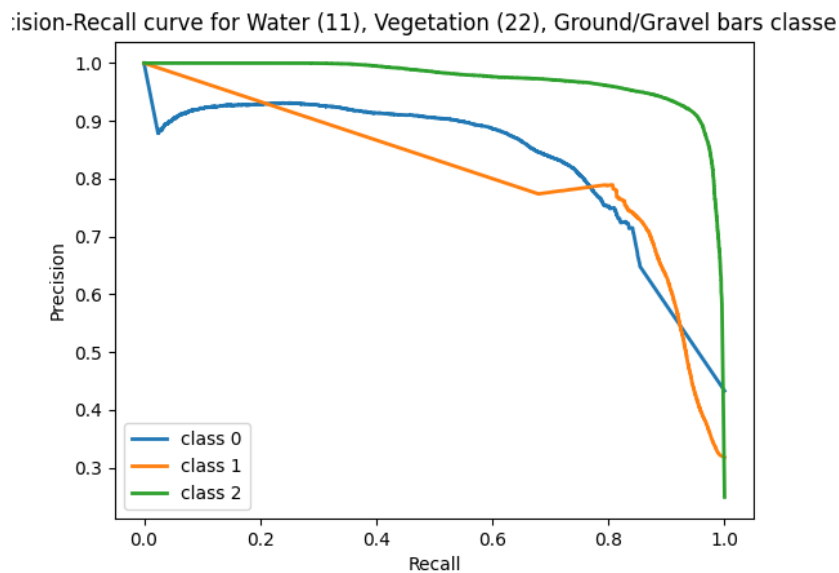


Figure 45. Precision-Recall curve of 1st test area- RGB dataset

4-1-3- Red-Edge + NIR dataset

Table 18 shows the results of Cross-validation for the Red-Edge + NIR dataset. Based on these results, 25 trees are used in a random forest and there is randomness in the selection of features.

Figure 46 shows the classification of the unseen testing area based on the multispectral dataset. As it can be seen riverbed and wet areas are correctly detected with a high level of accuracy. There seem to be some misclassifications between vegetation and ground classes.

Table 18. Cross-Validation Result for Red-Edge + NIR dataset

N-Estimators	25
Criterion	gini
Max-features	Auto
Min-samples-leaf	10
Min-samples-split	5
Random state	42

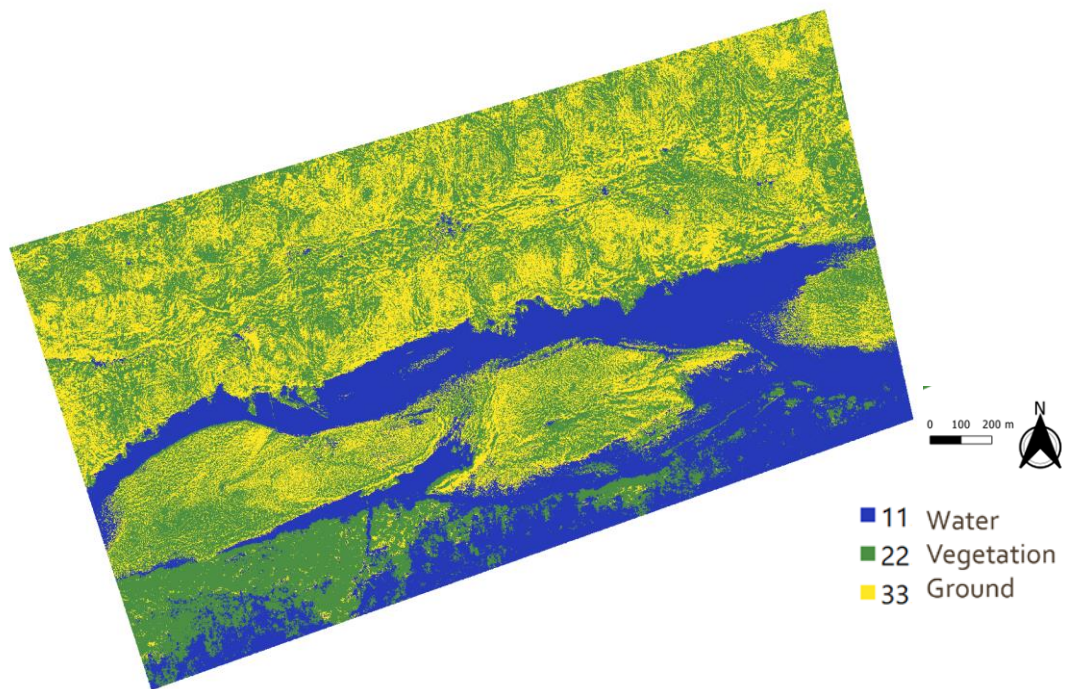


Figure 46. Predicted (classified) map of 1st test area- based on Red-Edge + NIR dataset

Evaluation of classification goodness in Python is based on the confusion matrix in Table 19, based on which misclassified pixels between vegetation and ground are present. This problem can also be derived from low precision in vegetation class and low recall in ground class in Table 20. As a result, the f-score of vegetation and ground is both low, compared to the water class. Because based on the results, all the pixels in the water class are water and almost all of the water pixels are detected and classified in the correct class.

Figure 47 is the area under curve representation. As it can be seen from the curve, the water class very high value of almost 1 and it tends to stay at 1 until the very end of it. Vegetation and ground, on the other hand, have problems in their precision-recall curve, and precision and recall values tend to decrease immediately for vegetation and ground respectively. Therefore, this dataset seems to perform very well for only wet area detection (water class), but considering the results of the other two classes, it fails to perform very well.

Table 19. Confusion Matrix of 1st test area based on Red-Edge + NIR dataset

Unit:m ²	Water	Vegetation	Ground
Water	998.7	0.07	0.04
Vegetation	2.5	704	26.7
Ground	0.4	172	402.2

Table 20. Accuracy parameters of 1st test area based on Red-Edge + NIR dataset

	Precision	Recall	F-score	AUC
Water	0.99	0.99	0.99	0.99
Vegetation	0.80	0.96	0.87	0.97
Ground	0.93	0.70	0.80	0.95

Precision-Recall curve for Water (11), Vegetation (22), Ground/Gravel bars classe

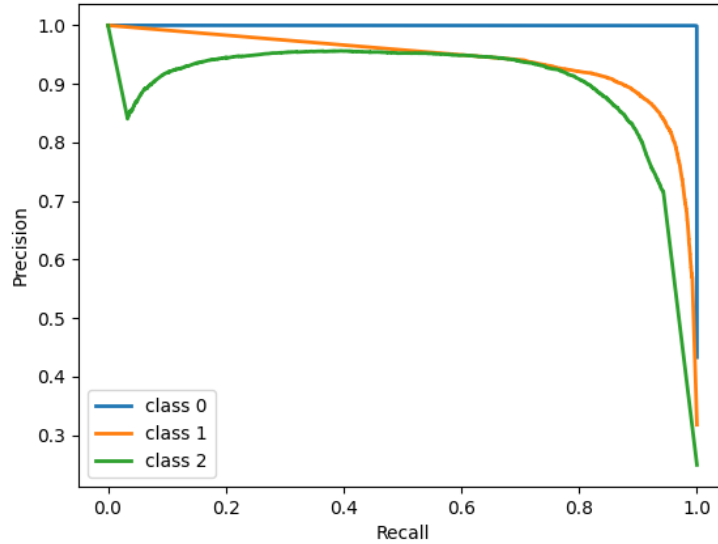


Figure 47. Precision-Recall curve of 1st test area based on Red-Edge + NIR dataset



Figure 48. Results of 1st test area using 3 different datasets

Based on Figure 48, the results of all three datasets for 1st test area are presented. In the RGB dataset precision and recall and consequently, f-score values are low for all classes. In the

multispectral dataset (RE+NIR) low recall has resulted for ground meaning that when it is ground, it has not been predicted as ground correctly, besides precision is low for vegetation meaning that most of the time that it is predicted as vegetation it is no vegetation.

Using the combined dataset (RGB+RE+NIR) the same pattern has remained, so low precision for vegetation class and low recall for ground class. However, with a slight improvement of 5% multispectral data alone performed better with respect to mixed data and about 20% better with respect to RGB data alone regarding the average f-score value of all classes.

Confusion of the vegetation and ground for the classifier can be a result of brownish and not completely green vegetation in the area during the winter season. Besides, the presence of shadows during the acquisition phase in April time has caused the main problems for the classifier to distinguish between ground and vegetation.

4-2- Random Forest- April Epoch- Second Test Area

4-2-1- RGB dataset

The left image in Figure 49 shows the second test area selected to test the random forest classifier. This test area is another part of the Salbertrand area and the reason for using the second test area is to produce some generalized results regarding the performance of datasets. The right image in Figure 49 is the classified map of the area based on the RGB dataset. As it is shown, there seems to be a lot of misclassifications between all couples of classes.

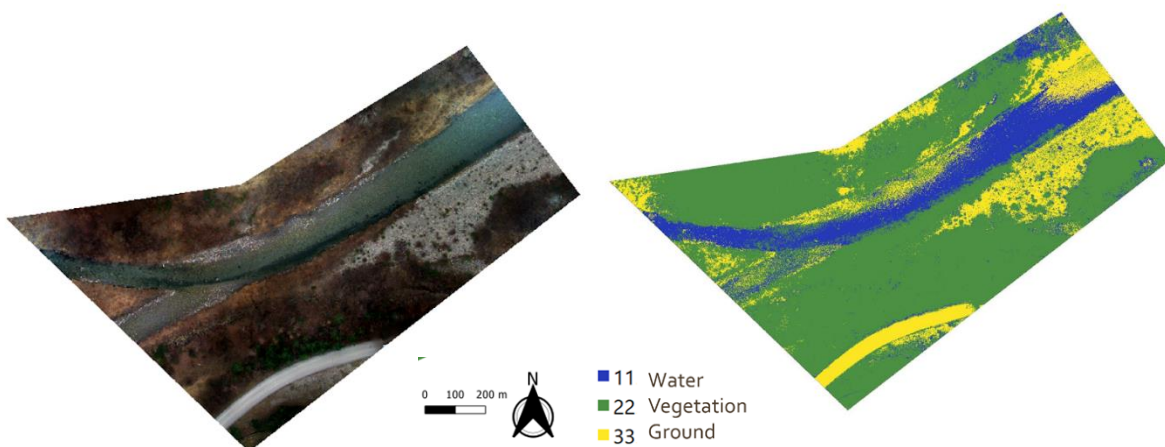


Figure 49. Left: 2nd test area. Right: classified map of 2nd test area

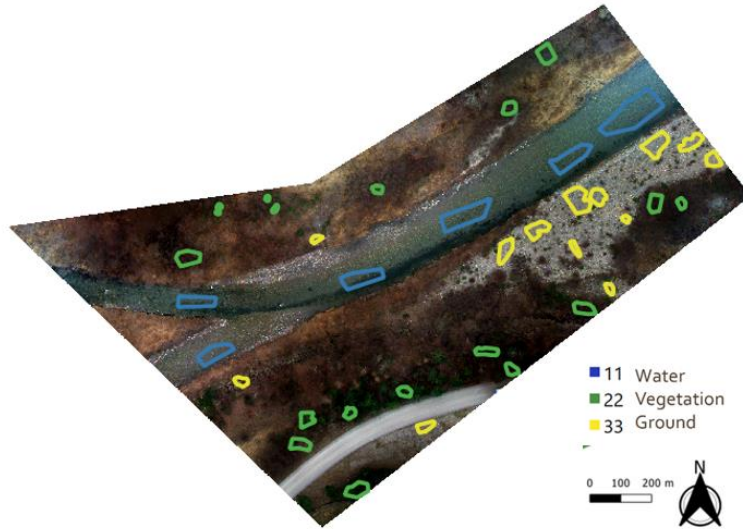


Figure 50. Validation polygons on the 2nd test area, Green (Vegetation), Blue (Water), Yellow (Ground)

In Figure 50, validation polygons on the testing area are presented, with the assumption that classes of the validation polygons are determined for us. This step is for assessing the classification goodness.

A numerical assessment of the results is in Table 21. Based on the results, there are high values of misclassification between vegetation\water, ground\water, vegetation\ground couples.

Table 21. Confusion matrix of 2nd test area- RGB dataset

Unit:m ²	Water	Vegetation	Ground
Water	299.3	38.17	75
Vegetation	21.2	258.3	0.64
Ground	3.5	62.8	215.8

Table 22. Accuracy parameters of 2nd test area- RGB

	Precision	Recall	F-score	AUC
Water	0.92	0.72	0.81	0.95
Vegetation	0.72	0.92	0.81	0.94
Ground	0.74	0.76	0.75	0.92
Average	0.79	0.80	0.79	0.94

Table 22 shows the accuracy measures of the second test area based on the RGB dataset. As it can be seen, there are low values of precision, recall, and consequently f-score for almost all the classes and the best-achieved result is 80%. Figure 51 shows the precision-recall curve for this dataset and their immediate decrease from 1 reference value in the water class as well as the other two classes, which proves the presence of high misclassification between all the classes.

Precision-Recall curve for Water (11), Vegetation (22), Ground/Gravel bars classe

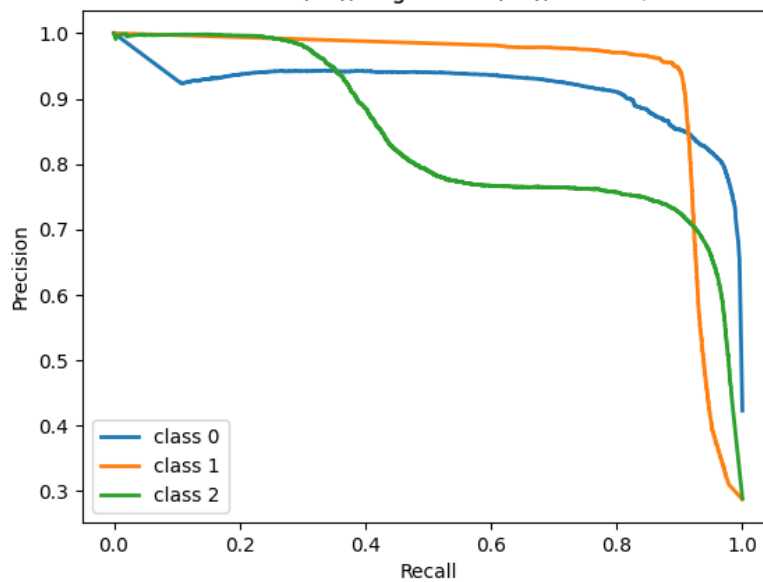


Figure 51. Precision-recall curves for 3 classes

4-2-2- Red-Edge + NIR dataset

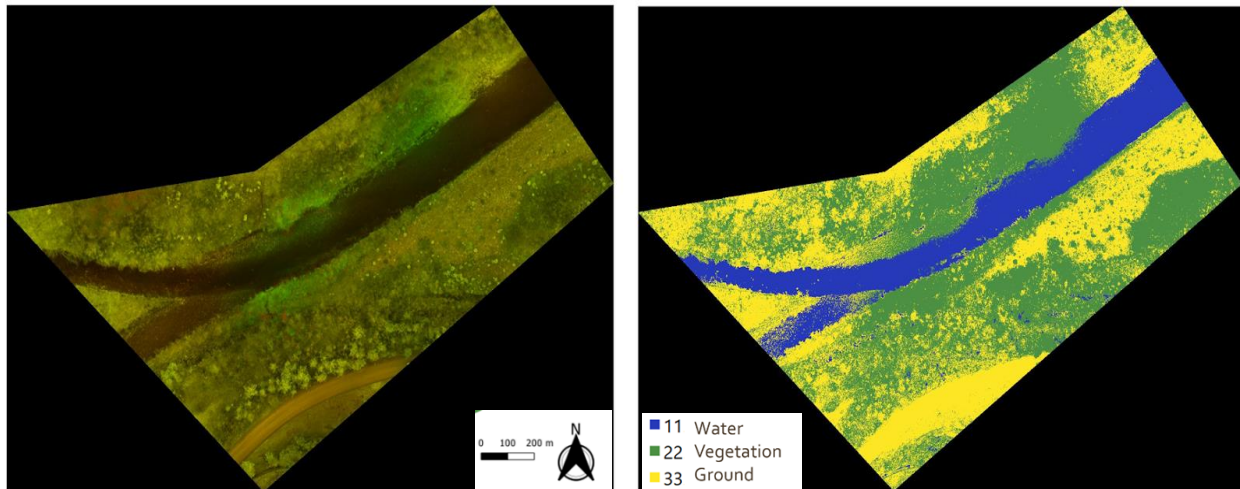


Figure 52. Left: 2nd Testing area- RE + NIR dataset. Right: segmented map of 2nd testing area based on RE + NIR dataset

Figure 52 shows the results of the classification of the second test area based on only multispectral data alongside with testing area itself is shown. The testing area in this figure (left) is a false-color representation with Red-Edge in the Red channel and NIR in the Green channel.

In the classified map, as it is evident visually, waterbed and wet areas are detected with almost good accuracy, but in the next figures also numerical measures are considered.

Table 23. Confusion matrix of 2nd Testing area- RE + NIR dataset

Unit:m ²	Water	Vegetation	Ground
Water	410.6	0.04	1.84
Vegetation	0.06	198.6	81.5
Ground	1.62	30.6	250

In table 23, the confusion matrix for the second test area for this dataset is reported. There seems to be no problem for water class, water pixels are mostly in water class, and the number of vegetation and ground pixels inside water class is not that much, but misclassification between ground and vegetation is still present in this testing area. The precision-recall curve in Figure 53 shows very high values of almost 1 for the water class. But for the other two classes, there is an immediate decrease in the AUC curve, which is proof of the classification problem. In Table 24, numerical results of precision, recall, and f-score for 3 classes prove our interpretation. Since there are low precision and recall values for vegetation and ground classes. But water class has higher precision and recall estimations.

Figure 53. Precision-Recall curve for Water (11), Vegetation (22), Ground/Gravel bars classe

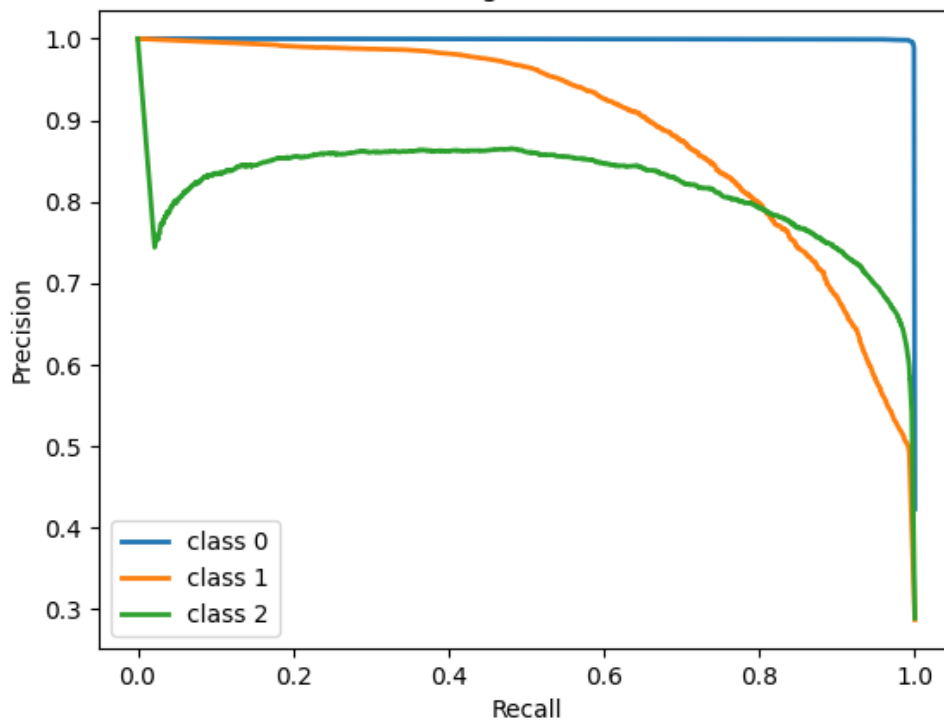


Figure 53. Precision-recall curves for 3 classes

Table 24. Accuracy parameters of 2nd Testing area- RE + NIR dataset

	Precision	Recall	F-score	AUC
Water	0.99	0.99	0.99	0.99
Vegetation	0.87	0.70	0.78	0.95
Ground	0.75	0.88	0.81	0.94
Average	0.89	0.88	0.88	0.98

4-2-3- RGB+ Red-Edge+ NIR dataset

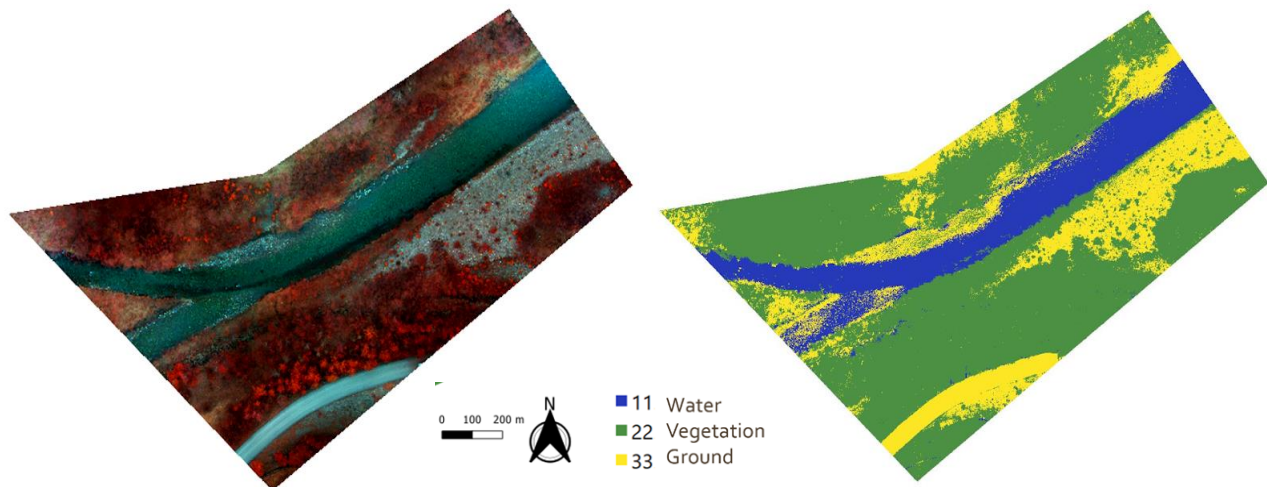


Figure 54. Left. 2nd testing area, RGB+ RE+ NIR dataset. Right: Segmented map of the 2nd testing area

Figure 54 shows the false-color representation of the testing area and the classified map of the area. As it is evident, most of the pixels seem to be classified correctly. Waterbed and moist areas are detected accurately and there is not that much noise between vegetation and ground classes.

Table 25. Confusion Matrix of 2nd testing area, RGB+ RE+ NIR dataset

Unit:m ²	Water	Vegetation	Ground
Water	405	0.01	7.4
Vegetation	0.003	280	0.09
Ground	2.67	15	264.5

Precision-Recall curve for Water (11), Vegetation (22), Ground/Gravel bars classe

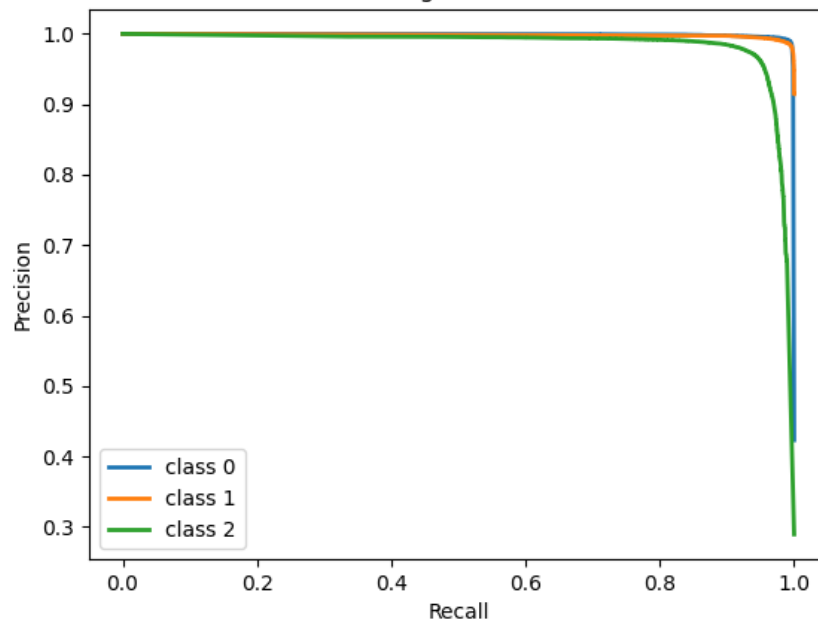


Figure 55. Precision- Recall curves

With the same token and same interpretations, the confusion matrix in Figure 55, Table 25, and Table 26 shows that precision, recall, and F-score values of all classes are high in this dataset, meaning that most of the classified pixels are in the right class and most of the pixels of each class

are detected. The precision-recall curve tends to stay 1 until the very end of it and the average F-score for all classes is about 97%.

Table 26. Accuracy Parameters of 2nd testing area, RGB+ RE+ NIR dataset

	Precision	Recall	F-score	AUC
Water	0.99	0.98	0.98	0.99
Vegetation	0.95	0.99	0.97	0.99
Ground	0.97	0.94	0.95	0.98
Average	0.97	0.97	0.97	0.99

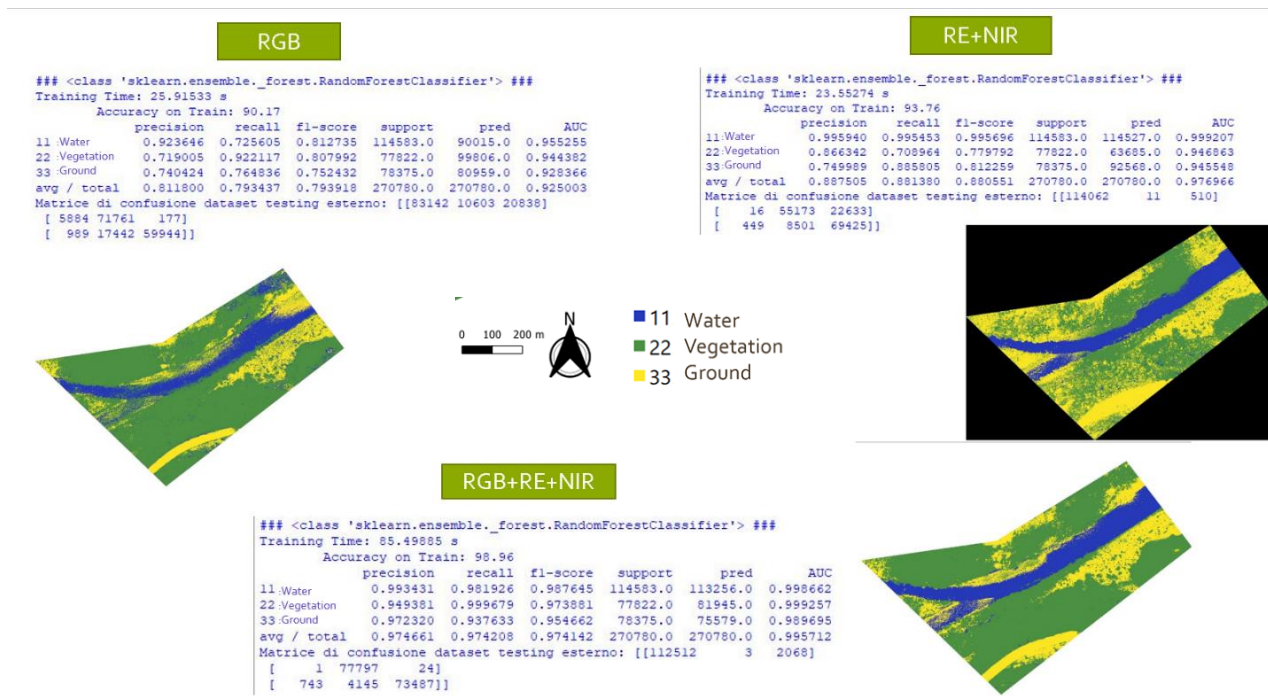


Figure 56. Results of 2nd test area using 3 different datasets

Figure 56 shows the results of all three datasets for the second test area. As expected RGB dataset could not provide accurate results for any of the classes. Using a multispectral dataset (RE+NIR) good results have been achieved for the water class mostly because of not so shallow depth of

water and clear boundaries between water and other areas. Although lower precision and lower recall values have been produced for both vegetation and ground classes, meaning that most of the points that are classified as vegetation or ground are not actually vegetation and ground respectively and most of the actual vegetation and ground points have not been predicted correctly, it is obvious that these parameters are correlated to each other and the level of confusion for the classifier is very high between vegetation and ground classes. And as mentioned before the most logical explanation for this issue is the radiance values in the winter which do not have a sharp difference between ground and vegetation in winter. However, this problem has been mostly resolved by using all available bands together including RGB and RE, and NIR. Therefore, with the combined dataset (RGB+RE+NIR), precision, recall, and consequently f-score values and considerably high for all classes.

4-3- Random Forest- April Epoch- Third Test Area

4-3-1- RGB dataset

Figure 57, the left map shows the true color representation of the third test area, and the right map shows the classified map of the third test area based on the RGB dataset. Figure 58 shows the validation polygons of the three classes which have been used to perform the evaluation of goodness for the classified map.

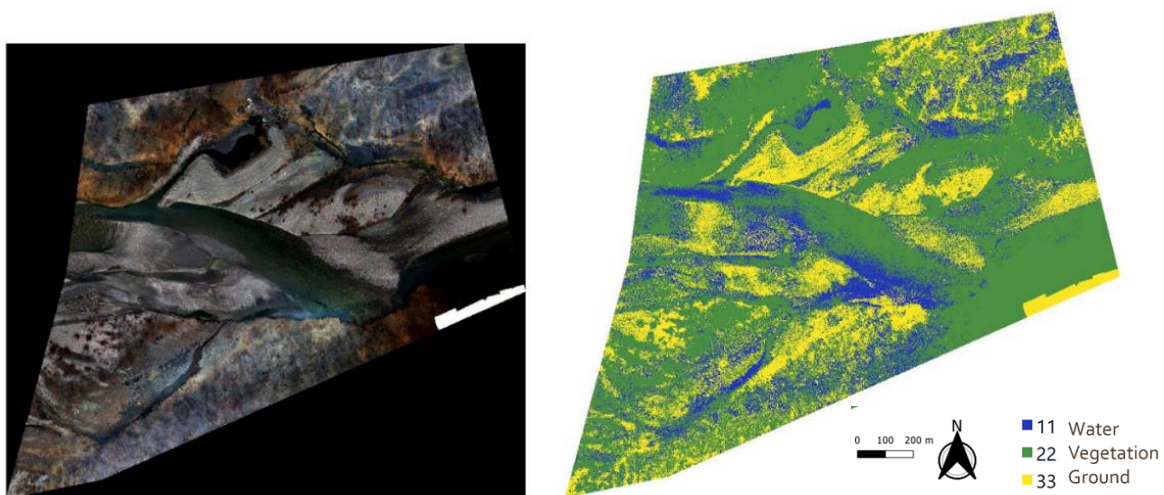


Figure 57. Left: 3rd testing area-RGB dataset. Right: segmented map of the 3rd testing area based on RGB dataset

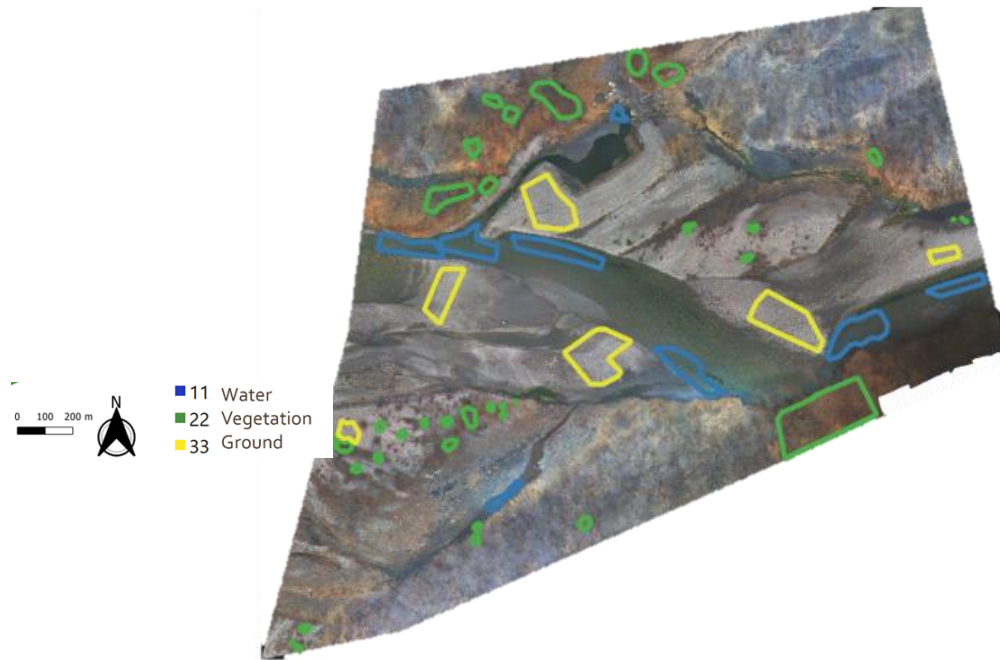


Figure 58. Validation Polygons on the 3rd testing area. Green (Vegetation), blue (Water), Yellow (Ground)

Table 27. Confusion Matrix of the 3rd testing area- based on RGB dataset

Unit:m ²	Water	Vegetation	Ground
Water	271.4	327.8	6.3
Vegetation	16	779	4.26
Ground	38.6	268.7	440.6

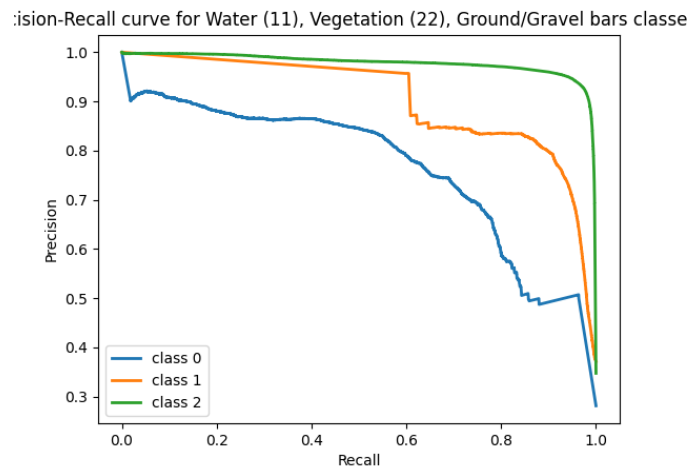


Figure 59. Precision-Recall curves

Based on the results reported in Table 28, Table 28, and Figure 59, there is misclassification between all of the classes. A large number of pixels are classified incorrectly, especially between the water\vegetation couple, and ground\vegetation couple of classes. The average F-score value produced for the water class is 58%, for vegetation class is 72% and for ground, class is 73%, and the overall average F-score for all classes is 68% which represents a very low value of precision and recall. The precision-recall curve has better results for the ground class compared to the two other classes, and the worst condition is related to the water class. Like the results of two previous test areas, the results of this test area proves that the RGB dataset cannot perform well neither for wet area detection nor for classification of two other classes.

Table 28. Accuracy parameters of the 3rd testing area- based on RGB dataset

	Precision	Recall	F-score	AUC
Water	0.83	0.44	0.58	0.89
Vegetation	0.57	0.97	0.72	0.93
Ground	0.98	0.59	0.73	0.99
Average	0.78	0.69	0.68	0.87

4-3-2- Red-Edge + NIR dataset

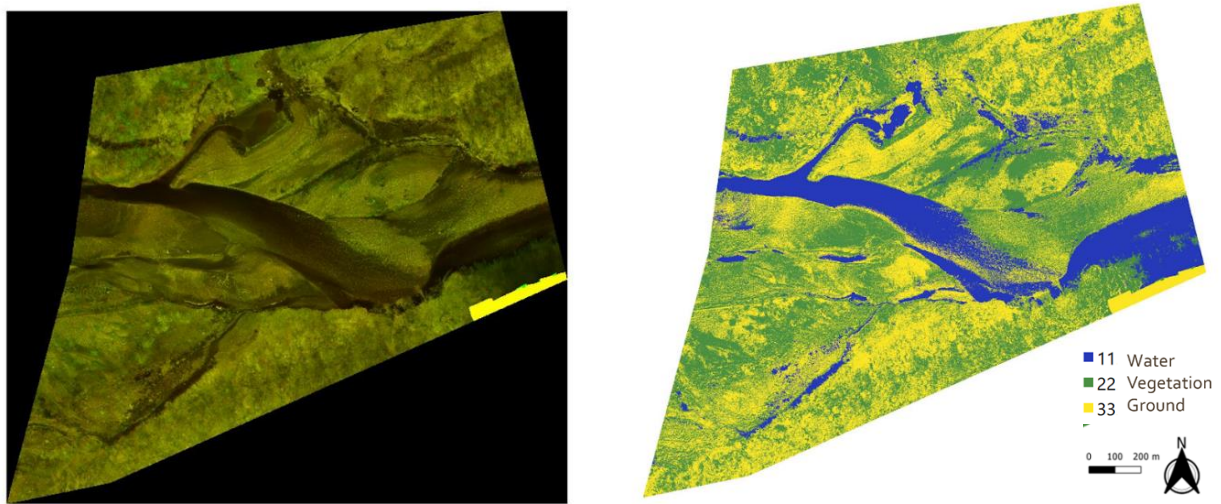


Figure 60. Left: 3rd testing area- Red-Edge + NIR dataset. Right: classified map of the 3rd testing area based on Red-Edge + NIR dataset

Figure 60, the left map shows a false-color representation of the third test area (Red-edge in the Red channel, and NIR in the green channel), and the right map shows the classified map of this area based on the Red-Edge and NIR dataset, in which blue represents water class, the yellow area is related to ground class and green classified areas are the vegetation class.

Based on the classified map, the water class seems to have very accurate results. The classifier was able to predict the water pixel even in the most challenging parts of the area (wet areas among the vegetation). For vegetation and ground, on the other hand, there seem to be some noises and misclassifications. Table 29, shows a high number of correctly classified water pixels, but a high number of falsely classified pixels for vegetation and ground.

Hence, as well as two other test areas, also in this test area, wet area and waterbed can be easily and accurately detected by Red-Edge and NIR dataset, but they have serious problems I classification of two other classes, it is worth mentioning that all accuracy measures of precision-recall numerical values, their curve and confusion matrix prove each other's results, which can be interpreted as their correct performance.

Table 29. Confusion Matrix of 3rd testing area- Red-Edge + NIR dataset

Unit:m ²	Water	Vegetation	Ground
Water	600.2	0.8	4.41
Vegetation	0.5	533.3	265.5
Ground	0.036	267.5	480.35

Precision-Recall curve for Water (11), Vegetation (22), Ground/Gravel bars classe

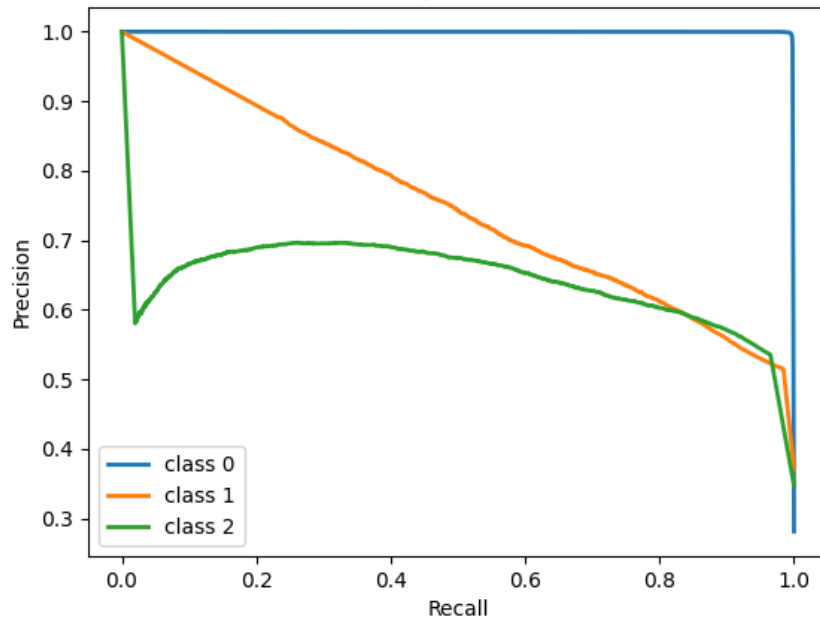


Figure 61. Precision-recall curve

Based on the precision-recall curve in Figure 61, the water class achieves an exact value of 1 in both axes, but vegetation and ground classes suffer from a large amount of misclassification. Low precision and recall in these two classes in Table 30 is proof of this interpretation.

Table 30. Accuracy Parameters of the 3rd testing area based on Red-Edge + NIR dataset

	Precision	Recall	F-score	AUC
Water	0.99	0.99	0.99	0.99
Vegetation	0.66	0.67	0.67	0.84
Ground	0.64	0.64	0.64	0.83
Average	0.75	0.75	0.75	0.91

4-3-3- RGB+ Red-Edge+ NIR dataset

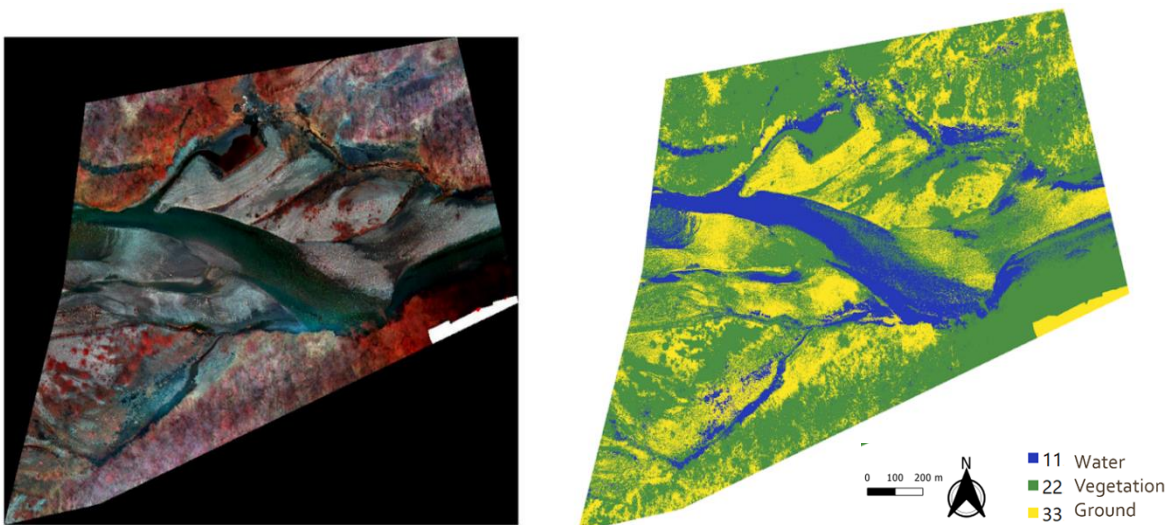


Figure 62. Left: 3rd testing area- RGB+ RE+ NIR dataset. Right: Segmented map of 3rd testing area based on RGB+ RE+ NIR dataset

The last set of analysis for the April epoch is depicted in this section. In Figure 62, the right map shows the false representation of the area. And the right map shows the classified map of the area

based on a dataset of all bands together. Table 31 depicts some problems in the classification results mostly in the water\vegetation and vegetation\ground couple. Figure 63 represents the precision-recall curve for three classes, in which again water class seems to perform better than the two other classes.

Table 31. Confusion Matrix of the 3rd testing area- RGB+ RE+ NIR dataset

Unit:m²	Water	Vegetation	Ground
Water	492.9	112	0.6
Vegetation	0.56	796	2.91
Ground	0.55	199	548.5

Table 32, shows the numerical results of the classification, low precision for vegetation, and low recall for ground class, showing the classification problem between these two classes of vegetation and ground. This misclassification can be accounted for by the presence of shadow in the area during the acquisition phase and the composition of brownish vegetation with the ground surface in this epoch. The average f-score values achieved for water, vegetation, and ground are 89%, 83%, and 84% respectively.

Figure 64 shows the results of the third test area based on all three datasets. Like the other two test areas, the RGB dataset performs weakly in classification. In the multispectral dataset (RE+NIR) precision and recall are low for both vegetation and ground classes meaning that there is some misclassification between actual and predicted points, especially between vegetation and ground pixels.

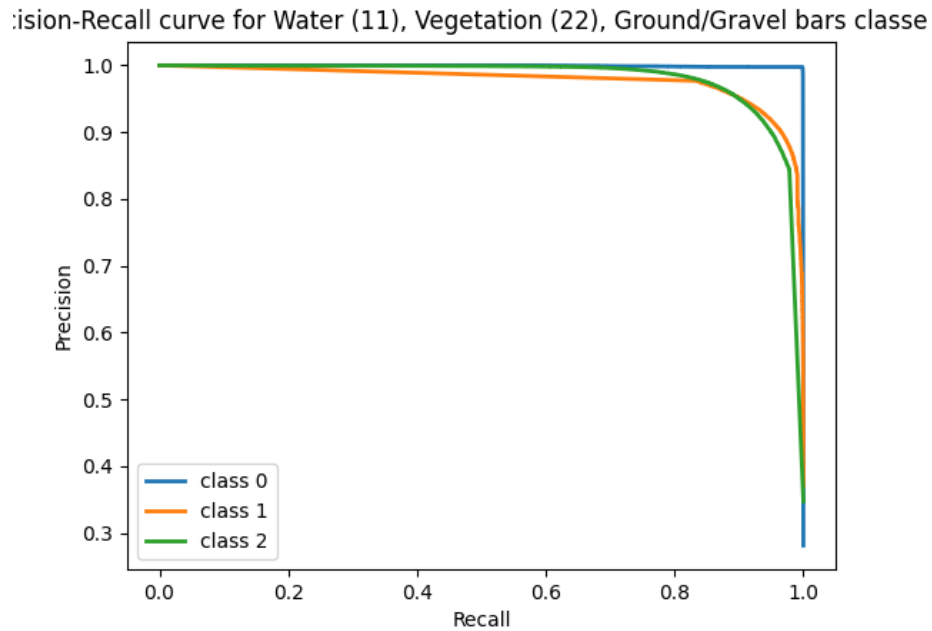


Figure 63. Precision-Recall curves

Table 32. Accuracy Parameters of the 3rd testing area based on RGB+ RE+ NIR dataset

	Precision	Recall	F-score	AUC
Water	0.99	0.81	0.89	0.99
Vegetation	0.72	0.99	0.83	0.98
Ground	0.99	0.73	0.84	0.98
Average	0.89	0.85	0.85	0.97

Results for the water class are promising. Using a combined dataset (RGB+RE+NIR), for water class, high precision values have been generated representing that most of the pixels that are classified as water are water, and also low recall value (not so low) meaning that a portion of the pixels that are actually water has not been predicted as water correctly.

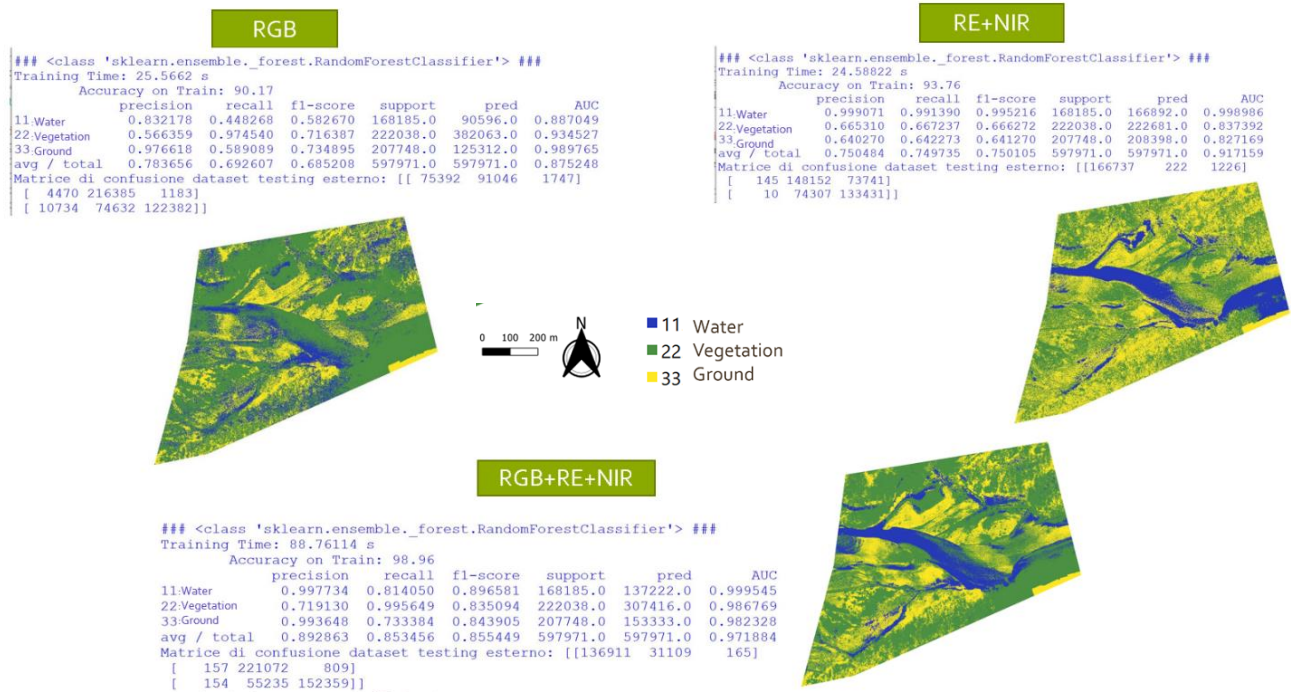


Figure 64. Results of 3rd test area using 3 different datasets

To sum up, for the water class, most of the points in the water class are water but still, there are a few points of water points in other classes as wrongly classified points.

Vegetation class resulted in low precision and high recall values meaning that points that are vegetation have been classified mostly correctly as vegetation but there are some other points in the vegetation class that belong to other classes and predicted incorrectly as vegetation which can be related to water points and explain lower recall value for water class. For ground class, high precision and low recall values have been observed showing that most of the points that are predicted as the ground are ground but there are some missing points from the ground which is present in other classes incorrectly, and it can be realized here that these missing points are most probably present in the vegetation class because of resulting low precision value for vegetation class. Generally, based on the average f-score value, the combined dataset (RGB+RE+NIR) performs better with respect to the other two datasets, but the results are still suffering from the grassy and brownish texture of the area during the winter season and even some shadow presence in the area. Table 33, shows all of the results for all classes for three test areas considering three datasets altogether, so it contains 9 scenarios.

Based on the results of Table 33, it can be recognized that generally RGB dataset cannot produce accurate results for classification purposes using a Random Forest classifier but adding data from other spectral bands to RGB dataset can improve classification results considerably.

Regarding 3 analyzed test areas, water class almost got detected in multispectral and combined datasets in all cases, but misclassification between ground and vegetation classes are still present even in the multispectral dataset for 1st and 3rd test area, although for 2nd test area such a problem was not an issue and RGB+RE+NIR dataset using Random Forest classifier did a good job for

Table 33. Results of all test areas for all available dataset

Dataset		Precision %	Recall %	F-score %	
Test 1	RGB	water	88	58	70
		vegetation	55	92	70
		ground	97	70	81
	RedEdge + NIR	water	99	99	99
		vegetation	80	96	87
		ground	94	70	80
	RGB+ RedEdge + NIR	water	99	82	90
		vegetation	70	99	82
		ground	98	86	86
Test 2	RGB	water	92	72	81
		vegetation	72	92	80
		ground	74	76	75
	RedEdge + NIR	water	99	99	99
		vegetation	87	70	78
		ground	75	88	81
	RGB+ RedEdge + NIR	water	99	98	98
		vegetation	95	99	97
		ground	97	97	97
Test 3	RGB	water	83	49	58
		vegetation	57	97	72
		ground	98	59	73
	RedEdge + NIR	water	99	99	99
		vegetation	66	66	66
		ground	64	64	64
	RGB+ RedEdge + NIR	water	99	81	89
		vegetation	72	99	83
		ground	99	73	84

classification. Following our aim of identifying wet areas effectively and as quickly as possible, It can be emphasized that the multispectral RE and NIR bands associated with RF are able to do so with an excellent degree of accuracy (in all 3 areas analyzed), with some errors mainly related to shadows due to the lack of light during the acquisition phase.

It is worth mentioning that multispectral data alone (Red-Edge and NIR) produce promising results for water class, so they can perform very well for wet area detection, but if detection of two other classes is also of importance for us, the combined dataset is preferable.

The composition of RGB bands with the multispectral ones tends to improve the classification also of the emerged areas with the consequence of a worsening of the wet areas' detection (especially in the 1st and 3rd sections). In general, the classified areas into Vegetation and Ground present classification problems, linked to the constitution of the riverbed and the non-evergreen vegetation present in the investigated area during the winter season. Such evidence could be severely limited in evergreen wooded areas or in summer, as will be exploited in the next stage.

4-4- Random Forest- July epoch

As discussed in the previous section, since our focus is to detect wet areas as well as the other two classes, the combined dataset of RGB+RedEdge+NIR have been selected as the best dataset for classification purpose. In addition, in this epoch, other features of elevation, spectral indices, and texture features have been added as the RF inputs.

The used 27 features in this epoch are:

- a) Spectral features: Red, Green, Blue, RE, NIR, and thermal.
- b) Vegetation Indexes: NDVI, NDWI, NDRE, ARI, EVI2, SAVI, SIPI
- c) Texture features: Angular Second Moment, Contrast, Correlation, Variance, Inverse Difference Moment, Sum Average, Sum Variance, Sum Entropy, Entropy, Difference Variance, Difference Entropy, Information Measures of Correlation, Maximal Correlation Coefficient. (ROBERT M. HARALICK, 1973)

Hence, in this section, the results of the classification of one of the test areas in the July epoch with all 27 features are presented. Table 34 shows the results of precision, recall, and f-score for this step. As presented in chapter 3, a selection process based on "Select from model" tool has been performed in this epoch to find a compromise between accuracy and number of features, and to detect the most important features for the classification purpose. Figure 65 shows the percentage of importance for each feature. As shown in this figure, spectral indices including

NDWI, EVI2, NDVI, SAVI, NDRE, and ARI are among the most effective features for classification, and from spectral bands, thermal and NIR and RE are the most important ones, and this is another proof for the fact that RGB dataset alone could not achieve to the acceptable classification accuracies, even in summer epoch.

Then, based on a median threshold, only 14 features are used to implement the classification and reclassify the area based on selected features, which can be considered the most important features. The result of performance analyzers with all features and with only the important ones are presented in Table 34. It is worth mentioning that Based on these results, it can be interpreted that with importance analysis, we can produce even better results with a lower number of features because sometimes less important features even tend to decrease the accuracy score and removing them from classification, not only improves the classification results but also decrease the processing time and required power for the classifier.

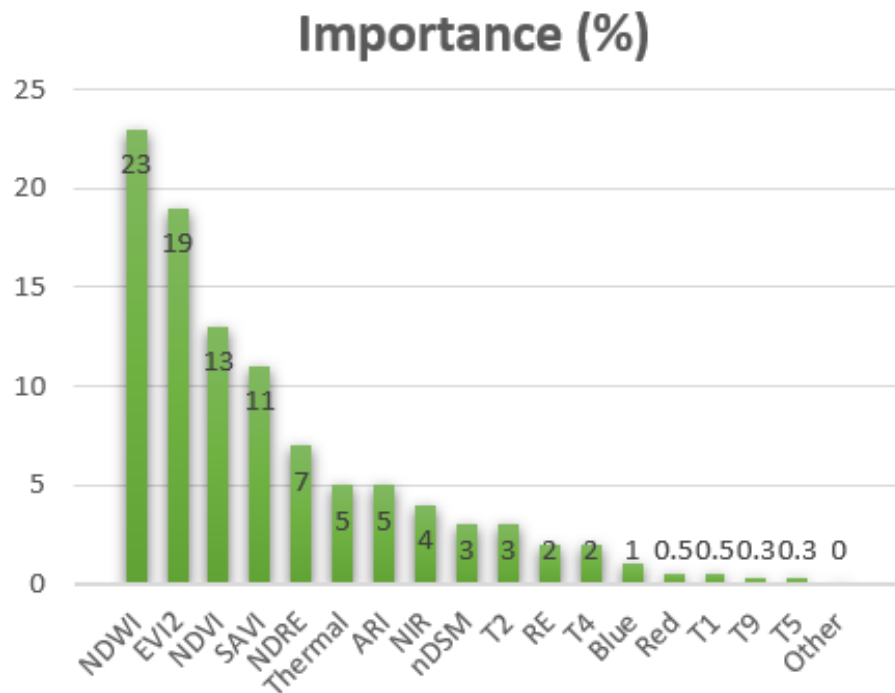


Figure 65. Importance of all features in percentage

Table 34. Results of performance analysis with all features vs only selected features.

	Precision (%)	Recall (%)	F-score (%)
27 features	91.6	91.5	91.3
14 features	93.2	92.6	92.7

In Figure 66, the top image shows the analyzed testing area in the summer epoch in RGB representation. The bottom image shows the result of classification for this area based on all the 27 features. The predicted map of the area based on only 14 features is not reported here, since it has a similar map as Figure 66, as are their precision, recall, and F-score values.

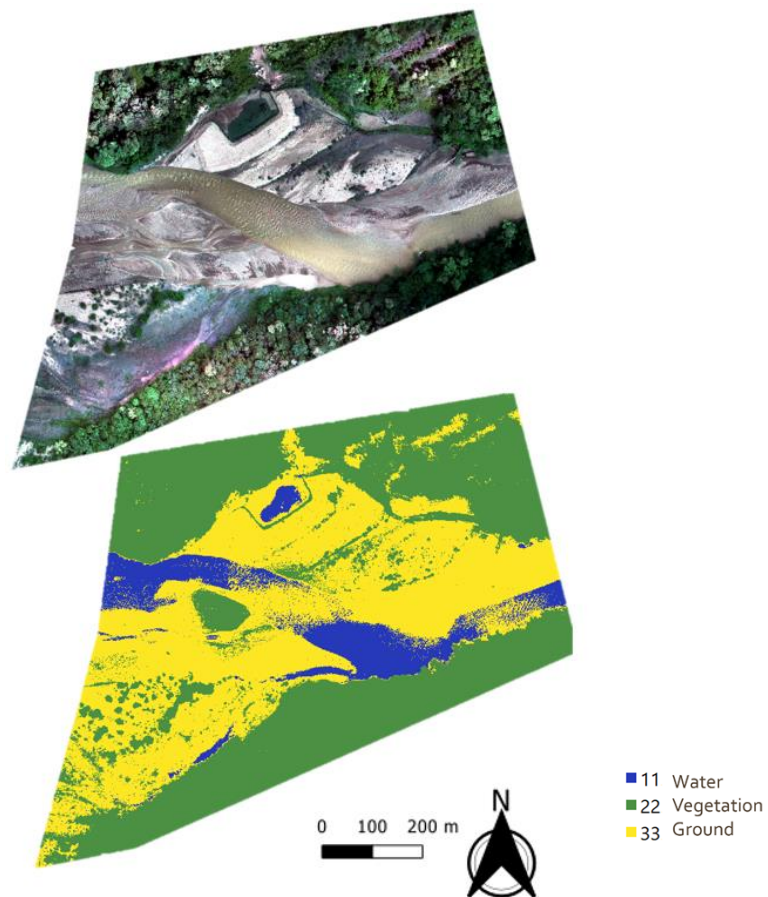


Figure 66. Classification of unseen dataset in summer epoch

Chapter 5

5- Conclusions and Suggestions

Riparian river areas are of high importance for landscape and environmental planning. The river area and its surrounding landscape are highly effective in the judgments of decision-makers for climate change measures. Taking all these considerations into account, the classification of the riparian area of the Salbertrand river with emphasis on wet area detection is performed in this project.

Starting from Raw UAV multispectral images, the orthophotos of the area based on the Structure from Motion approach are produced with a high level of accuracy at the centimeter level. The produced orthophotos were then used as inputs of the machine learning classifier named Random Forest.

Following our aim of identifying wet areas effectively and as soon as possible, along with the classification of two other classes of vegetation and ground, it can be emphasized that the multispectral radiometric features associated with the Random Forest classifier were able to do so with an excellent degree of accuracy, either in the cold season in April time epoch or the summertime in July time epoch.

There were some errors in all the scenarios mainly related to shadows due to the lack of light during the acquisition phase and constitution of the riverbed and the non-evergreen vegetation present in the investigated area in the April epoch.

In the July time epoch, the composition of radiometric features with additional features, including elevation feature of the Normalized Digital Elevation Model (nDSM), thermal data acquired by a thermal camera, vegetation indexes of NDVI, NDWI, NDRE, ARI, EVI2, SAVI, SIPI, and textures features of Angular Second Moment, Contrast, Correlation, Variance, Inverse Difference Moment, Sum Average, Sum Variance, Sum Entropy, Entropy, Difference Variance, Difference Entropy, Information Measures of Correlation, Maximal Correlation Coefficient, tends to improve the classification results even more in respect to previous time epoch.

Meanwhile, a compromise between the number of features and classification accuracy results in a more realistic conclusion about selected features. Based on the performed importance analysis, spectral indices including NDWI, EVI2, NDVI, SAVI, NDRE, and ARI are among the most effective features for classification, and from spectral bands, thermal and NIR and Red-Edge are the most important ones. By recognizing the most effective features, researchers can focus on the most important ones in their studies, to decrease the processing time and required power alongside achieving high accuracy for the classification.

In future works, other machine learning methods, such as Support Vector Machine (SVM) and deep learning methods based on Convolutional Neural Networks (CNNs), can be taken into consideration to have a comprehensive analysis of the performance of different methods beside different datasets for wet area detection.

In order to perform the classification with CNNs, one way is to take a model and train the model by our multispectral dataset of Salbertrand, but the problem with this action is overfitting. Another way would be to find a pretrained network with an available weighting matrix and test it with our Salbertrand dataset. But the problem with this method is that the given network should be trained on exactly similar data as ours considering the number of bands, wavelength, and all radiometric characteristics. The third possible way is to find a set of datasets (images) and train the network with that unknown dataset and then use the Salbertrand data as testing data for the network (Ronald Kemker C. S., 2017), but similar to the previous method, also in this case we should have exactly same characteristics of the dataset as ours because the model will be trained on it and different characteristics of data may result in problematic results (Bin Pan, 2019). Because of lack

of processing power and time, CNNs have not been performed in this research work, but considering the performed vast literature review on it, it can be the focus of our future work.

References

- (2022, 07 05). Retrieved from Random Forest Models: <https://www.ml-science.com/random-forest>
- (2022, 07 05). Retrieved from QGIS: <https://www.qgis.org/en/site/about/index.html>
- (2022, 07 03). Retrieved from Python Programming Language: <https://www.python.org/>
- Ahamed, T., Tian, L., Zhang, Y., & Ting, K. C. (2011). A review of remote sensing methods for biomass feedstock production. *Biomass & Bioenergy*, 2455-2469.
- Alabi, T. R., Abebe, A. T., Chigeza, G., & Kayode R. Fowobaje. (2022). Estimation of soybean grain yield from multispectral high-resolution UAV data with machine learning models in West Africa,. *Remote Sensing Applications: Society and Environment*,27, 100782, ISSN 2352-9385, <https://doi.org/10.1016/j.rsase.2022.100782>.
- Al-Awar, B., Awad, M., Jarlan, L., & Courault, D. (2022). Evaluation of Nonparametric Machine-Learning Algorithms for an Optimal Crop Classification Using Big Data Reduction Strategy. *Remote Sens Earth Syst Sci*, <https://doi.org/10.1007/s41976-022-00072-7>.
- Ayala-Izurieta, J., Márquez, C., García, V., Recalde-Moreno, C., Rodríguez-Llerena, M., & Damián-Carrión, D. (2017). Land Cover Classification in an Ecuadorian Mountain Geosystem Using a Random Forest Classifier, Spectral Vegetation Indices, and Ancillary Geographic Data. *Geosciences* 7 , 34. <https://doi.org/10.3390/geosciences7020034>.
- Bannari, A., Morin, D., Bonn, F., & Huete, A. R. (1995). A review of vegetation indices. *Remote Sensing Reviews*, 25.
- Barrett Lowe, A. K. (2015). Multispectral Image Analysis Using Random Forest. *Computer Science Faculty Publications and Presentations*, 15.
- Bassier, M., Vergauwen, M., & Poux, F. (2020). Point Cloud vs. Mesh Features for Building Interior Classification. *Remote Sens.* 12, 2224. <https://doi.org/10.3390/rs12142224>.
- Bin Pan, Z. S. (2019). CoinNet: Copy Initialization Network for Multispectral Imagery Semantic Segmentation. *IEEE GEOSCIENCE AND REMOTE SENSING LETTERS*, 5.
- Ceccato, P., Gobron, N., Flasse, S., Pinty, B., & Tarantola, S. (2002). Designing a spectral index to estimate vegetation water content from remote sensing data: Part 1: Theoretical approach. *Remote Sensing of Environment*, 188-197.
- Clara Skuse, A. G.-S. (2021). Can emerging membrane-based desalination technologies. *Desalination*.

- Clarke, T. R., Moran, M. S., Barnes, E. M., Pinter, P. J., & Qi, J. (2001). Planar domain indices: a method for measuring a quality of a single component in two-component pixels. *Geoscience and Remote Sensing Symposium, 2001. IGARSS '01. IEEE 2001 International*, 1279-1281.
- Darren Turner *, A. L. (2012). An Automated Technique for Generating Georectified Mosaics. *Remote Sensing*, 19.
- Dong, S., Han, S., Yin, Y., Zhang, Z., & Yao, T. (2021). The method for accurate acquisition of pavement macro-texture and corresponding finite element model based on three-dimensional point cloud data,. *Construction and Building Materials*, 312, 125390, ISSN 0950-0618, <https://doi.org/10.1016/j.conbuildmat.2021.125390>.
- F.Y., O., J.E.T., A., O., A., O., H. J., O., O., & J., A. (2017). Supervised Machine Learning Algorithms: Classification and Comparison. *International Journal of Computer Trends and Technology (IJCTT) V48(3):*, 128-138, ISSN:2231-2803.
- Feng, Q., Liu, J., & Gong, J. (2015). UAV Remote Sensing for Urban Vegetation Mapping Using Random Forest and Texture Analysis. *Remote Sens.* 7, 1074-1094. <https://doi.org/10.3390/rs70101074>.
- Francisco Agüera-Vega, F. C.-R.-C.-H.-C.-F.-P. (2018). Reconstruction of extreme topography from UAV structure from motion. *Measurement*, 12.
- Franklin, S. E., & Ahmed, O. S. (2018). Deciduous tree species classification using object-based analysis and machine learning with unmanned aerial vehicle multispectral data. *International Journal of Remote Sensing*, 39, 5236-5245, 10.1080/01431161.2017.1363442.
- Gevaert, C., Persello, C., Sliuzas, R., & G. Vosselman. (2017). Informal settlement classification using point-cloud and image-based features from UAV data,. *ISPRS Journal of Photogrammetry and Remote Sensing*,125, 225-236, ISSN 0924-2716, <https://doi.org/10.1016/j.isprsjprs.2017.01.017>.
- Gitelson, A. A., Merzlyak, M. N., Zur, Y., Stark, R., & Gritz, U. (2001). Non-destructive and remote sensing techniques for estimation of vegetation status. *Third European Conference on Precision Agriculture*, 301-306.
- Iglhaut, J., Cabo, C., Puliti, S., Piermattei, L., O'Connor, J., & Rosette, J. (2019). Structure from Motion Photogrammetry in Forestry: a Review. *Remote Sensing, Curr Forestry Rep* 5, 155–168,<https://doi.org/10.1007/s40725-019-00094-3>.
- Impollonia, G., Croci, M., Ferrarini, A., Brook, J., Martani, E., Blandinières, H., . . . Amaducci, S. (2022). UAV Remote Sensing for High-Throughput Phenotyping and for Yield Prediction of Miscanthus by Machine Learning Techniques. *Remote Sens.* 14,, 2927.

- Kotsiantis, S., Zaharakis, I., & Pintelas, P. (2006). Machine learning: a review of classification and combining techniques. . *Artif Intell Rev* 26, 159–190, <https://doi.org/10.1007/s10462-007-9052-3>.
- Koutalakis, P., Tzoraki, O., Gkiatas, G., & Zaimes, G. (2020). Using UAV to Capture and Record Torrent Bed and Banks, Flood Debris, and Riparian Areas. *Drones*, 4, 77. <https://doi.org/10.3390/drones4040077>.
- Lowe, B., & Kulkarni, A. (2015). Multispectral Image Analysis Using Random Forest. *International Journal on Soft Computing (IJSC)*, 6, 1-14, 10.5121/ijsc.2015.6101.
- Lowe, D. G. (2004). Distinctive Image Features from Scale-Invariant Keypoints. *International Journal of Computer Vision*, 28.
- Mahboubi, M. ., Fernandes, A., Fibaek, C., & Dabove, P. (2022). Geospatial Analysis of Safe Delivery App Events Based on Geographically Weighted Regression Tool. *{AGILE: GIScience Series*, 3, 10.5194/agile-giss-3-47-2022 (p. 47). <https://agile-giss.copernicus.org/articles/3/47/2022/>.
- Mahboubi, M., Belcore, E., Pontoglio, E., Matrone, F., & Lingua, A. (2022). Detection of Wet Riparian Areas using Very High Resolution Multispectral UAS Imagery Based on a Feature-based Machine Learning Algorithm. *AGILE: GIScience Series*, 3, 10.5194/agile-giss-3-46-2022 (p. 46). <https://agile-giss.copernicus.org/articles/3/46/2022/> .
- Maimaitijiang, M., Sagan, V., Sidike, P., Daloye, A., Erkbol, H., & Fritschi, F. (2020). Crop Monitoring Using Satellite/UAV Data Fusion and Machine Learning. *Remote Sens.*, 12(9), 1357, <https://doi.org/10.3390/rs12091357>.
- Marin, D. B., Ferraz, G. A., Santana, L. S., Barbosa, B. D., Barata, R. A., Osco, L. P., . . . Guimarães, P. H. (2021). Detecting coffee leaf rust with UAV-based vegetation indices and decision tree machine learning models,. *Computers and Electronics in Agriculture*,190, 106476,ISSN 0168-1699, <https://doi.org/10.1016/j.compag.2021.106476>.
- Maxwell, A. E., Warner, T. A., & Fang, F. (2018). Implementation of machine-learning classification in remote sensing: an applied review. *International Journal of Remote Sensing*, 39(9), 2784-2817, <https://doi.org/10.1080/01431161.2018.1433343>.
- Miura, T., Yoshioka, H., Fujiwara, K., & Yamamoto, H. (2008). Inter-Comparison of ASTER and MODIS Surface Reflectance and Vegetation Index Products for Synergistic Applications to Natural Resource Monitoring. *Sensors*, 2480-2499.
- Nasir, N., Kansal, A., Alshaltone, O., Barneih, F., Sameer, M., Shanableh, A., & Al-Shamma'a, A. (2022). Water quality classification using machine learning algorithms,. *Journal of Water Process Engineering*, 48, 102920, ISSN 2214-7144, <https://doi.org/10.1016/j.jwpe.2022.102920>.

- Nikolakopoulos, K., Kyriou, A., & Koukouvelas, I. (2022). Developing a Guideline of Unmanned Aerial Vehicle's Acquisition Geometry for Landslide Mapping and Monitoring. *Appl. Sci.* 12, 4598. <https://doi.org/10.3390/app12094598>.
- Osco, L. P., Junior, J. M., Ramos, A. P., Jorge, L. A., Fatholahi, S. N., Silva, J. d., . . . Li, J. (2021). A review on deep learning in UAV remote sensing,. *International Journal of Applied Earth Observation and Geoinformation*, 102, 102456, ISSN 1569-8432, <https://doi.org/10.1016/j.jag.2021.102456>.
- Ramos, A. P., Osco, L. P., Furuya, D. E., Gonçalves, W. N., Santana, D. C., Teodoro, L. P., . . . Roj, F. H. (2020). A random forest ranking approach to predict yield in maize with uav-based vegetation spectral indices,. *Computers and Electronics in Agriculture*, 178, 105791,ISSN 0168-1699, <https://doi.org/10.1016/j.compag.2020.105791>.
- ROBERT M. HARALICK, K. S. (1973). Textural Features for Image Classification. *IEEE TRANSACTIONS ON SYSTEMS, MAN, AND CYBERNETICS*, 12.
- Ronald Kemker, C. S. (2017). High-Resolution Multispectral Dataset for Semantic Segmentation. *Computer Vision and Pattern Recognition*, 9.
- Ronald Kemker, C. S. (2018). Algorithms for Semantic Segmentation of Multispectral. *ISPRS Journal of Photogrammetry and Remote Sensing*, 45.
- Rusnák, M., Goga, T., Michaleje, L., Šulc Michalková, M., Máčka, Z., Bertalan, L., & Kidová, A. (2022). Remote Sensing of Riparian Ecosystems. *Remote Sens.* 14, 2645. <https://doi.org/10.3390/rs14112645>.
- Schneider, T., O'Gorman, P. A., & and Levine, X. J. (2010). Water vapor and the dynamics of climate changes. *Rev. Geophys.*, 48, RG3001, doi:10.1029/2009RG000302.
- Shen, Y., Mercatoris, B., Cao, Z., Kwan, P., Guo, L., Yao, H., & Cheng, Q. (2022). Improving Wheat Yield Prediction Accuracy Using LSTM-RF Framework Based on UAV Thermal Infrared and Multispectral Imagery. *Agriculture*, 12, , 892. <https://doi.org/10.3390/agriculture12060892>.
- Shin, J.-i., Seo, W.-w., Kim, T., Park, J., & Woo, C.-s. (2019). Using UAV Multispectral Images for Classification of Forest Burn Severity—A Case Study of the 2019 Gangneung Forest Fire. *Forests* 10, 1025. <https://doi.org/10.3390/f10111025>.
- Singh, A. P., Yerudkar, A., Mariani, V., Iannelli, L., & Glielmo, L. (2022). A Bibliometric Review of the Use of Unmanned Aerial Vehicles in Precision Agriculture and Precision Viticulture for Sensing Applications. *Remote Sensing* 14:7, , pages 1604.
- Su, J. X. (2017). Significant Remote Sensing Vegetation Indices: A Review of Developments and Applications. *Sensors*, 17.

- Tao, W., Lei, Y., & Mooney, P. .. (2011). Dense point cloud extraction from UAV captured images in forest area. *Proceedings 2011 IEEE International Conference on Spatial Data Mining and Geographical Knowledge Services* (pp. 389 - 392. 10.1109/). ICSDM 2011 - .
- Tavakol, m. h., Tali, M. G., Sadough, H., & Alinoori, K. (2022). Random forest model to identify changes in micro-landforms using UAV images (Case study: Afjeh region in Jajroud basin 1397-1397). *Quantitative Geomorphological Research*, doi: 10.22034/gmpj.2022.324517.1331.
- Westoby, M., Brasington, J., Glasser, N., Hambrey, M., & J.M. Reynolds. (2012). 'Structure-from-Motion' photogrammetry: A low-cost, effective tool for geoscience applications,. *Geomorphology*, 179, 300-314, ISSN 0169-555X, <https://doi.org/10.1016/j.geomorph.2012.08.021>.
- Xue, J., & Su, B. (2017). Significant Remote Sensing Vegetation Indices: A Review of Developments and Applications. *Sensors*, 1687-725X, <https://doi.org/10.1155/2017/1353691>.
- Zan, X., Zhang, X., Xing, Z., Liu, W., Zhang, X., Su, W., . . . Li, S. (2020). Automatic Detection of Maize Tassels from UAV Images by Combining Random Forest Classifier and VGG16. *Remote Sens.* 12, 3049. <https://doi.org/10.3390/rs12183049>.
- Zeybek, M. (2021). Classification of UAV point clouds by random forest machine learning algorithm. *Turkish Journal of Engineering* , 5 (2), 48-57 . DOI: 10.31127/tuje.669566.
- Zhang, F., Chen, Y., Wang, W., Jim, C. Y., Zhang, Z., Tan, M. L., . . . Rahman, H. A. (2022). Impact of land-use/land-cover and landscape pattern on seasonal in-stream water quality in small watersheds,. *Journal of Cleaner Production*, 357, 131907, ISSN 0959-6526, <https://doi.org/10.1016/j.jclepro.2022.131907>.
- Zhang, L., Song, Z., Wu, D., Luo, Z., Zhao, S., Wang, Y., & Deng, J. (2022). Prediction of coal self-ignition tendency using machine learning. *Fuel*, 325, 124832, ISSN 0016-2361, <https://doi.org/10.1016/j.fuel.2022.124832>.

Statement of Independent Work

I hereby confirm that this thesis was written independently by myself without the use of any sources beyond those cited, and all passages and ideas taken from other sources are cited accordingly.